Exploring Naturalness in Supersymmetry at the High-Luminosity Large Hadron Collider

by

Mari Røysheim

Thesis

for the degree of

Master of science

Faculty of Mathematics and Natural Sciences

University of Oslo

December 2016

Abstract

We explore the naturalness reach of the high-luminosity Large Hadron Collider (HL-LHC) at $\sqrt{s} = 14$ TeV in future experiments searching for supersymmetry, quantifying naturalness in terms of the Barbieri–Giudice measure. Based on work presented in [1], we compare with similar results at a possible International Linear Collider (ILC) at $\sqrt{s} = 0.5$ and 1 TeV, to investigate how the two can complement each other.

In the framework of the minimal supersymmetric Standard Model with conservation of R-parity, we scan the parameter spaces of three different scenarios, where one of them represents a so-called Natural supersymmetry model. We set exclusion limits at the 95% confidence level, defining what parameter values and sparticle masses are disfavored by experiment.

With Bayesian parameter estimation we also find posterior probability distributions for naturalness from the planned searches for supersymmetry at CERN, which indicate that very natural models may remain even after the HL-LHC searches. The information gain in the update of our prior beliefs is quantified in terms of the Kullback–Leibler divergence. From the literature, it appears that this measure has never previously been used in the context of particle physics.

Takk

Først av alt vil jeg takke min veileder professor Are Raklev ved Universitetet i Oslo for uvurderlig oppklaring og hjelp under arbeidet med denne masteroppgaven. Jeg har satt stor pris på din åpne kontordør, og jeg er glad du har vist deg som en meget tålmodig sjel. En stor takk går også til Anders Kvellestad — du har vært intet mindre enn en guru. The CPU intensive parameter scans in this work was carried out using the Abel Cluster, owned by the Univeristy of Oslo and the Norwegian metacenter for High Performance Computing (NOTUR), and operated by the Research Computing Services group at USIT, the University of Oslo IT-department. The computing time was given by NOTUR allocation NN9284K, financed through the Research Council of Norway.

Takk også til alle flotte mennesker på teorigruppa ved Universitetet i Oslo, særlig Ola Liabøtrø og Marius Meyer, som har bistått med programmeringskunnskaper og generelt godt humør. Jeg vil også takke Jørgen Eriksson Midtbø for hjelp med Higgskorreksjoner og brødmotivasjon. Tusen takk Marte Julie, for at du underholder, dikter og alltid byr på deg selv. Takk til Elise for at du alltid så trygg og varm å møte på. Takk til Matilde Linde for all ærlighet, sarkasme, ironi og løpings. Takk til Malin for alle frokoster og Lieblingdater. Du er et unikum.

Takk til Steinar Bakken som gjorde fysikk morsomt i løpet av tredjeklasse på videregående. Det var verken tåkekammeret vi laget eller bilkjøringa i timen som gjorde utslaget, men din uhøytidelige tilnærming til faget, entusiasme og evne til å gjøre det ganske forståelig. Videre må jeg takke Inga for at du inspirerte meg ytterligere den gangen du tok master på NTNU, og svarte på mailen jeg sendte med spørsmål om hvor vanskelig det var. Du løy sikkert så det rant av deg, men jeg er glad du pynta på sannheten, ellers hadde jeg nok aldri møtt deg på fysikkonferanse seks år seinere. Jeg håper du fortsetter å fortelle om hyllene dine på kontoret, og at vi løper Feynmandiagram når du besøker Oslo. Og la oss aldri legge bloggen død.

Kjære Henrik. Tusen takk for alt ubegripelig du har gjort forståelig de siste fem åra. Tusen takk for alle Ellingparodier, kaffepauser hos tyrkern, lørdagskvelder med non-stop og vin på Grünerløkka.

Kjære Edel. Jeg er så glad vi tok den skogsturen den høsten. Da fant jeg ut at du kunne være dum nok til å bli med på gåtur fra Oslo til Trondheim med telt på ryggen. Sammen med Tina er dere verdens beste kollektiv, både å komme hjem til og å våkne opp med. Mer gamlehjem, Gilmore Girls og kaffe, takk.

Kjære Eli. Jeg veit ikke hvem jeg må takke for at vi har etternavn som likner, men det var ganske avgjørende for fadderuka i 2011, og tilværelsen min på Blindern de neste fem åra. At to så ulike personer skulle vise seg å ha så like arbeidsvaner og -metoder er ganske utrolig, og det har stadig vært min redning.

Du har vært min desidert viktigste støttespiller og beste venninne gjennom hele studietida. Uten deg hadde aldri denne masteren blitt til.

Takk til Åse Minde på Gaustad for at du alltid hørte på meg og hadde tro på meg. Takk for at du lærte meg at man ikke trenger å være enten eller.

Til mitt store forbilde bestefar. Takk for at du alltid har vist en enorm interesse for det jeg holder på med, og alltid har ønsket å høre hvordan arbeidet med masteroppgaven har gått. Dine *råd fra en gammel bestefar* har alltid vært gode å støtte seg på. Du er en stor inspirasjon, og jeg håper jeg blir like nysgjerrig og kunnskapssøkende som deg når jeg blir 80 år.

Til kjæreste Erik. Takk for alle kveldene i høst du har tatt imot meg og latt meg få sovne i armkroken din. Din omsorg har betydd mer enn jeg har klart å gi uttrykk for.

Til den beste mammaen, pappaen og lillebroren. Takk for at dere trøsta meg da jeg lå på fysikkplenen etter tre dager på universitetet og gråt fordi det var for mange komplekse tall og greske bokstaver. Jeg er så glad jeg ikke visste at det bare var starten. Takk for at det alltid er så godt å komme hjemhjem til Lillehammer. Men aller mest takk for at dere aldri ga meg opp.

Blindern, 20.desember 2016,
Mari Røysheim.

Contents

Introduction

Within the framework of the minimal supersymmetric Standard Model with conservation of R-parity, this thesis investigates the naturalness reach of the high-luminosity Large Hadron collider at $\sqrt{s} = 14$ TeV with integrated luminosities of $\mathcal{L} = 300$ fb^{-1} and $\mathcal{L} = 3000$ fb^{-1}. We quantify naturalness in terms of the widely adopted Giudice–Barbieri sensitivity criterium. By the use of Monte Carlo event generators, we scan the parameter spaces of two minimal supergravity scenarios, and one Natural supersymmetry scenario. The goal of the scans is to set exclusion limits at the 95% confidence level, defining what parameter values and sparticle masses are disfavored by experiment, as well as which naturalness scores are excluded. Taking the same approach as Allanach et al. in [2], we use these exclusion bounds to define the naturalness reach of the HL-LHC in terms of the minimum non-excluded score. As a more sophisticated measure of the naturalness reach, we also find posterior probability distributions of naturalness, using Bayesian parameter estimation and likelihoods taken from the parameter scans. These distributions indicate how likely we consider the various naturalness values to be. We quantify the information gain in the update of our prior beliefs in terms of the Kullback–Leibler divergence, and from the literature it appears that this measure has never previously been used in the context of particle physics. Based on work presented in [1], we compare with similar results at a possible International Linear Collider at $\sqrt{s} = 0.5$ TeV and 1 TeV, to investigate how the two can complement each other.

We begin with an introduction to the underlying principles of the Standard Model in chapter 1. Many of the shortcomings of this theory can be solved with supersymmetric models, which we elaborate on in chapter 2, culminating in the definition of the minimal supersymmetric Standard Model. In chapter 3 we present the hierarchy problem of the Standard Model and clarify why supersymmetry can offer an attractive solution. We also explain how this impacts the scale at which we believe supersymmery can be realized. Chapter 4 desribes the statistical framwork of this thesis, where we outline the concept of Bayesian parameter estimation, and define the Kullback–Leibler divergence. In chapter 5 we give a detailed description of the simulation of future experiments, searching for various supersymmetric signatures at the HL-LHC. The practical software and scan set-up is given, the analyses are described in detail, and we validate our implementations

by benchmark testing. In chapter 6 we present and discuss our results, before we finally make our conclusions.

Chapter 1

The Standard Model of particle physics

The Standard Model (SM) of elementary particle physics has had great success in describing the fundamental particles and their interactions. As of today, it is our best description of the subatomic world. The final confirmation of its viability came in 2012, after the Higgs boson was discovered by the CMS and ATLAS experiments at CERN [3, 4]. Despite its great success, there are good reasons for believing the Standard Model constitutes only the low energy part of a more fundamental theory. The Standard Model offers no candidate for dark matter (DM), and gravitation is ignored as a fundamental force. In addition, the Standard Model suffers large quantum corrections to the Higgs mass, a topic we will return to in chapter 3.

1.1 The Standard Model as a quantum field theory

The Standard Model is a quantum field theory, described by a Lagrangian density $\mathcal{L}$ (from now on referred to simply as the Lagrangian), a function of the field content of the theory and their derivatives. It is related to the action S by

$$S = \int_R \mathrm{d}^4x \; \mathcal{L}. \tag{1.1}$$

The dynamics are obtained from the Lagrangian via the Euler–Lagrange equation, which for a field ϕ_i is

$$\partial_\mu \left(\frac{\partial \mathcal{L}}{\partial(\partial_\mu \phi_i)} \right) - \frac{\partial \mathcal{L}}{\partial_\mu \phi_i} = 0. \tag{1.2}$$

Symmetries play a crucial rôle in physics, as they have a deep underlying connection to conserved physical quantities. In field theory, a symmetry transformation is defined as a transformation that leaves the equations of motion invariant.

This is guaranteed if the action is left invariant under the transformation. Invariance of the action is in turn obtained if the Lagrangian changes by a total derivative,

$$\mathcal{L} \to \mathcal{L}' = \mathcal{L} + \partial_\mu f(x), \tag{1.3}$$

when we take $f(x)$ to be zero on the surface $S(R)$ of the integration boundary.

The connection between symmetries and conservation laws is summarized in *Noethers theorem* from 1918. The theorem states that every continous symmetry of the Lagrangian, has a corresponding conservation law [5]. As an example, energy and momentum conservation are consequences of the invariance of the Lagrangian under space and time translations.

Using the *interaction amplitude* $\mathcal{M}$ found from the Lagrangian, we can calculate physical quantities like the decay width of a particle or the cross section of a scattering process. As the exact expression of $\mathcal{M}$ is often unknown, an approximation in power series of the interaction strength is done, so-called perturbation theory. Richard Feynman visualized and organized the calculation of the perturbation series using diagrams, known as Feynman diagrams [6]. The expansion is in principle an infinite sum of terms (diagrams) with increasing complexity and decreasing importance. Hence it is often sufficient to evaluate only the first terms (usually the leading and next-to-leading order) of the approximation.

1.1.1 Obtaining a finite theory

A problem arising when calculating the subleading contributions in scattering processes, is diverging integrals. They appear when the corrections contain closed loops, since the loop momenta are unknown, and integration therefore must be carried out over all possible momenta. *Regularization* is the parametrization of the mathematical infinities appearing in the field theory, and there exist several ways to do this.

One method is the *cut-off* regularization, where the integration is performed only up to a finite *cut-off* scale Λ, evoking a finite answer

$$\int_0^\infty \mathrm{d}^4k \to \int_0^\Lambda \mathrm{d}^4k, \tag{1.4}$$

where the physical limit is found when $\Lambda \to \infty$. The cut-off is a large scale, typically the Planck scale $\mathcal{O}(10^{18})$ GeV, indicating the invalidity of the Standard Model at these energies and above. This regularization procedure is applied when we calculate the Higgs mass corrections in appendix B.

Another approach is dimensional regularization (DR), where one substitutes the four spacetime dimensions by $d = 4 - \epsilon$, where ϵ is a small parameter,

$$\int_0^\infty \mathrm{d}^4k \to \int_0^\infty \mathrm{d}^dk. \tag{1.5}$$

The physical limit is found when $\epsilon \to 0$.

Despite the parametrization of the infinities, they still appear in field theory calculations. *Renormalization* is the removal of these infinities, and introduces a fixed scale μ at which the parameters (couplings) of the Lagrangian are defined. This means that for example the electron charge has different values depending on what scale your experiment takes place. The renormalized parameters of the Lagrangian correspond to the physical observables we can measure, in contrast to the unphysical *bare* (infinite) parameters before renormalization took place.

The evolution of the couplings with energy is described by the renormalization group equations, and is referred to as the *running of the coupling constants*. We return to this in chapter 2.

In order for a theory to make meaningful physical predictions, it must be renormalizable. Attempts at incorporating gravity into the Standard Model, by the interaction with gravitons, results in a non-renormalizable theory, which explains why it is not one of the fundamental forces in the Standard Model.

1.2 External symmetries

From Einstein's special relativity, we know that the laws of physics should be invariant under rotations and boosts between different reference frames. These transformations are captured in the Lorentz group L, and is the group of all linear transformations

$$x^{\mu'} = \Lambda^{\mu}{}_{\nu} x^{\nu}, \tag{1.6}$$

such that $x_\mu x^\mu$ is invariant.

Any *proper* Lorentz transformation $\Lambda \in L_+^\uparrow$ can be written as[1]

$$\Lambda^{\mu}{}_{\nu} = \left[\exp\left(-\frac{i}{2}\omega^{\rho\sigma} M_{\rho\sigma}\right)\right]^{\mu}{}_{\nu}, \tag{1.7}$$

where $\omega_{\rho\sigma}$ are the (antisymmetric) parameters of the transformation, and $M_{\rho\sigma}$ are the generators of the proper Lorentz group. The Lie algebra for L is formed by the elements of $M_{\rho\sigma}$, and are given by

$$M = \begin{pmatrix} 0 & -K_1 & -K_2 & -K_3 \\ K_1 & 0 & J_3 & -J_2 \\ K_2 & -J_3 & 0 & J_1 \\ K_3 & J_2 & -J_1 & 0 \end{pmatrix}, \tag{1.8}$$

with K_i and J_i being the generators of boosts and rotations, respectively.

The external symmetries of the Standard Model are space and time translations, and proper Lorentz transformations. These transformations are summarized in

[1] Improper transformations would include space and time reflections.

the (proper) Poincaré group, which is an extension of the Lorentz group with a constant spacetime translation a^μ, giving the transformation

$$x^\mu \to x'^\mu = \Lambda^\mu{}_\nu x^\nu + a^\mu. \tag{1.9}$$

The behaviour of the Poincaré group (locally), as for any Lie group, is determined by its algebra. The algebra is made up of the commutators of the generators of the group, i.e. the translation generator P_μ and the generators of boosts and rotations $M_{\rho\sigma}$. The behaviour of the Poincaré group is therefore determined by

$$[P_\mu, P_\nu] = 0, \tag{1.10}$$
$$[M_{\mu\nu}, P_\rho] = -i(g_{\mu\rho}P_\nu - g_{\nu\rho}P_\mu), \tag{1.11}$$
$$[M_{\mu\nu}, M_{\rho\sigma}] = -i(g_{\mu\rho}M_{\nu\sigma} - g_{\mu\sigma}M_{\nu\rho} - g_{\nu\rho}M_{\mu\sigma} + g_{\nu\sigma}M_{\mu\rho}). \tag{1.12}$$

1.3 Internal gauge symmetries

The Standard Model is based on the principle of *gauge invariance* under the Lie groups $SU(3)_C \times SU(2)_L \times U(1)_Y$. A gauge refers to redundant degrees of freedom in the Lagrangian which are not physical observable, and is a continous local symmetry.

1.3.1 Abelian gauge theories

We illustrate the gauge principle by looking at an abelian group,[2] which will reproduce the theory of quantum electrodynamics (QED). The conserved quantity for this group is electric charge q, and the underlying symmetry group is $U(1)_{\text{em}}$.

Fermions are described by Dirac spinors $\psi(x)$, for simplicity referred to as ψ in the following. Ignoring the fact that they — for reasons to be discussed later — initially need to be treated as massless, the free Lagrangian of a free fermion field is

$$\mathcal{L} = \bar{\psi}(i\gamma^\mu\partial_\mu - m)\psi, \tag{1.13}$$

where $\bar{\psi} = \psi^\dagger\gamma^0$. We observe that this Lagragian is invariant under the global phase transformation $\psi' = U(\alpha)\psi = e^{i\alpha}\psi$, where α is a real number. This transformation belongs to the global $U(1)$ transformations, where the elements $U(\alpha)$ are 1×1 'matrices', satisfying the unitary condition $UU^\dagger = 1$.

Imposing gauge invariance means we require the transformation to hold also on a *local* basis, i.e. we take $\alpha = \alpha(x)$, an arbitrary real differentiable function of spacetime. The transformed Lagrangian then takes the form

$$\begin{aligned} \mathcal{L}' &= \bar{\psi}e^{-iq\alpha(x)}(i\gamma^\mu\partial_\mu - m)e^{iq\alpha(x)}\psi \\ &= \mathcal{L} - q\bar{\psi}\left(\partial_\mu\alpha(x)\right)\psi, \end{aligned} \tag{1.14}$$

[2] Abelian means the elements of the group commute.

where q is a constant. This is no longer invariant due to the additional derivative term. To recover the original $\mathcal{L}$, we introduce a *covariant derivative* D_μ to replace ∂_μ, containing a four-component spin-1 (gauge) vector field $A_\mu(x)$ — describing the photon. The covariant derivative we define as

$$D_\mu = \partial_\mu + iqA_\mu, \tag{1.15}$$

and require it to be gauge invariant, meaning

$$\bar{\psi}' D'_\mu \psi' = \bar{\psi} D_\mu \psi, \tag{1.16}$$

which again implies that the vector field must transform according to

$$A'_\mu = A_\mu - \partial_\mu \alpha(x). \tag{1.17}$$

We also notice we can construct a gauge invariant term $F_{\mu\nu}F^{\mu\nu}$, where $F_{\mu\nu} \equiv \partial_\nu A_\mu - \partial_\mu A_\nu$. This is known as the vector field strength, and describes free photons. From eq. (1.17), we see that a possible photon mass term $\propto m^2 A_\mu A^\mu$ would break gauge invariance, and is hence forbidden. This also applies to the gauge bosons in non-abelian theories, to be discussed in section 1.3.2.

The full QED Lagrangian is then

$$\mathcal{L}_{\text{QED}} = i\bar{\psi}\gamma^\mu \partial_\mu \psi - m\bar{\psi}\psi - \frac{1}{4}F^{\mu\nu}F_{\mu\nu} - q\bar{\psi}\gamma^\mu \psi A_\mu, \tag{1.18}$$

and describes a massive fermion and its interaction with a massless photon, where the coupling strength q between ψ and A_μ is the electric charge.

1.3.2 Non-abelian gauge theories

We can generalize the abelian case to non-abelian theories, where commutation of the group elements is not trivial. The procedure is similar to that of QED, but gives some additional terms due to the non-commuting properties. This generalization enables the description of the weak and strong interactions, through the $SU(2)_L$ and $SU(3)_C$ groups, respectively.

In the fundamental representation, an $SU(n)$ group consist of all complex unitary $n \times n$ matrices A, with $\det A = 1$. A general $SU(n)$ transformation can be written

$$\psi'(x) = e^{ig\alpha^a(x)T^a}\psi(x), \tag{1.19}$$

where g is the *charge* of the field $\psi(x)$ under the gauge group, related to the interaction strength, $\alpha^a(x)$ are the transformation parameters, and T^a are the non-abelian generators of the group. Summation in a is implicit. The covariant derivative now takes the form

$$D_\mu = \partial_\mu + igA^a_\mu T^a, \tag{1.20}$$

where the number of gauge vector fields A^a_μ equals the (n^2-1) generators of the group. Due to the non-abelian properties of the generators, the field strength tensor needs an additional term to preserve gauge invariance, and now takes the form

$$F^a_{\mu\nu} = \partial_\mu A^a_\nu - \partial_\nu A^a_\mu + g f^{abc} A^b_\mu A^c_\nu, \tag{1.21}$$

where f^{abc} are the (antisymmetric) structure constants given by the algebra of the group

$$[T^a, T^b] = i f^{abc} T^c. \tag{1.22}$$

As the Standard Model gauge group is $G = SU(3)_C \times SU(2)_L \times U(1)_Y$, the complete covariant derivative is

$$D_\mu = \partial_\mu + i g_s \frac{\lambda^a}{2} C^a_\mu + i g \frac{\sigma^i}{2} W^i_\mu + i g' \frac{Y}{2} B_\mu. \tag{1.23}$$

We identify C^a_μ, W^i_μ and B_μ as gauge fields, and g_s, g and g' as coupling constants of the $SU(3)_C, SU(2)_L$ and $U(1)_Y$ gauge groups, respectively, where $\frac{1}{2}\lambda^a$ and $\frac{1}{2}\sigma^i$ are the group generators of the two former (composed of the Gell–Mann and Pauli matrices).[3] In section 1.6 we will see how spontaneous symmetry breaking of $SU(2)_L \times U(1)_Y \to U(1)_{\text{em}}$ mixes the gauge bosons W^i_μ and B_μ, which in turn represent the physical gauge bosons $W^\pm, Z^0$ and γ, mediating the weak and electromagnetic force. The strong force is mediated by the gluons, described by the gauge fields C^a.

The subscripts of the gauge groups refer to the conserved color charge of $SU(3)_C$, and the weak hypercharge Y for $U(1)_Y$. The weak hypercharge relates to units of the electron charge Q and the projection of weak isospin I_3 by

$$Y = 2(Q - I_3). \tag{1.24}$$

The conserved quantity for $SU(2)_L$ is isospin I, but here the subscript is a reminder that only left chiral particles carry charge under this group. We will return to this in section 1.5.

A tabulation of the fields in the Standard Model and their charges under G can be seen in table 1.1.

1.4 Gauge multiplets

We have seen that the symmetry group of the weak interaction is the $SU(2)_L$ group, where the generators are proportional to the 2×2 Pauli–matrices. Hence, an $SU(2)_L$ transformation

$$\psi \to \psi' = e^{i g \alpha^i(x) \frac{1}{2}\sigma^i} \psi, \tag{1.25}$$

[3]The generators are defined with a factor of 1/2 to avoid accumulation of numerical factors.

Table 1.1: Electromagnetic charge Q, projection of weak isospin I_3 and weak hypercharge Y for the SM fermions. The right handed neutrinos are not charged under any of the SM gauge groups, and – if they exist – are difficult to probe.

	Left chiral			Right chiral		
	Q	I_3	Y	Q	I_3	Y
ν_e, ν_μ, ν_τ	0	$+\frac{1}{2}$	-1	0	0	0
e, μ, τ	-1	$-\frac{1}{2}$	-1	-1	0	-2
u, c, t	$+\frac{2}{3}$	$+\frac{1}{2}$	$+\frac{1}{3}$	$+\frac{2}{3}$	0	$+\frac{4}{3}$
d, s, b	$-\frac{1}{3}$	$-\frac{1}{2}$	$+\frac{1}{3}$	$-\frac{1}{3}$	0	$-\frac{2}{3}$

needs a two dimensional vector ψ to act upon. As we know from experiments only left chiral components of a fermion is affected by the weak force,[4] we combine these in $SU(2)_L$ *doublets*. For the quarks and leptons, they are

$$Q_L^i = \begin{pmatrix} u_L^i \\ d_L^i \end{pmatrix}, \qquad L_L^i = \begin{pmatrix} \nu_L^i \\ e_L^i \end{pmatrix}, \tag{1.26}$$

where $i = 1, 2, 3$ is the generation index. The right chiral fermions are put in $SU(2)_L$ singlets, as they are not charged under this group, and are

$$e_R^i, \quad u_R^i, \quad d_R^i, \tag{1.27}$$

and are acted upon by the $U(1)_Y$ gauge group only.

Only color charged fermions — the quarks — are subject to the strong interaction, and an $SU(3)_C$ transformation,

$$\psi' = e^{ig_s \alpha^a(x) \frac{1}{2} \lambda^a} \psi, \tag{1.28}$$

for $a = 1, ...8$, acts on color neutral so-called *triplets* of quarks

$$q = \begin{pmatrix} q_r \\ q_g \\ q_b \end{pmatrix}, \tag{1.29}$$

where the indices refer to the red, green and blue color charge. The mathematical description of the strong interaction in terms of a gauge field theory is called quantum chromodynamics (QCD).

[4] We return to chirality in section 1.5.

1.5 Parity violation of the weak force

The weak interaction was confirmed to violate parity in 1957 [7],[5] and is today manifest through the Standard Model being a *chiral theory*, where the $SU(2)_L$ gauge group describes the interaction with *left chiral* components of a fermion. We will in the following clarify the concept of chirality.

A four-component Dirac spinor can, in the fundamental representation of the Lorentz group, be represented by two two-component Weyl spinors ψ_L and ψ_R,

$$\psi = \begin{pmatrix} \psi_L \\ \psi_R \end{pmatrix}, \tag{1.30}$$

where the subscripts refer to the chirality of the Weyl spinor. Using the projection operators

$$P_L = \frac{1-\gamma^5}{2}, \quad P_R = \frac{1+\gamma^5}{2}, \tag{1.31}$$

we can project out the different components of the Dirac fermion

$$\psi_L = P_L\psi, \qquad \psi_R = P_R\psi, \tag{1.32}$$

and by using that $P_L + P_R = 1$, the representation of a Dirac fermion can hence be written as

$$\psi = (P_L + P_R)\psi = \psi_L + \psi_R. \tag{1.33}$$

We can express the free fermion Dirac Lagrangian from eq. (1.13) in terms of the chiral components by

$$\begin{aligned} \bar{\psi}(i\gamma^\mu\partial_\mu - m)\psi = i\bar{\psi}_L\gamma^\mu\partial_\mu\psi_L + i\bar{\psi}_R\gamma^\mu\partial_\mu\psi_R \\ - m(\bar{\psi}_R\psi_L - \bar{\psi}_L\psi_R). \end{aligned} \tag{1.34}$$

The kinetic term nicely treats the chiral components separately, while the mass term mix the two. Since only the left chiral component is charged under $SU(2)_L$, mass terms are not gauge invariant. This is why fermions initially must be treated as massless, and we will see how they aquire their mass in section 1.6.

1.6 The Higgs mechanism

As seen in sections 1.4 and 1.5, Lagrangian mass terms are forbidden in the Standard Model for both fermions and gauge bosons, as they are not gauge invariant. From experimental measurements we know they are massive, with the exception of the photon, and we need a mechanism by which they can aquire their masses — respecting our renormalizable theory.

[5]The chinese phycisists C.N. Yang and T.D. Lee were rewarded the Nobel Prize after suggesting this in 1950 [8].

The Higgs mechanism of spontaneous symmetry breaking was introduced almost simultaneously by three independent groups in 1964 [9–12], and showed how gauge invariant mass terms could be present in the Lagrangian if the gauge fields interact with a neutral scalar field $h(x)$, later known as the Higgs field. As we are about to see, the particles acquire their masses through the non-zero vacuum expectation value (vev) of the Higgs field, its value in the lowest energy state. The vacuum does not obey the symmetry of the underlying Lagrangian, and this is what provides us the fermion and boson masses.

We begin by introducing an additional weak isospin doublet of two complex scalar fields ϕ_a and ϕ_b, with hypercharge $Y = 1$, known as the Higgs doublet,

$$\Phi = \begin{pmatrix} \phi_a \\ \phi_b \end{pmatrix}. \tag{1.35}$$

As $Y = 1$, this implies ϕ_a has positive charge, while ϕ_b is neutral. The gauge invariant renormalizable Lagrangian of the Higgs doublet is

$$\begin{aligned} \mathcal{L}_{\mathcal{H}} &= (D_\mu \Phi)^\dagger (D^\mu \Phi) - V(\Phi) \\ &= (D_\mu \Phi)^\dagger (D^\mu \Phi) - \mu^2 \Phi^\dagger \Phi - \lambda (\Phi^\dagger \Phi)^2, \end{aligned} \tag{1.36}$$

where $V(\Phi)$ is the Higgs potential.

We want to investigate the stable vacuum state of the system described by Φ. This forces $\lambda > 0$, as the potential ought to be bound from below, but no such constraint is required for μ^2. For $\mu^2 > 0$, the potential has one minimum at $\Phi = 0$, but for $\mu^2 < 0$, the vev of the field is non-zero. This property of the vacuum state is the essence of spontaneous symmetry breaking. The field value minimizing the potential in eq. (1.36), is

$$\Phi^\dagger \Phi = -\frac{\mu^2}{2\lambda}. \tag{1.37}$$

This vacuum is degenerate, since a global phase transformation (a rotation around the origin) of the field $\Phi \to e^{i\alpha}\Phi$, leaves the potential unchanged. See figure 1.1 for an illustration of the Higgs potential with $\phi_a = 0$.

As the energy decreases and the Higgs field falls to the bottom of this degenerate circle, it is forced into a non-zero vacuum state. Since the potential only depends on $\Phi^\dagger\Phi$ and not on Φ, we can use the degeneracy of the vacuum to rotate the state, such that

$$\Phi_0 = \frac{1}{\sqrt{2}} \begin{pmatrix} 0 \\ v \end{pmatrix}, \tag{1.38}$$

where $v \equiv \sqrt{\frac{-\mu^2}{\lambda}}$ is the vacuum expectation value. We can parametrize the Higgs doublet as a perturbation around this vacuum by

$$\Phi = \frac{1}{\sqrt{2}} \begin{pmatrix} \eta_1(x) + i\eta_2(x) \\ v + h(x) + i\eta_3(x) \end{pmatrix}, \tag{1.39}$$

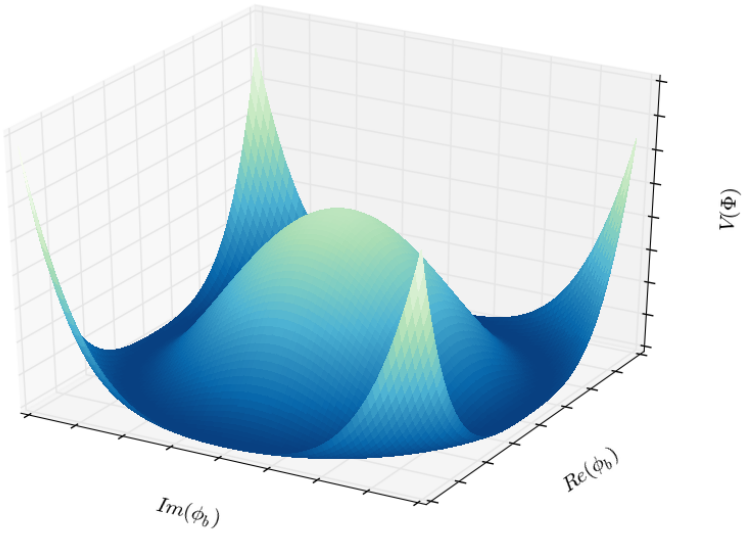

Figure 1.1: The Higgs potential for $\phi_a = 0$ with $\lambda > 0$ and $\mu^2 < 0$.

where the $\eta_i(x)$ and $h(x)$ are real scalar fields. The three fields $\eta_i(x)$ turn out to be unphysical fields, so-called *Goldstone bosons*, and are exactly what we need for the gauge bosons to be massive.

Using the gauge freedom of the $SU(2)_L \times U(1)_Y$ group, we can transform the upper component of Φ to be zero, and the lower component to be real. This choice of gauge is called the *unitary gauge*, and the Higgs doublet can be written as

$$\Phi = \frac{1}{\sqrt{2}} \begin{pmatrix} 0 \\ v + h(x) \end{pmatrix}, \tag{1.40}$$

where $h(x)$ now represents the physical Higgs field.

After the gauge transformations, the Goldstone bosons $\eta_i(x)$ are no longer present. The interpretation is that they are absorbed into $W^{\pm}$ and Z^0, providing them with an extra longitudinal degree of freedom, needed for massive vector bosons.

What remains is to identify the gauge boson masses. They arise from the kinetic term of the Lagrangian in eq. (1.36) using eq. (1.40), and are

$$\begin{aligned} \mathcal{L}_{\mathcal{H}} = &\frac{g^2 v^2}{8} \left(W_\mu^1 W^{\mu 1} + W_\mu^2 W^{\mu 2} \right) \\ &+ \frac{v^2}{8} \left(g W_\mu^3 - g' B_\mu \right) \left(g W^{\mu 3} - g' B^\mu \right) \end{aligned} \tag{1.41}$$

This can be written in matrix form,

$$\begin{aligned}\mathcal{L}_{\mathcal{H}} = &\frac{1}{2}(W_\mu^1 \;\; W_\mu^2)\begin{pmatrix} m_W^2 & 0 \\ 0 & m_W^2 \end{pmatrix}\begin{pmatrix} W^{\mu 1} \\ W^{\mu 2}\end{pmatrix} \\ &+ \frac{1}{2}(A_\mu \;\; Z_\mu)\begin{pmatrix} 0 & 0 \\ 0 & \left(\frac{v}{2}\right)^2(g^2+g'^2)\end{pmatrix}\begin{pmatrix} A^\mu \\ Z^\mu\end{pmatrix},\end{aligned} \tag{1.42}$$

where we have diagonalized the second mass matrix. The physical gauge fields are the normalized eigenvectors of the diagonal mass matrices from eq. (1.42),

$$W_\mu^\pm = \frac{1}{\sqrt{2}}(W_\mu^1 \mp iW_\mu^2), \quad Z_\mu^0 = \frac{gW_\mu^3 - g'B_\mu}{\sqrt{g^2+g'^2}}, \quad A_\mu = \frac{g'W_\mu^3 + gB_\mu}{\sqrt{g^2+g'^2}}, \tag{1.43}$$

where A_μ describes the photon. Their masses are

$$m_W = \frac{1}{2}gv, \quad m_Z = \frac{1}{2}v\sqrt{g^2+g'^2}, \quad m_A = 0, \tag{1.44}$$

and from the Higgs potential we find the Higgs mass to be

$$m_h = \sqrt{2\lambda}v. \tag{1.45}$$

Since the photon does not aquire mass through the Higgs mechanism, we have broken the $SU(2)_L \times U(1)_Y$ symmetry down to a $U(1)_{\text{em}}$ symmetry, and electric charge is conserved.

The fermion masses are induced by the same mechanism as described above, as the Higgs field can couple a left handed $SU(2)_L$ doublet L_L^i to a right-handed $SU(2)_L$ singlet e_R^i in a gauge invariant way, through the terms $\bar{L}_L^i \Phi e_R^i + \text{h.c.}$ An $SU(2)_L$ gauge transformation U on these terms is

$$\bar{L}_L^{i'}\Phi' e_R^{i'} = \bar{L}_L^i U^\dagger U \Phi e_R^i = \bar{L}_L^i \Phi e_R^i. \tag{1.46}$$

Taking the electron mass as an example,[6] the vacuum state provides us with the gauge invariant mass term in the following way

$$\begin{aligned}\mathcal{L}_e &= -y_e \bar{L}_L \Phi e_R + \text{h.c.} \\ &= -\frac{y_e}{\sqrt{2}}\begin{pmatrix}\bar{\nu}_L & \bar{e}_L\end{pmatrix}\begin{pmatrix}0 \\ v\end{pmatrix} e_R + \text{h.c.} \\ &= -\frac{y_e v}{\sqrt{2}}\bar{e}_L e_R + \text{h.c.}\end{aligned} \tag{1.47}$$

From this we identify the electron mass as $m_e = \frac{y_e v}{\sqrt{2}}$, where y_e is the *Yukawa coupling* of the electron, giving the coupling strength with the Higgs field. The

[6] And omitting the generation indices.

size of the Yukawa couplings y_f is not predicted by the Higgs mechanism, but can be chosen to be in compliance with the measured fermion masses, i.e.,

$$y_f = \frac{\sqrt{2}m_f}{v}. \tag{1.48}$$

With the Higgs vacuum expectation value of $v \sim 246$ GeV [13], this implies Yukawa couplings of the top and bottom quarks of $y_t \approx 1$ and $y_b \approx 0.02$, respectively. In comparison, the Yukawa coupling of the electron is $y_e \approx 0.3 \cdot 10^{-6}$.

Since the non-zero vev occurs for the lower component in the Higgs doublet, it can only give masses to charged leptons and down-type quarks. Ignoring the question of neutrino masses, we also need to generate the masses of the up-type quarks. This is done using the charge conjugate field $\tilde{\Phi} = i\sigma^2\Phi^*$, where the terms $\bar{Q}^i_L(i\sigma^2\Phi^*)u^i_R + \text{h.c.}$ are gauge invariant.[7]

1.7 Shortcomings of the Standard Model

Despite its success, the Standard Model cannot be the final theory of particle physics. One of the reasons is the lack of the fourth fundamental force, gravity. As the Standard Model is considered to be a low-energy part of a more fundamental theory, we also believe that the three interactions of the Standard Model unite at some high energy, and act as one single interaction under a larger gauge group. This gives rise to a so-called grand unified theory (GUT). If such a unification is to be realized, the three gauge couplings must be equal at the GUT scale, but they fail to unify if the Standard Model is taken to high energies.

Further, the postulation of dark matter attempts to explain the discrepancy between the predicted and observed angular motion of galaxies [14]. The dark matter is assumed to be made up of at most weakly interacting particles, and the Standad Model has no such viable candidate. The neutrino masses are too small to make up all the missing mass, as the sum of the three generations is constrained by cosmological measurements to be approximately $\sum_i m_{\nu_i} \leq 1$ eV [15].

Finally, the quantum corrections to the Higgs mass give rise to the hierarchy problem of the Standard Model, and introduces a large degree of *fine-tuning* in order for experiment and theory to coincide. As this topic is central to the thesis, we have devoted chapter 3 to it. Possible extensions of the Standard Model are numerous, and one of the most popular are theories of supersymmetry, which will be the subject of the next chapter.

[7] With σ^2 being a Pauli matrix.

Chapter 2

Supersymmetry

Various theories extending the Standard Model exist, and theories with supersymmetry (SUSY) are perhaps the most popular, as they can solve many of the shortcomings of the Standard Model mentioned in section 1.7. They propose a solution to the hierarchy problem, have cold dark matter candidates, and can make the gauge couplings unite at high energies. These are all compelling reasons for the theory to be realised in nature.

In this chapter, we look at how supersymmetry arose as a concept and study the framework of the model. We will first take a general approach, before we introduce the minimal supersymmetric Standard Model (MSSM) — holding only the minimal number of fields needed to reconstruct the particles and interactions of the Standard Model.

2.1 Extending the Poincaré algebra

We have seen in sections 1.2 and 1.3 how the Standard Model has both external and internal symmetries, desribed by the Poincaré group and gauge groups $SU(3)_C \times SU(2)_L \times U(1)_Y$. In additin to these, supersymmetry introduces yet another symmetry, a symmetry between fermions and bosons. A supersymmetric operator Q acts on fermionic and bosonic states as

$$Q\,|\text{fermion}\rangle = |\text{boson}\rangle \quad \text{and} \quad Q\,|\text{boson}\rangle = |\text{fermion}\rangle\,. \tag{2.1}$$

The transformation alters the particle spin by 1/2, while all other quantum numbers remain unchanged. As none of the particles in the Standard Model can be superpartners of each other, a new set of particles is needed, and consequently a whole new range of interactions appear.

Theories with supersymmetry arose during the 1970s, from a desire to extend the spacetime symmetries of the Poincaré group to also include the internal gauge symmetries in a non-trivial way. By non-trivial we mean that there should exist non-zero commutation relations between the generators of the internal gauge

groups and the external ones in the Lie algebra. Unfortunately, Coleman and Mandula proved that such a non-trivial extension was impossible [16], known as the Coleman and Mandula no-go theorem.

To succeed in a non-trivial extension, Haag, Łopuszański and Sohnius introduced the concept of a *graded Lie algebra*, also called a *superalgebra* [17]. The superalgebra L is a direct sum of two Lie algebras, $L = L_0 \oplus L_1$, with a binary operation $\cdot$ called grading. For $x_i \in L_i$, the grading is given by

$$x_i \cdot x_j = x_k \in L_{i+j \bmod 2}, \tag{2.2}$$

meaning the superalgebra is a so-called $\mathbb{Z}_2$ graded algebra.

By combining the Poincaré algebra with an algebra spanned by four supersymmetry operators in a Majorana spinor Q_a, Haag et al. constructed such a superalgebra. By relating the Majorana spinors to a two-component Weyl spinor Q_A and its hermitian conjugate $\bar{Q}_{\dot{A}}$ as

$$Q_a = \begin{pmatrix} Q_A \\ \bar{Q}^{\dot{A}} \end{pmatrix}, \tag{2.3}$$

the superalgebra is given by the following commutation and anti-commutation relations

$$\{Q_A, Q_B\} = \{\bar{Q}_{\dot{A}}, \bar{Q}_{\dot{B}}\} = 0, \tag{2.4}$$
$$\{Q_A, \bar{Q}_{\dot{B}}\} = 2\sigma^{\mu}_{A\dot{B}} P_\mu, \tag{2.5}$$
$$[Q_A, P_\mu] = [\bar{Q}_{\dot{A}}, P_\mu] = 0, \tag{2.6}$$
$$[Q_A, M^{\mu\nu}] = \sigma_A^{\mu\nu B} Q_B, \tag{2.7}$$

where now $\sigma^{\mu\nu} = \frac{i}{4}(\sigma^\mu \bar{\sigma}^\nu - \sigma^\nu \bar{\sigma}^\mu)$.

Unfortunately, with only one Majorana spinor, the internal gauge symmetries must still commute trivially with all the operators in the superalgebra, and the original idea of merging them with the external symmetries fails. They can appear if one further extends the algebra with more sets of Majorana spinor charges Q_a^n where $n = 1, ...N$. These theories are called $N > 1$ supersymmetries, but introduces an extensive number of extra particles that are difficult to reconcile with experiment.

2.2 Superfields

The fields we are familiar with from the Standard Model live in Minkowski space and are objects that transform under the Poincaré and gauge transformations. In supersymmetry, it is conventient to replace these fields with superfields Φ, that transform under supersymmetry transformations, and are functions of *superspace*.

Table 2.1: The component fields of a general superfield $\Phi(x, \theta, \bar{\theta})$, and their degrees of freedom.

Component field	Type	Degrees of freedom
$f(x), m(x), n(x)$	Complex (pseudo) scalars	2
$\psi_A(x), \phi_A(x)$	Left-handed Weyl spinors	4
$\bar{\chi}^{\dot{A}}(x), \bar{\lambda}^{\dot{A}}(x)$	Right-handed Weyl spinors	4
$V_\mu(x)$	Lorentz four-vector	8
$d(x)$	Complex scalar	2

Table 2.2: The component fields of a left-handed scalar superfield $\Phi(y, \theta)$, and their degrees of freedom.

Component field	Type	Degrees of freedom
$A(y), F(y)$	Complex scalars	2
$\psi_A(y)$	Left-handed Weyl spinor	4

Superspace is a manifold spanned by spacetime x^μ and four additional anti-commuting Grassmann numbers θ and $\bar{\theta}$,

$$z^\pi = (x^\mu, \theta^A, \bar{\theta}^{\dot{A}}), \tag{2.8}$$

with $A = 1, 2$ and $\dot{A} = \dot{1}, \dot{2}$.

A general superfield can be expanded in a power series of θ and $\bar{\theta}$,

$$\begin{aligned}\Phi(x, \theta, \bar{\theta}) = f(x) + \theta^A \phi_A(x) + \bar{\theta}_{\dot{A}} \bar{\chi}^{\dot{A}}(x) + \theta\theta m(x) + \bar{\theta}\bar{\theta} n(x) \\ + \theta\sigma^\mu \bar{\theta} V_\mu(x) + \theta\theta\bar{\theta}_{\dot{A}} \bar{\lambda}^{\dot{A}}(x) + \bar{\theta}\bar{\theta}\theta^A \psi_A(x) + \theta\theta\bar{\theta}\bar{\theta} d(x),\end{aligned} \tag{2.9}$$

where the series terminate due to the anti-commuting properties of the Grassmann numbers. Here, $\sigma^\mu = (\mathbf{1}_{2\times 2}, \sigma^i)$, with σ^i being the Pauli matrices. The properties of the component fields in eq. (2.9) are found in table 2.1, and are deduced from the requirement of Φ being a Lorentz (pseudo) scalar, as this makes Φ invariant under Lorentz transformations.

In order to represent particles with the superfields, we need both scalar and vector superfields, to be defined shortly. The superfield in eq. (2.9) contains too many degrees of freedom to represent only the known fermions and bosons of the Standard Model, and is how the supersymmetric partners — the *sparticles* — enter the theory.

Due to the commutation of the supersymmetry operators Q and $Q^\dagger$ with the operators of the gauge transformations, all component fields of the same superfield

Table 2.3: The component fields of a general vector superfield $V(x, \theta, \bar{\theta})$, and their degrees of freedom.

Component field	Type	Degrees of freedom
$f(x), d(x)$	Real scalar fields	1
$\phi_A(x), \lambda_A(x)$	Left-handed Weyl spinors	4
$m(x)$	Complex scalar field	2
$V_\mu(x)$	Real Lorentz four-vector	4

must be equally charged under each of the three Standard Model gauge groups. As the supersymmetry operators also commute with the squared momentum operator $P^2 = P_\mu P^\mu$, particles originating from the same superfield are also initially equal in mass. As none of the supersymmetric particles have been discovered, they must be heavier than their Standard Model partners, and supersymmetry is therefore a broken theory. The supersymmetry breaking will be discussed in section 2.4.

2.2.1 Scalar superfields

A superfield Φ is defined to be a scalar superfield if

$$\bar{D}_{\dot{A}}\Phi(x, \theta, \bar{\theta}) = 0 \quad \text{(left-handed)}, \tag{2.10}$$

$$D_A\Phi^\dagger(x, \theta, \bar{\theta}) = 0 \quad \text{(right-handed)}, \tag{2.11}$$

where we have introduced covariant supersymmetry invariant derivatives,

$$D_A = \partial_A + i(\sigma^\mu\bar{\theta})_A\partial_\mu, \tag{2.12}$$

$$\bar{D}_{\dot{A}} = -\partial_{\dot{A}} - i(\theta\sigma^\mu)_{\dot{A}}\partial_\mu, \tag{2.13}$$

where $\partial_A = \partial/\partial\theta^A$.

We observe that a coordinate change $y^\mu = x^\mu + i\theta\sigma^\mu\bar{\theta}$ simplifies $\bar{D}_{\dot{A}}$, namely $\bar{D}_{\dot{A}} = -\partial_{\dot{A}}$. This impacts the left-handed scalar fields, as no dependence upon $\bar{\theta}$ can occur in the new set of coordinates. Hence, we can write a general left-handed scalar superfield as

$$\Phi(y, \theta) = A(y) + \sqrt{2}\theta\psi(y) + \theta\theta F(y), \tag{2.14}$$

where the properties of the component fields are listed in table 2.2. By undoing the coordinate change, we can see that the field $F(x)$ is auxillary as it has no derivatives, and can be eliminated after applying the equations of motion in eq. (1.2). They also eliminate two of the four fermion degrees of freedom from the Weyl spinor. Hence, from a left-handed scalar superfield we get one complex scalar and one left-handed Weyl fermion, giving a total of two fermionic and two

bosonic degrees of freedom. The same procedure can be followed for right-handed superfields, with the coordinate change $y^\mu = x^\mu - i\theta\sigma^\mu\bar{\theta}$, giving one right-handed Weyl fermion and one complex scalar.

As seen in eq. (1.30), a Weyl spinor on its own cannot describe a Dirac fermion. To do this, we combine the left-handed Weyl spinor ψ_A and the right-handed Weyl spinor $\bar{\chi}^{\dot{A}}$ to the Dirac spinor ψ_a as

$$\psi_a = \begin{pmatrix} \psi_A \\ \bar{\chi}^{\dot{A}} \end{pmatrix}. \tag{2.15}$$

Therefore, when finding a representation of Dirac fermions in section 2.5.1, we construct it from the Weyl spinor from one left-handed scalar superfield Φ_i, and the Weyl spinor from a *different* right-handed scalar superfield $\Phi_j^\dagger$. Constructing the Dirac fermion from the Weyl spinor from Φ_i and $\Phi_i^\dagger$, would give a Majorana fermion.

2.2.2 Vector superfields

A superfield Φ is defined to be a vector superfield if

$$\Phi(x, \theta, \bar{\theta}) = \Phi^\dagger(x, \theta, \bar{\theta}), \tag{2.16}$$

and this affects what type of component fields we have in the vector superfield. Comparing the two sides of eq. (2.16), we find that they must be as listed in table 2.3. Some of the remaining auxillary degrees of freedom in the vector superfield is removed in the so-called *Wess–Zumino gauge*, which is a certain choice of *superfield gauge transformation* of the vector superfield V, generally defined as

$$V'(x, \theta, \bar{\theta}) = V(x, \theta, \bar{\theta}) + i(\Lambda(x, \theta, \bar{\theta}) - \Lambda^\dagger(x, \theta, \bar{\theta})), \tag{2.17}$$

where $\Lambda(x, \theta, \bar{\theta})$ is a scalar superfield. In this gauge, the vector superfield then takes the form

$$\begin{aligned} V_{WZ}(x, \theta, \bar{\theta}) = {} & (\theta\sigma^\mu\bar{\theta})[V_\mu(x) + i\partial_\mu(A(x) - A^*(x))] \\ & + \theta\theta\bar{\theta}\bar{\lambda}(x) + \bar{\theta}\bar{\theta}\theta\lambda(x) + \theta\theta\bar{\theta}\bar{\theta}d(x), \end{aligned} \tag{2.18}$$

where A is a complex scalar field from Λ.[1]

After the equations of motions are applied, and all redundant degrees of freedom are eliminated, a vector field gives us one left-handed Weyl spinor λ_A, the hermitian conjugate right-handed Weyl spinor $\bar{\lambda}^{\dot{A}}$, and one massless vector boson V_μ, and we are also here left with two fermionic and two bosonic degrees of freedom.

[1] The remaining ordinary gauge degree of freedom is found in the imaginary part of A.

2.3 The supersymmetric Lagrangian

Not surprisingly, we want to construct a Lagrangian that is invariant under the supersymmetry transformations generated by Q_a. As we have seen in chapter 1, the action is invariant if the Lagrangian changes by a total derivative. It can be shown that the highest order component fields (in θ and $\bar{\theta}$) of a superfield always have this property [18]. The following redefinition of the action integral isolates the highest order component fields, and therefore guarantees invariance

$$S = \int_R \mathrm{d}^4x \int \mathrm{d}^4\theta \ \mathcal{L}. \tag{2.19}$$

The integration over the four Grassmann numbers has a projecting effect, where only the highest order component fields in θ and $\bar{\theta}$ give contributions to the integral.

For the theory to be renormalizable, we can have at most three powers of scalar superfields [19], and since the action must be real, the most general expression for a supersymmetric invariant Lagrangian with scalar superfields is restricted to

$$\mathcal{L} = \Phi_i^\dagger \Phi_i + \theta\theta W[\Phi] + \bar{\theta}\bar{\theta} W[\Phi^\dagger], \tag{2.20}$$

where $\Phi_i^\dagger \Phi_i$ is the *kinetic term*[2] and $W[\Phi]$ is the superpotential

$$W[\Phi] = g_i \Phi_i + m_{ij} \Phi_i \Phi_j + \lambda_{ijk} \Phi_i \Phi_j \Phi_k, \tag{2.21}$$

where the *tadpole term* has coupling g_i, the *mass term* m_{ij} and the *Yukawa term* λ_{ijk}. The dimensions of the couplings can be derived from the fact that the action is dimensionless, and we find that $[g_i] = [M^2]$, $[m_{ij}] = [M]$, $[\lambda_{ijk}] = 1$.

2.3.1 Supersymmetric gauge theories

As supersymmetric theories are usually extensions of the Standard Model, they must reproduce its field content and interactions. Therefore, supersymmetric theories must also be gauge theories.

We start by defining a local (super) gauge transformation on a left-handed scalar superfield Φ in the following way[3]

$$\Phi_i \to \Phi_i' = e^{-iq_i \Lambda^a T^a} \Phi_i, \tag{2.22}$$

where q_i is the charge of Φ_i under the gauge group, T^a are the group generators, and $\Lambda^a = \Lambda^a(x, \theta, \bar{\theta})$ are the parameters of the transformation. As the transformed

[2] And in fact a vector field, since $(\Phi_i^\dagger \Phi_i)^\dagger = (\Phi_i^\dagger \Phi_i)$.

[3] We have already given the non-abelian (super) gauge transformation for a vector superfield in eq. (2.17).

field Φ_i' must also be a left-handed superfield, i.e. $\bar{D}_{\dot{A}}\Phi_i' = 0$, it follows that the Λ^a must be too.

Gauge invariance must also be satisfied by the superpotential $W[\Phi]$, restricting the allowed couplings in the superpotential. For the kinetic term to be invariant, we must introduce gauge compensating vector superfields V^a, transforming under supersymmetry transformations in such a way that the gauge invariance is fulfilled. The coupling of scalar and vector superfields is introduced into the kinetic terms of the Lagrangian by writing them as

$$\Phi_i^\dagger e^{q_i V^a T^a}\Phi_i. \tag{2.23}$$

The kinetic term after a gauge transformation of $\Phi_i \to \Phi_i'$ is now

$$\Phi^\dagger e^{iq_i\Lambda^{\dagger a}T^a} e^{q_i V'^a T^a} e^{-iq_i\Lambda^a T^a}\Phi_i, \tag{2.24}$$

which is gauge invariant given that the vector field transforms according to[4]

$$e^{q_i V'^a T^a} = e^{-iq_i\Lambda^{a\dagger}T^a} e^{q_i V^a T^a} e^{iq_i\Lambda^a T^a}. \tag{2.25}$$

This procedure reproduces the Standard Model couplings between fermions and bosons for the component fields.

In order to write down the complete (supersymmetric) Lagrangian, we lack the gauge field strengths. These interactions can be covered through the gauge invariant traces $\mathrm{Tr}[W^A W_A]$ and $\mathrm{Tr}[\bar{W}^{\dot{A}}\bar{W}_{\dot{A}}]$, where the left-handed superfield W_A is given by

$$W_A = -\frac{1}{4}\bar{D}\bar{D}e^{-V^a T^a} D_A e^{V^a T^a}. \tag{2.26}$$

From the above arguments, the most general form of a gauge invariant supersymmetric Lagrangian can be written

$$\mathcal{L} = \Phi_i^\dagger e^{q_i V^a T^a}\Phi_i + \bar{\theta}\bar{\theta}W[\Phi] + \theta\theta W[\Phi^\dagger] + \frac{1}{2T(R)}\bar{\theta}\bar{\theta}\mathrm{Tr}[\mathrm{W^A W_A}]. \tag{2.27}$$

Here, $T(R)$ is the so-called *Dynkin index*, a numerical factor included to ensure correct energy densities of the gauge fields. It is related to the representation R of the gauge group, and the generators are normalized by the relation

$$\mathrm{Tr}[T^a, T^b] = T(R)\delta^{ab}. \tag{2.28}$$

2.4 Supersymmetry breaking

As the supersymmetric particles remain undiscovered, supersymmetry must be a broken theory. Just as properties of the vacuum provide masses to the gauge

[4]The expression in eq. (2.17) is the special case of eq. (2.25) for non-abelian gauge fields.

bosons in the Standard Model, we seek to construct a similar mechanism by which the supersymmetric masses can be driven upwards. In other words, we assume spontaneous symmetry breaking to be the breaking mechanism also in supersymmetry.

From the complete scalar potential,[5] including also contributions from gauge interactions and vector superfields,

$$V(A_i, A_i^*) = \sum_{i=1}^{n} \left| \frac{\partial W[A_1, ..., A_n]}{\partial A_i} \right|^2 + \frac{1}{2} \sum_a g_a^2 (A^* T^a A)^2 > 0, \tag{2.29}$$

we want to break the $SU(2)_L \times U(1)_Y$ symmetry. Unfortunately, spontaneous supersymmetry breaking is hard to make work in practice, due to a property of the *supertrace*. The supertrace is effectively the difference between the (squared) scalar and fermionic masses, and can be proven to vanish (at tree level) [20]. The physical consequence of the vanishing supertrace is that only *some* of the scalar partners can be heavier than the known fermions — but not all of them.

To solve this problem, the assumption is made that spontaneous supersymmetry breaking originates at some high energy scale inaccessible to us, before it is mediated down to our scale by some unknown mechanism, leaving particles at high scale to fulfill the supertrace requirement. One of the suggested mechanisms leads to the model of minimal supergravity, to be discussed in section 2.7.1. To paramterize our ignorance of the true spontaneous symmetry breaking, we simply add certain breaking terms into the Lagrangian explicitly, under the name *soft terms*. They are terms which do not introduce new quadratic[6] divergencies in loop contributions to scalar masses. Written in terms of component fields, the possible allowed soft terms are[7]

$$\begin{aligned} \mathcal{L}_{\text{soft}} = & -\frac{1}{2} M_i \lambda_i^A \lambda_{iA} + \left(\frac{1}{6} a_{ijk} A_i A_j A_k + \frac{1}{2} b_{ij} A_i A_j + t_i A_i \right) + \text{c.c.} \\ & - m_{ij}^2 A_i^* A_j. \end{aligned} \tag{2.30}$$

As the soft terms include a gaugino mass M for each gauge group, and scalar mass terms m_{ij}^2 and b_{ij}, these may drive the gaugino and sfermion masses upwards. We will later see that the soft terms are responsible for most of the parameters in supersymmetric models.

[5] The scalar potential are those terms of the Lagrangian with no derivatives, holding only scalar fields.

[6] Or worse.

[7] We have here omitted a type of term that might be soft, $-\frac{1}{2} c_{ijk} A_i^* A_j A_k + \text{c.c.}$, depending on the gauge structure of the model.

2.5 The minimal supersymmetric Standard Model

The minimal supersymmetric Standard Model (MSSM) introduces the minimal number of superfields needed in order to recover all the known particles and interactions of the Standard Model. Based on the previous sections of this chapter, we now go on constructing the MSSM Lagrangian and find its particle content.

2.5.1 Field content

To construct a Dirac fermion, we need one left-handed and one right-handed Weyl spinor from two *different* scalar superfields, as argued in section 2.2.1. They give us the four degrees of freedom required by a Dirac fermion and its anti-particle. As each of the scalar superfields also contain a (complex) scalar component field, we gain two scalar particle anti-particle pairs in constructing the Dirac fermion. These are known as *sfermions* and are the superpartners of the Dirac fermions.

Similar to the multiplets of quantum fields in the Standard Model, we now put superfields in *supermultiplets*, to be acted upon by the relevant gauge symmetry group. For the leptons we introduce three $SU(2)_L$ superfield doublets and singlets

$$L_i = \begin{pmatrix} \nu_i \\ e_i \end{pmatrix} \quad \text{and} \quad \bar{E}_i, \tag{2.31}$$

for each generation $i = 1, 2, 3$. The bar is not to be confused with a conjugate field, it is simply a part of the singlet name. From these superfields[8] we recover the known Standard Model leptons, in addition to their spin-0 superpartners — the *sleptons*.

Similar, for the three generations of up- and down-type quarks, we introduce

$$Q_i = \begin{pmatrix} u_i \\ d_i \end{pmatrix}, \quad \bar{U}_i \quad \text{and} \quad \bar{D}_i, \tag{2.32}$$

and from this we recover all the known Standard Model quarks, and their spin-0 superpartners — the *squarks*.

For the Standard Model gauge bosons we must introduce twelve vector superfields, for the generators of the SM gauge groups. They are

$$C^a, \quad W^i, \quad B^0, \tag{2.33}$$

from the gauge groups $SU(3)_C, SU(2)_L$ and $U(1)_Y$, respectively. From this we recover the SM spin-1 gauge bosons $W^\pm, Z$ and γ from the mixing between the vector fields in W^i and B^0. In addition we gain their fermionic supersymmetric partners. The *gluinos*, $\tilde{g}^a$, come from the Weyl spinors of C^a, the *winos*, $\tilde{W}^i$, from

[8] And their conjugate fields.

the Weyl spinors of W^i and the *bino*, $\tilde{B}^0$, from the Weyl spinor of B^0. They are gauge eigenstates, and in section 2.6.3 we will see how they mix into observable mass eigenstates, knwon as the *charginos* and *neutralinos*.

In order to give masses to both up-, and down-type leptons,[9] we need to introduce two Higgs $SU(2)_L$ doublets. As seen in section 1.6, the up-type fermions of the Standard Model are given mass through a rotation of the Higgs field using one of the generators of the $SU(2)_L$ gauge group. The same trick can not be applied now, as the construction generating the mass of up-type quarks relies on the term $-i(H^\dagger\sigma^2)^T$. With H being a superfield, this would mix left- and right-handed superfields in the superpotential. Hence, we must introduce one $SU(2)_L$ doublet generating the up-type masses, and another for the down-type masses. They must have opposite hypercharge $Y = \pm 1$ due to the need of *anomaly cancellation*, which ensures gauge invariance also at loop level.[10] Hence, the two Higgs doublets are composed of four scalar superfields H_u^+, H_u^0, H_d^0 and H_d^- in the following way

$$H_u = \begin{pmatrix} H_u^+ \\ H_u^0 \end{pmatrix}, \quad H_d = \begin{pmatrix} H_d^0 \\ H_d^- \end{pmatrix}, \tag{2.34}$$

where the indices indicate what quark type they give mass to.

The doublets extend the Higgs sector of the Standard Model, as they predict a total of five Higgs bosons after giving mass to the gauge bosons, in addition to their fermionic superpartners known as *higgsinos*. We return to the Higgs bosons in section 2.6.1, and treat the higgsinos in section 2.6.3.

All Standard Model superpartners and the extended Higgs sector predicted by the MSSM are given in table 2.4.

2.5.2 The Lagrangian

With the field content of the MSSM defined, we can construct the kinetic terms of the Lagrangian, describing the interactions between matter and gauge particles. For readability, we will abbreviate $\lambda^a C^a$ to λC etc. The kinetic terms of eq. (2.27) are then

$$\begin{aligned} \mathcal{L}_{\text{kin}} = {} & L^\dagger e^{\frac{1}{2}g\sigma W - \frac{1}{2}g'B} L + Q^\dagger e^{\frac{1}{2}g_s\lambda C + \frac{1}{2}g\sigma W + \frac{1}{3}\frac{1}{2}g'B} Q \\ & + \bar{U}^\dagger e^{\frac{1}{2}g_s\lambda C - \frac{4}{3}\frac{1}{2}g'B}\bar{U} + \bar{D}^\dagger e^{\frac{1}{2}g_s\lambda C + \frac{2}{3}\frac{1}{2}g'B}\bar{D} \\ & + \bar{E}^\dagger e^{2\frac{1}{2}g'B}\bar{E} + H_u^\dagger e^{\frac{1}{2}g\sigma W + \frac{1}{2}g'B} H_u + H_d^\dagger e^{\frac{1}{2}g\sigma W - \frac{1}{2}g'B} H_d. \end{aligned} \tag{2.35}$$

The normalized gauge terms of supersymmetric field strengths are

$$\mathcal{L}_V = \frac{1}{2}\text{Tr}\left[W^A W_A\right]\bar{\theta}\bar{\theta} + \frac{1}{2}\text{Tr}\left[C^A C_A\right]\bar{\theta}\bar{\theta} + \frac{1}{4}B^A B_A \bar{\theta}\bar{\theta} + \text{h.c.}, \tag{2.36}$$

[9] Ignoring the question of neutrino masses.

[10] This happens automatically in the Standard Model due to its field content, but is no longer valid in the MSSM as the content has changed.

Table 2.4: The gauge and mass eigenstates of the MSSM sparticles, in addition to the extended Higgs sector of the SM.

Name	Spin	P_R	Gauge eigenstates	Mass eigenstates
Higgs bosons	0	$+1$	$H_u^+\ H_u^0\ H_d^-\ H_d^0$	$h^0\ H^0\ A^0\ H^\pm$
Squarks	0	-1	$\tilde{u}_L\ \tilde{u}_R\ \tilde{d}_L\ \tilde{d}_R$ $\tilde{s}_L\ \tilde{s}_R\ \tilde{c}_L\ \tilde{c}_R$ $\tilde{t}_L\ \tilde{t}_R\ \tilde{b}_L\ \tilde{b}_R$	$\tilde{u}_L\ \tilde{u}_R\ \tilde{d}_L\ \tilde{d}_R$ $\tilde{s}_L\ \tilde{s}_R\ \tilde{c}_L\ \tilde{c}_R$ $\tilde{t}_1\ \tilde{t}_2\ \tilde{b}_1\ \tilde{b}_2$
Sleptons	0	-1	$\tilde{e}_L\ \tilde{e}_R\ \tilde{\nu}_e$ $\tilde{\mu}_L\ \tilde{\mu}_R\ \tilde{\nu}_\mu$ $\tilde{\tau}_L\ \tilde{\tau}_R\ \tilde{\nu}_\tau$	$\tilde{e}_L\ \tilde{e}_R\ \tilde{\nu}_e$ $\tilde{\mu}_L\ \tilde{\mu}_R\ \tilde{\nu}_\mu$ $\tilde{\tau}_1\ \tilde{\tau}_2\ \tilde{\nu}_\tau$
Neutralinos	1/2	-1	$\tilde{B}^0\ \tilde{W}^0\ \tilde{H}_u^0\ \tilde{H}_d^0$	$\tilde{\chi}_1^0\ \tilde{\chi}_2^0\ \tilde{\chi}_3^0\ \tilde{\chi}_4^0$
Charginos	1/2	-1	$\tilde{W}^\pm\ \tilde{H}_u^+\ \tilde{H}_d^-$	$\tilde{\chi}_1^\pm\ \tilde{\chi}_2^\pm$
Gluino	1/2	-1	$\tilde{g}$	$\tilde{g}$

where the field strengths are given by

$$B_A = -\frac{1}{4}\bar{D}\bar{D}D_A B, \qquad B = \frac{1}{2}g'B^0, \tag{2.37}$$

$$W_A = -\frac{1}{4}\bar{D}\bar{D}e^{-W}D_A e^W, \quad W = \frac{1}{2}g\sigma^a W^a, \tag{2.38}$$

$$C_A = -\frac{1}{4}\bar{D}\bar{D}e^{-C}D_A e^C, \quad C = \frac{1}{2}g_s\lambda^a C^a. \tag{2.39}$$

Having defined the kinetic terms and field strengths of the Lagrangian, what remains is to identify the gauge invariant terms of the superpotential from eq. (2.21). Since none of the superfields of the MSSM in eq. (2.35) are singlets under all gauge groups, no tadpole terms are allowed in the superpotential. Furthermore, to preserve $U(1)_Y$ gauge invariance, the mass terms need $Y_i + Y_j = 0$ and the Yukawa terms need $Y_i + Y_j + Y_k = 0$, where Y_i is the hypercharge of the superfield. This reduces the number of possible superfield combinations, and the only allowed superpotential terms are

$$\begin{aligned}\mathcal{L}_W = {} & \mu H_u H_d + \mu' L_i H_u + y^e_{ij} L_i H_d \bar{E}_j + y^u_{ij} Q_i H_u \bar{U}_j + y^d_{ij} Q_i H_d \bar{D}_j \\ & + \lambda_{ijk} L_i L_j \bar{E}_k + \lambda'_{ijk} L_i Q_j \bar{D}_k + \lambda''_{ijk} \bar{U}_i \bar{D}_j \bar{D}_k.\end{aligned} \tag{2.40}$$

We have here contracted the superfield doublets, e.g. $H_u H_d$, as shorthand for $H_u^T i\sigma^2 H_d$, since this construction preserves $SU(2)_L$ gauge invariance.

The total MSSM Lagrangian can then be expressed as

$$\mathcal{L}_{\text{MSSM}} = \mathcal{L}_{\text{kin}} + \mathcal{L}_V + \mathcal{L}_{\text{soft}} + \mathcal{L}_W. \tag{2.41}$$

2.5.3 R-parity

The terms $L_i H_u$, $L_i L_j \bar{E}_k$ and $L_i Q_j \bar{D}_k$ of the superpotential in eq. (2.40), violate lepton number conservation, while $\bar{U}_i \bar{D}_j \bar{D}_j$ violates baryon number conservation, and together they allow for phenomenological inconsistencies such as rapid proton decay. As such decays have never been observed, the lifetime of a proton has a known lower limit of $\sim 10^{33}$ years [13] This puts heavy restrictions on the values of some of the couplings in the superpotential. To avoid all such couplings — and hence remove the terms mentioned at the beginning of this section — R-parity conservation was introduced by Fayet in in 1975 [21], where he defined a new multiplicative quantum number P_R as

$$P_R = (-1)^{2s+3B+L}. \tag{2.42}$$

Here, s is the particle spin, B is the baryon number and L is the lepton number. This means all Standard Model particles have $P_R = 1$, while all supersymmetry particles have $P_R = -1$. Note that the two Higgs doublets extend the Higgs sector of the Standard Model, as all five Higgs bosons have $P_R = 1$.

Conservation of R-parity has some important phenomenological consequences. The lightest supersymmetric particle (LSP) must be stable, and every other supersymmetric particle must decay into the LSP, often through so-called *decay cascades* via other sparticles. Further, supersymmetric particles from collider experiments must be pair produced, as they originate from Standard Model particles with $P_R = 1$.

2.5.4 Supersymmetry breaking terms

Gauge invariance and R-parity conservation also restricts what soft terms from eq. (2.30) are allowed in the MSSM Lagrangian. Written in component fields, they are

$$\begin{aligned}
\mathcal{L}_{\text{soft}} = &-\frac{1}{2}\left(M_1 \tilde{B}^0 \tilde{B}^0 + M_2 \tilde{W}^i \tilde{W}^i + M_3 \tilde{g}^a \tilde{g}^a\right) + \text{c.c.} \\
&- \left(a^e_{ij} \tilde{L}_i H_d \tilde{e}^*_{jR} + a^u_{ij} \tilde{Q}_i H_u \tilde{u}^*_{jR} + a^d_{ij} \tilde{Q}_i H_d \tilde{d}^*_{jR}\right) + \text{c.c.} \\
&- (m^L_{ij})^2 \tilde{L}^\dagger_i \tilde{L}_j - (m^Q_{ij})^2 \tilde{Q}^\dagger_i \tilde{Q}_j \\
&- (m^e_{ij})^2 \tilde{e}^*_{iR} \tilde{e}_{jR} - (m^u_{ij})^2 \tilde{u}^*_{iR} \tilde{u}_{jR} - (m^d_{ij})^2 \tilde{d}^*_{iR} \tilde{d}_{jR} \\
&- m^2_{H_u} H^\dagger_u H_u - m^2_{H_d} H^\dagger_d H_d - (b H_u H_d + \text{c.c.}).
\end{aligned} \tag{2.43}$$

Removing all the freedom we can from the MSSM Lagrangian in terms of the field redefinitions, we are left with 105 new parameters, in addition to those of the Standard Model. All of them origin from the soft terms above, except the higgsino mass parameter μ from the superpotential in eq. (2.40).

The soft terms of eq. (2.43) give the main contribution to the sparticle masses, and are responsible for driving them above their Standard Model partners'.

2.5.5 Gauge coupling unification

In section 1.1.1, we introduced renormalization as a way to remove infinities from quantum field calculations. The prize to pay for a finite theory, was the introduction of a scale μ, at which the parameters of the Lagrangian are defined.[11] As the scale is not a physical measurable quantity, but simply a choice of how we define our theory, the action should be invariant under a change of μ. This invariance is expressed in terms of the renormalization group equation (RGE):

$$\left(\mu\frac{\partial}{\partial\mu}+\mu\frac{\partial\lambda}{\partial\mu}\frac{\partial}{\partial\lambda}\right)S(Z\Phi,\lambda,\mu)=0, \tag{2.44}$$

where λ are the couplings (from the superpotential) of the theory and $Z\Phi$ represent the renormalized superfields.[12] From this, we define the *β-function*, controlling how the couplings behave away from the energy where they were defined

$$\beta_\lambda \equiv \frac{\partial\lambda}{\partial t}, \tag{2.45}$$

with $t=\ln\mu$.

Taking the MSSM field content and its three couplings,

$$g_1=\sqrt{\frac{5}{3}}g', \quad g_2=g, \quad g_3=g_s, \tag{2.46}$$

it can then be showed that the one-loop β-functions of the inverse coupling constants $\alpha_i^{-1}\equiv\frac{g_i^2}{4\pi}$ are

$$\beta_{\alpha_i^{-1}}=-\frac{b_i}{2\pi}, \tag{2.47}$$

where in the MSSM, $b_i=(\frac{33}{5},1,-3)$. This means the strong interaction strength decreases as we go to higher scales, while the weak and hypercharge increase. In the MSSM, the inverse couplings α_i^{-1} unite at $\sim 10^{16}$ GeV, the so-called *GUT scale*, as illustrated in figure 2.1 (left).

[11] This is not to be confused with the Higgs mass parameter in the superpotential.

[12] The coupling constants of the superpotential do not need renormalization in unbroken SUSY [22].

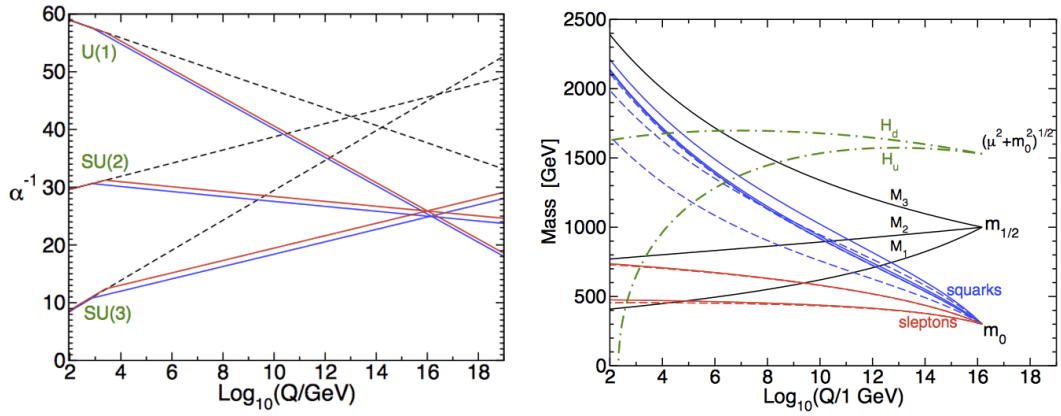

Figure 2.1: Left: evolution of the gauge couplings with energy in the Standard Model (dashed) and in supersymmetry (solid). Right: Soft masses and their evolution with energy in the MSSM. Both illustrations taken from [23].

Assuming GUT-unification of the couplings, $g_1 = g_2 = g_3 = g_u$, in addition to a common gaugino mass $M_1 = M_2 = M_2 = m_{1/2}$ at the same scale, the following ratio between the gaugino masses at 1 TeV can be showed to hold at all scales (at one-loop),

$$M_3 : M_2 : M_1 = 6 : 2 : 1. \tag{2.48}$$

2.5.6 Radiative electroweak symmetry breaking

In the Standard Model, the gauge bosons gain mass through the electroweak symmetry breaking (EWSB), as described in section 1.6. It is induced by the shape of the Higgs scalar potential $V(\Phi)$ in eq. (1.36), and the requirement for breaking was $\lambda > 0$ and $\mu^2 < 0$, to ensure the potential is bounded from below, and that the Higgs field has a vev, respectively. Rather than putting this mechanism in by hand, supersymmetry gives an explanation to why it occurs, through the RGE equation and running of the Higgs masses m_{H_u} and m_{H_d}.

From eq. (2.29), the MSSM scalar potential for the scalar Higgs component fields (not superfields) is

$$\begin{aligned} V(H_u, H_d) = {} & |\mu|^2(|H_u^0|^2 + |H_u^+|^2 + |H_d^0|^2 + |H_d^-|^2) \\ & + \frac{1}{8}(g^2 + g'^2)(|H_u^0|^2 + |H_u^+|^2 - |H_d^0|^2 - |H_d^-|^2)^2 \\ & + \frac{1}{2}g^2|H_u^+ H_d^{0*} + H_u^0 H_d^{-*}|^2 \\ & + m_{H_u}^2(|H_u^0|^2 + |H_u^+|^2) + m_{H_d}^2(|H_d^0|^2 + |H_d^-|^2) \\ & + (bH_u^+ H_d^- - bH_u^0 H_d^0 + \text{c.c.}). \end{aligned} \tag{2.49}$$

Here, the first line comes from so-called *D-terms* from the first part of eq. (2.21), the second line from *F-terms* from the second part, while the three last lines have their origin in the soft breaking terms.

Just like in the Standard Model, we now seek to use the shape of the potential to break the $SU(2)_Y \times U(1)_Y$ symmetry in order to provide the fermion and gauge boson masses while keeping $U(1)_{\text{em}}$. To do this, eq. (2.49) must fulfill the following three requirements:

i) the potential must have a minimum for finite, *i.e. non-zero*, field values,

ii) the minimum must have a remaining $U(1)_{\text{em}}$ symmetry,

iii) the potential must be bound from below.

We will restrict our analysis to tree-level, ignoring loop effects on the potential. As we have a gauge invariant theory, we are free to use the $SU(2)_L$ gauge transformation to rotate away any field value of H_u^+ at the minimum of the potential, preventing it from having a possible vev. Without loss of generality, we therefore put $H_u^+ = 0$. Further, since $\partial V/\partial H_d^+ = 0$ in the minimum, this implies $H_d^- = 0$ when $H_d^+ = 0$. Hence, the charged fields cannot have vevs in the minimum, and electromagnetism is unbroken as required in ii). With these changes, the potential can be written

$$\begin{aligned} V(H_u^0, H_d^0) = (|\mu|^2 + m_{H_u}^2)|H_u^0|^2 + (|\mu|^2 + m_{H_d}^2)|H_d^0|^2 \\ + \frac{1}{8}(g^2 + g'^2)(|H_u^0|^2 - |H_d^0|^2)^2 - (bH_u^0 H_d^0 + \text{c.c.}) \end{aligned} \tag{2.50}$$

The parameter b can be taken to be real and positive, as we can absorb a phase in H_u^0 or H_d^0. For the b-term to give a maximal negative contribution, $H_u^0 H_d^0$ must be real and positive in the minimum. This means the vacuum expectation values v_u and v_d of H_u^0 and H_d^0, respectively, must have opposite phases. However, we use our $U(1)_Y$ gauge freedom to transform v_u and v_d to both be real and of same sign.

For the potential to have a minimum for non-zero field values, we need negative mass terms. This is now fulfilled by eq. (2.50) if

$$b^2 > (|\mu|^2 + m_{H_u}^2)(|\mu|^2 + m_{H_d}^2). \tag{2.51}$$

For the potential to be bound from below also outside the vacuum, usually dominated by the H^4 terms, we need to take care of the situation $|H_u^0| = |H_d^0|$, which will require

$$2b < 2|\mu|^2 + m_{H_u}^2 + m_{H_d}^2. \tag{2.52}$$

Negative values of $m_{H_u}^2$ or $m_{H_u}^2$ help satisfy eqs. (2.51) and (2.52), but do not guarantee EWSB. Assuming a common mass $m_{H_u} = m_{H_d}$ at some high scale, e.g. the GUT scale $\sim 10^{16}$ GeV, these two inequalities can not be satisfied

simultaneously *at that scale*. However, both $m_{H_u}^2$ and $m_{H_d}^2$ run down with energy, to an extent determined by the Yukawa couplings y_t and y_b of the top and bottom quarks, respectively. As $y_t \gg y_b$, $m_{H_u}^2$ runs down much faster than $m_{H_d}^2$, and may in fact become negative as we go to the electroweak scale, as illustrated in figure 2.1 (right). If we also have that $m_{H_u}^2 \sim |\mu|^2$, the first term of eq. (2.51) is zero and automatically fulfilled, which means we only have to make sure that $2b < |\mu|^2 + m_{H_d}$. This is called *radiative* electroweak symmetry breaking (REWSB), and is caused by the soft terms of the MSSM Lagrangian. This is in contrast to the Standard Model, where the breaking must be put in by hand.

The two vacuum expectation values are related to the masses of the Standard Model vector bosons by

$$v_u^2 + v_d^2 = v^2 = \frac{2m_Z^2}{g^2 + g'^2} \approx (246 \text{ GeV})^2. \tag{2.53}$$

This relation can be used to define one free parameter from the two Higgs vevs,

$$\tan\beta \equiv \frac{v_u}{v_d}, \tag{2.54}$$

where by convention $0 < \beta < 2\pi$. Hence the Higgs scalar potential of the MSSM has four real parameters; $b, \mu, m_{H_u}^2$ and $m_{H_d}^2$. By the property

$$\partial V/\partial H_u^0 = \partial V/\partial H_d^0 = 0 \tag{2.55}$$

at the minimum, we can eliminate b and $|\mu|$ as free parameters, however, not the sign of μ. This means we can parametrize the scalar MSSM Higgs sector with

$$\tan\beta, m_{H_u}^2, m_{H_d}^2, \text{sgn}(\mu). \tag{2.56}$$

Alternatively we may eliminate $m_{H_u}^2$ and $m_{H_d}^2$, keeping b and μ. It is then common to trade b against $m_A^2 = 2b/\sin 2\beta$, where m_A is the mass of the Higgs pseudo scalar.

2.6 Sparticle masses and phenomenology

2.6.1 The extended Higgs sector

The MSSM predicts five Higgs bosons from the two Higgs supermultiplets.[13] Three of the eight degrees of freedom in the scalar potential in eq. (2.49) are absorbed into $W^\pm$ and Z^0 as they turn massive. The five remaining form two neutral scalars h, H, two charged scalars $H^\pm$, and one neutral pseudo-scalar A.

[13] In addition, the supermultiplets also contain a total of four higgsinos, $\tilde{H}_u^0, \tilde{H}_u^+, \tilde{H}_d^0, \tilde{H}_d^-$.

At tree level, the Higgs masses are

$$m_A^2 = \frac{2b}{\sin 2\beta} = 2|\mu|^2 + m_{H_u}^2 + m_{H_d}^2, \tag{2.57}$$

$$m_{h,H}^2 = \frac{1}{2}\left(m_A^2 + m_Z^2 \mp \sqrt{(m_A^2 - m_Z^2)^2 + 4m_Z^2 m_A^2 \sin^2 2\beta}\right), \tag{2.58}$$

$$m_{H^\pm}^2 = m_A^2 + m_W^2. \tag{2.59}$$

From this we see that $H, H^\pm$ and A are all in principle unbound in mass, since they grow as $b/\sin 2\beta$. The lightest Higgs boson h, however, is restricted from (2.58) to have a tree-level mass

$$m_h < m_Z |\cos 2\beta|. \tag{2.60}$$

Unfortunately, this is not in accord with the experimental measurements of the Higgs mass of $m_h \simeq 125$ GeV. To the rescue comes large loop corrections, otherwise the MSSM would have been excluded already. The dominant corrections come from scalar top (stop) and top quark loops, due to their large Yukawa couplings, given in eq.(B.25). Taking these, and other corrections into consideration, the bound on m_h is weaker,

$$m_h \leq 135 \text{ GeV}, \tag{2.61}$$

when assuming a common sparticle mass $m_{\text{SUSY}} \leq 1$ TeV. The bound is not very sensitive to higher values of the sparticle mass scale m_{SUSY} due to a logarithmic dependence in the correction term, and is weakened very little as m_{SUSY} increases. However, the larger the sparticle masses, the larger the *fine-tuning*, a topic we will discuss in chapter 3.

2.6.2 Sfermions and gluinos

The soft terms of the MSSM Lagrangian give multiple contributions to the sfermion masses. For the two first generations, many of the contributions are negligible due to small Yukawa couplings. To avoid flavour changing neutral currents from the soft terms, the mass matrix must to a good approximation be diagonal. The sfermion masses are

$$m_F^2 = m_{F,\text{soft}}^2 + \Delta_F, \tag{2.62}$$

where $m_{F,\text{soft}}$ are contributions from the soft terms on the form $-m^2 \tilde{F}_i^\dagger \tilde{F}_i$ and $-m^2 \tilde{f}_{iR}^* \tilde{f}_{iR}$, and $\Delta_F = (I_3 g^2 - Y g'^2)(v_d^2 - v_u^2)$. The isospin I_3 and hypercharge Y belong to the left-handed supermultiplet from which the sfermion originates.

The third generation of sfermions $\tilde{t}, \tilde{b}$ and $\tilde{\tau}$ are slightly more complicated, as they receive a larger number of non-negligible contributions due to their large Yukawa and trilinear couplings. Taking the stop as an example, the mass term of

the Lagrangian is given as

$$\mathcal{L}_{\tilde{t}} = -(\tilde{t}_L^* \ \tilde{t}_R^*)\mathbf{M}_{\tilde{t}}^2 \begin{pmatrix} \tilde{t}_L \\ \tilde{t}_R \end{pmatrix}, \tag{2.63}$$

where we have that

$$\mathbf{M}_{\tilde{t}}^2 = \begin{pmatrix} m_{Q_3}^2 + m_t^2 + \Delta\tilde{u}_L & v(a_t^* \sin\beta - \mu y_t \cos\beta) \\ v(a_t \sin\beta - \mu^* y_t \cos\beta) & m_{u_3}^2 + m_t^2 + \Delta\tilde{u}_R \end{pmatrix}. \tag{2.64}$$

The particle masses can be found by diagonalizing $\mathbf{M}_{\tilde{t}}^2$, writing it in terms of the mass eigenstates $\tilde{t}_1$ and $\tilde{t}_2$, mixing with the gauge eigenstates $\tilde{t}_L$ and $\tilde{t}_R$. By convention, $m_{\tilde{t}_1} < m_{\tilde{t}_2}$. The mass matrices for $\tilde{b}$ and $\tilde{\tau}$ both have the same structure.

The gluino is a color octed Majorana fermion, and has nothing to mix with in the MSSM. The tree-level mass of the gluino is therefore simply given by the soft term M_3. As the gluino interacts strongly, $M_3(\mu)$ runs quickly with energy. It is therefore useful to talk about the scale-independent pole-mass. Including effects of gluon exchange and squark loops to one-loop order, it is given by

$$m_{\tilde{g}} = M_3(\mu)\left[1 + \frac{\alpha_s}{4\pi}\left(15 + 6\ln\frac{\mu}{M_3(\mu)} + \sum_{\text{all } \tilde{\text{q}}} A_{\tilde{q}}\right)\right], \tag{2.65}$$

where $A_{\tilde{q}}$ is the first order squark loop corrections,

$$A_{\tilde{q}} = \int_0^1 x \ln\left(x\frac{m_{\tilde{q}}^2}{M_3^2} + (1-x)\frac{m_q^2}{M_3^2} - (1-x) - i\epsilon\right) \mathrm{d}x. \tag{2.66}$$

The gluino mass is therefore mainly driven by the M_3 gaugino soft mass, but is also dependent upon the squark masses from the loop corrections.

2.6.3 Charginos and neutralinos

Due to electroweak symmetry breaking, we get mixing between the electroweak gauginos $\tilde{W}^i, \tilde{B}^0$ and the higgsinos $\tilde{H}_u^+, \tilde{H}_u^0, \tilde{H}_d^0, \tilde{H}_d^-$ from the Higgs doublets. The remaining $U(1)_{\text{em}}$ symmetry only allows fields of equal charge to mix, and the mass eigenstates of the allowed mixings give us what is known as charginos and neutralinos.

The neutral gauginos mix with the neutral higgsinos to form four neutral mass eigenstates $\tilde{\chi}_i^0$ — the neutralinos. We can define a vector $\tilde{\chi}^0$ in the gauge eigenstate basis

$$\tilde{\chi}^0 = \begin{pmatrix} \tilde{B}^0 \\ \tilde{W}^0 \\ \tilde{H}_d^0 \\ \tilde{H}_u^0 \end{pmatrix}, \tag{2.67}$$

with the relevant mass terms in the Lagrangian

$$\mathcal{L}_{\tilde{\chi}^0} = -\frac{1}{2}(\tilde{\chi}^0)^T \mathbf{M}_{\tilde{\chi}^0} \tilde{\chi}^0 + \text{c.c.}, \tag{2.68}$$

where the mass matrix $\mathbf{M}_{\tilde{\chi}^0}$ is given as

$$\mathbf{M}_{\tilde{\chi}^0} = \begin{pmatrix} M_1 & 0 & -\frac{1}{\sqrt{2}}g'v_d & \frac{1}{\sqrt{2}}g'v_u \\ 0 & M_2 & \frac{1}{\sqrt{2}}gv_d & -\frac{1}{\sqrt{2}}gv_u \\ -\frac{1}{\sqrt{2}}g'v_d & \frac{1}{\sqrt{2}}gv_d & 0 & -\mu \\ \frac{1}{\sqrt{2}}g'v_u & -\frac{1}{\sqrt{2}}gv_u & -\mu & 0 \end{pmatrix}. \tag{2.69}$$

We recognize the M_1 and M_2 gaugino mass parameters from the soft breaking terms, and the higgsino mass parameter μ from the superpotential.

The neutralino mass eigenstates $\tilde{\chi}_i^0$ and their corresponding masses $m_{\tilde{\chi}_i^0}$ are found by diagonalizing the mass matrix by a unitary matrix $\mathbf{N}$ such that

$$\mathbf{N}^* \mathbf{M} \mathbf{N}^{-1} = \text{diag}(m_{\tilde{\chi}_1^0}, m_{\tilde{\chi}_2^0}, m_{\tilde{\chi}_3^0}, m_{\tilde{\chi}_4^0}). \tag{2.70}$$

The mass eigenstates are then given by

$$\tilde{\chi}_i^0 = \mathbf{N}_{i1}\tilde{B}^0 + \mathbf{N}_{i2}\tilde{W}^0 + \mathbf{N}_{i3}\tilde{H}_d^0 + \mathbf{N}_{i4}\tilde{H}_u^0. \tag{2.71}$$

As with the stops, the labels $i = 1, 2, 3, 4$ describe the neutralinos by increasing mass.

An interesting limit is when $m_Z \ll |\mu \pm M_1|, |\mu \pm M_2|$ and when $M_1 < M_2 \ll |\mu|$, as argued for GUT motivated models in eq. (2.48). The neutralinos can here be approximated as

$$\begin{aligned} \tilde{\chi}_1^0 &\approx \tilde{B}^0, \\ \tilde{\chi}_2^0 &\approx \tilde{W}^0, \\ \tilde{\chi}_{3,4}^0 &\approx \frac{1}{\sqrt{2}}\left(\tilde{H}_u^0 \pm \tilde{H}_d^0\right). \end{aligned} \tag{2.72}$$

The charged gauginos, $\tilde{W}^\pm = \frac{1}{\sqrt{2}}(\tilde{W}^1 \mp i\tilde{W}^2)$, mix with the charged higgsinos forming the mass eigenstates known as charginos. Again, we can write the gauge eigenstate basis as

$$\tilde{\chi}^\pm = \begin{pmatrix} \tilde{W}^+ \\ \tilde{H}_u^+ \\ \tilde{W}^- \\ \tilde{H}_d^- \end{pmatrix}, \tag{2.73}$$

with the corresponding Lagrangian mass terms

$$\mathcal{L}_{\tilde{\chi}^\pm} = -\frac{1}{2}(\tilde{\chi}^\pm)^T \mathbf{M}_{\tilde{\chi}^\pm} \tilde{\chi}^\pm + \text{c.c}, \tag{2.74}$$

where the mass matrix is given by

$$\mathbf{M}_{\tilde{\chi}^{\pm}} = \begin{pmatrix} 0 & 0 & M_2 & gv_d \\ 0 & 0 & gv_u & \mu \\ M_2 & gv_u & 0 & 0 \\ gv_d & \mu & 0 & 0 \end{pmatrix}. \tag{2.75}$$

Taking the same limit as for eq. (2.72), the charginos can be approximated as

$$\begin{aligned} \tilde{\chi}_1^{\pm} &\approx \tilde{W}^{\pm} \\ \tilde{\chi}_2^{\pm} &\approx \tilde{H}_u^{+}/\tilde{H}_d^{-}. \end{aligned} \tag{2.76}$$

This limit, and the stronger assumption in eq. (2.48) allows us to reach the following usefull sparticle mass relations,

$$\begin{aligned} m_{\tilde{\chi}_1^{\pm}} \approx m_{\tilde{\chi}_2^0} &\approx 2m_{\tilde{\chi}_1^0}, \\ m_{\tilde{g}} &\approx 6m_{\tilde{\chi}_1^0}. \end{aligned} \tag{2.77}$$

However, the table turns if we assume $|\mu| < |M_1|, |M_2|$, as this gives $\tilde{\chi}_1^0 \approx \tilde{H}_u^0/\tilde{H}_d^0$, $\tilde{\chi}_2^0 \approx \tilde{H}_u^0/\tilde{H}_d^0$ and $\tilde{\chi}_1^{\pm} \approx \tilde{H}_u^{+}/\tilde{H}_d^{-}$, while $\tilde{\chi}_2^{\pm} \approx \tilde{W}^{\pm}$.

2.7 GUT motivated supersymmetric models

2.7.1 Minimal supergravity

Perhaps the most studied — although not the best motivated — MSSM based model is minimal supergravity (mSUGRA), also known as the constrained MSSM (CMSSM). The constraint is manifest in the minimal number of free parameters, making it relatively easy to study. The model assumes some gravity mechanism at the Planck scale $M_P \sim 10^{18}$ GeV is responsible for the spontaneous supersymmetry breaking. Motivated by the wish for unification at high scale, the 105 free parameters of the MSSM are reduced to four, plus a sign. They are

$$m_0, m_{1/2}, \tan\beta, A_0, \mathrm{sgn}(\mu), \tag{2.78}$$

where m_0 is the common scalar soft mass, $m_{1/2}$ the common gaugino soft mass, $\tan\beta$ is the ratio of the Higgs vacuum expectation values, A_0 is the common trilinear coupling constant, and μ the Higgs superpotential mass parameter. All parameters except $\tan\beta$ are defined at the GUT scale, and the RGE equations in section 2.5.5 define the corresponding sparticle masses at low scale. An example of their running from the GUT scale to electroweak scale can be seen in figure2.1.

2.7.2 Non-universal Higgs mass

In mSUGRA, all soft scalar masses are described at the GUT scale by the universal soft mass parameter m_0, motivated by the need to suppress unwanted flavour changing processes [24]. However, this motivation does not apply to the soft breaking Higgs masses. This has been the inspiration behind more general forms of mSUGRA, allowing for non-universal Higgs masses (NUHM) at the GUT scale. In these models, the soft Higgs masses m_{H_u} and m_{H_d} are free parameters.

In the NUHM1 model, the assumption is that they are non-universal by the same amount, i.e. $m_{H_u} = m_{H_d} = m_H$, giving one extra parameter m_H in addition to those of mSUGRA. In the NUHM2 model, the Higgs masses are allowed also to have an internal splitting, i.e. $m_{H_u} \neq m_{H_d}$. From the conditions for electroweak symmetry breaking in eqs. (2.51) and (2.52), we may trade the GUT scale parameters m_{H_u} and m_{H_d} with the weak scale values of μ and m_A, and we can parametrize NUHM2 by the set

$$m_0, m_{1/2}, \tan\beta, A_0, \mu, m_A. \tag{2.79}$$

Certain choices of these parameters are well motivated by their low fine-tuning and fulfillment of the sparticle and Higgs mass constraints, e.g. see [25]. This framework is dubbed *Radiatively-driven Natural Supersymmetry* (RNS), as the required value of $m_{H_u}^2 \simeq -m_Z^2$ at the weak scale is generated radiatively via running from the GUT scale. This running of m_{H_u} can only be realized once its GUT scale value is decoupled from the matter scalar masses m_0.

We will return to the phenomenology of natural supersymmetry in section 3.3.

Chapter 3

Naturalness

Naturalness is a concept in physics concerning how comfortable we are with accidental cancellations of physical quantitites. In the Standard Model, this is relevant for the quantum corrections of the Higgs mass, as the theoretical predicted mass is off by approximately 10^{16} orders of magnitude compared to what is measured, being such magical cancellations. Concidering the Standard Model alone, this is regarded *unnatural*, as it offers no explanation to why this happens. In this chapter, we will first introduce the hierarchy problem of the Higgs mass, before we explain why and how supersymmetry can protect it from such cancellations. We then give the typical phenomenological consequences of a natural supersymmetry model, before we quantify the naturalness in terms of the so-called Barbieri–Giudice fine-tuning criteria.

3.1 The hierarchy problem in the Standard Model

The tree level mass term of the Higgs field h is present in the Standard Model Lagrangian as

$$-\mu^2 h^\dagger h, \tag{3.1}$$

and its Feynman diagram representation can be seen in figure 3.1. Since the Higgs field interacts with the other particles in the Standard Model, there is an infinite number of diagrams with identical initial and final state as those in

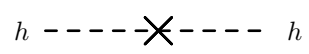

Figure 3.1: Tree level mass term og the Higgs particle.

figures 3.2(a) and 3.2(b). They contribute to the same process, and are the loop corrections to the Higgs mass. Their naïve mathematical evaluation gives infinity, and regularization is necessary to parametrize these infinities. A cut-off scale Λ can be introduced,[1] a scale above which we expect the Standard Model to be invalid. This is often taken to be the Planck scale at the order of $M_P \sim 10^{18}$ GeV, as we know gravitational effects are no longer negligible at this scale.

To leading order in Λ, the resulting Higgs mass is (see appendix B for detailed calculations)

$$\begin{aligned} m_h^2 &= \mu^2 + \Delta m_h^2 \\ &= \mu^2 + \left(\frac{\lambda_S}{16\pi^2} - \frac{|\lambda_f|^2}{8\pi^2} \right) \Lambda^2, \end{aligned} \tag{3.2}$$

where the first correction comes from the scalar loop, and the second from the fermion loop. This means the Higgs mass is quadratically sensitive to the scale of where new physics takes over. From experiments the Higgs mass is known to be ~ 125 GeV [13], but the theoretical prediction seemingly wants to push it to the order of 10^{18} GeV. This extreme disagreement between theory and experiment is known as the *hierarchy problem* of the Standard Model, where the name refers to the hierarchy of scales between the Planck scale and the electroweak scale.

For theory and experiment to agree, the terms of eq. (3.2) must cancel almost completely. In terms of the Standard Model alone, this is regarded as improbable, as the theory gives no mechanism or explanation to why these numbers are almost identical. As we are about to see, supersymmetry does.

3.2 Solving the hierarchy problem with supersymmetry

As we have seen in chapter 2, supersymmetry introduces a whole new range of elementary particles, and the Higgs boson is accompanied by many other scalars. The number of particles running in loops increases, and so does the number of correction terms.

From eq. (3.2), we see that a cancellation to leading order in Λ means the couplings must be related by $\lambda_S = |\lambda_f|^2$, in addition to a factor of two in the scalar correction. This is exactly what happens in unbroken supersymmetry. To see this, we go back to the super- and scalarpotential of the MSSM Lagrangian, defined in eqs. (2.21) and (2.29), respectively. From this we see that the superpotential term $\lambda_{ijk}\Phi_i\Phi_j\Phi_k$ contains terms with component fields of the form

$$W \sim \lambda_{ijk}\psi_i\psi_j A_k, \tag{3.3}$$

[1] But a dimensional regularization could also be done.

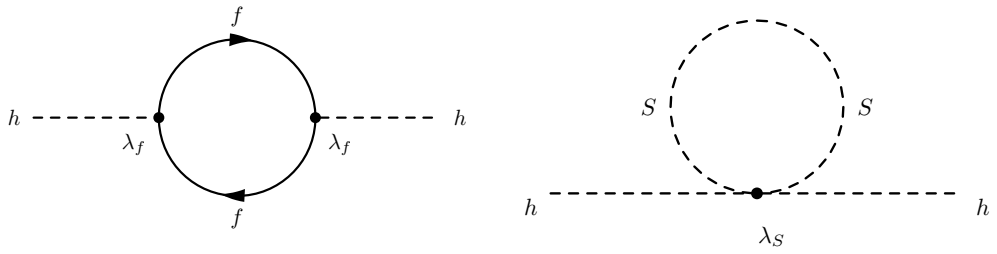

(a) Fermion loop with coupling λ_f.

(b) Scalar loop with coupling λ_S.

Figure 3.2: Fermion and scalar loop corrections to the Higgs mass.

which describe the interaction of a scalar particle A_k with two fermions ψ_i, ψ_j, as in figure 3.2(a). From the scalar potential in eq. (2.29) we identify the following term coming from the same superpotential term

$$V \sim \left| \frac{\partial W[A]}{\partial A_i} \right|^2 = |\lambda_{ijk}|^2 A_j^* A_k^* A_j A_k, \tag{3.4}$$

which describes the interaction of two scalar fields A_j and A_k, illustrated in figure 3.2(b). Since both interactions come from the same superpotential term, it is then clear that if we write $|\lambda_{ijk}|^2 = \lambda_S$, then $\lambda_{ijk} = \lambda_f$, and we have the relation

$$\lambda_S = |\lambda_f|^2, \tag{3.5}$$

which was one of the two conditions needed for a cancellation to leading order in Λ from eq. (3.2).

The remaining factor of two enters as every Standard Model fermion has two superpartners, so there are twice as many scalar as fermionic degrees of freedom running around in loops, see table 2.4. The cancellation of these quadratic divergencies in the loop corrections to the Higgs mass[2] holds to all orders in perturbation theory in both broken and unbroken supersymmetry [23].

However, in broken supersymmetry there is a remaining logarithmic dependency, see eq. (B.21),

$$\frac{\lambda_S}{16\pi^2}\ m_S^2 \ln\left(\frac{\Lambda^2}{m_S^2}\right), \tag{3.6}$$

where m_S is the scalar soft mass parameter, driving the scalar masses. We now encounter what is called the *little hierarchy problem*. As the logarithmic correction increases with increasing soft masses, the superpartner masses should be restricted in order not to reintroduce the hierarchy problem.

[2]Or in fact, any scalar mass.

In order to keep the cancellations fairly natural, it is often claimed that the lightest superpartner masses should not be much greater than the TeV scale [23]. This provides a Higgs vev from the MSSM scalar potential in compliance with the gauge boson masses m_W and m_Z, without suffering miraculous cancellations.

It should be noted that the historical motivation for developing supersymmetry was not to solve the hierarchy problem. The fact that it does, is therefore even more impressive.

3.3 Natural supersymmetry

Introducing supersymmetry cancelled the quadratic divergencies in the Higgs mass corrections, but left us with a term depending upon the mass splitting between the Standard Model particles and their superpartners, known as the little hierarchy problem. From this it is clear that the supersymmetric masses can not be too large, in order not to reintroduce the hierarchy problem.

This constraint is also manifest if one expresses the Z-boson mass as a function of supersymmetric parameters, by minimizing the MSSM one-loop scalar potential. At tree-level, this dictates the relation [2][3]

$$\frac{1}{2}m_Z^2 = \frac{m_{H_u}^2 - m_{H_d}^2 \tan^2\beta}{\tan^2\beta - 1} - \mu^2, \tag{3.7}$$

which correlates the higgsino mass parameter μ with the soft masses $m_{H_u}^2$ and $m_{H_d}^2$ and $\tan\beta$. Equation (3.7) serves as the starting point for a qualitative discussion of naturalness, as well as raising an interesting question concerning the scales of the parameters on the right hand side. The MSSM is regarded as natural if the individual terms of eq. (3.7) are of the same order as m_Z. Otherwise, they will give large contributions to the right hand side, and consequently, all individual contributions need to be finely tuned for the equation to hold. As $m_{H_u}^2$ and $m_{H_d}^2$ are from the part of the MSSM Lagrangian breaking supersymmetry, they have an expected scale m_{SUSY}, common to all the soft masses. For the equation to hold for the observed Z-boson mass, this means μ must be at the same scale. However, μ does not originate from the supersymmetry breaking part of the MSSM Lagrangian, and there is no explanation in the MSSM for why its scale should be that of the soft breaking terms. This is known as the *μ-problem*.

Assuming there is an explanation to why the scale of μ is correlated to that of $m_{H_u}^2$, there is still a fine-tuning problem in eq. (3.7), as parameters at the scale of m_{SUSY} must be fine-tuned in order to obtain the observed m_Z at the electroweak scale.

[3] We will here for simplicity work with the parameters at the low energy scale. If the model is defined by parameters at some high scale, as it is elsewhere in this thesis, the low scale parameters must be regarded as functions of these.

Inspired by the wish for a minimally fine-tuned model, *Natural supersymmetry models* have been developed [26, 27]. In general, keeping the fine-tuning as low as possible requires that $m_{H_u}^2, m_{H_d}^2$ and μ are kept fairly low. For simplicity, we will use eq. (3.7) to discuss some phenomenological consequences in Natural SUSY, even though the fine-tuning is alleviated somewhat if one includes also higher order corrections [28].

As μ is the higgsino mass parameter, Natural SUSY models thus predict light higgsinos. A very natural scenario would be $|\mu| \leq m_Z$, but this is already excluded by LEP results [13]. Unless either the gaugino soft mass parameters M_1 or M_2 are also small, this means the two lightest neutralinos and the lightest chargino will be dominantly higgsinos, with masses of similar size.

The dominant one-loop corrections to $m_{H_u}^2$ are driven by the soft breaking parameters governing the masses of stops and left-handed sbottoms, due to the large Yukawa strengths. It is therefore expected that these squarks are rather light in Natural SUSY. The gluino mass parameter M_3 enters the two-loop corrections to $m_{H_u}^2$, hence gluinos are neither expected to be too heavy.

To summarize the above, models of Natural SUSY predict light higgsinos, stops and left-handed sbottoms, and gluinos accessible to the LHC [29]. However, Natural SUSY models out of kinematic reach at the LHC can also be motivated, see e.g. [25].

3.4 Measuring fine-tuning

To measure the fine-tuning, we will take on the commonly used Giudice–Barbieri-measure defined in [30]. The definition consideres the electroweak scale represented by the Z-boson mass, expressed in terms of the most general set of model parameters $\{\theta_i\}$. The amount of fine-tuning c_i is defined as the sensitivity of the electroweak scale with respect to the model parameter θ_i,

$$c_i = \left| \frac{\partial \ln m_Z^2}{\partial \ln \theta_i} \right| = \left| \frac{\theta_i}{m_Z^2} \frac{\partial m_Z^2}{\partial \theta_i} \right|, \tag{3.8}$$

with the naturalness score or overall fine-tuning c determined by the most sensitive parameter,

$$c = \max\{c_i\}. \tag{3.9}$$

We will in this thesis focus on the specific model parameters of the MSSM, and take the scan parameters — to be defined in chapter 5 — as the fundamental parameters.

3.4.1 Example

We give a simple example to illustrate how this criteria measures fine-tuning, and how it reflects the problem of cancellation discussed previously in this chapter.

We have from eq. (3.7) the correlation of the Z-boson mass with the higgsino mass parameter $\mu, \tan\beta$ and the soft masses $m_{H_u}^2$ and $m_{H_d}^2$. This serves as the starting point for a qualitative discussion of naturalness.

Now we can find how sensitive eq. (3.7) is to changes in for instance μ, by

$$c_\mu = \left| \frac{\mu}{m_Z^2} \frac{\partial m_Z^2}{\partial \mu} \right| = \left| \frac{4\mu^2}{m_Z^2} \right|. \tag{3.10}$$

Taking μ to be positive, $m_{H_d}^2$ to be negative, and $\mu^2 > |m_{H_d}^2|$, we can simplify eq. (3.7) in the limit where $\tan\beta \gg 1$ as

$$c_\mu = \left| \frac{4\mu^2}{m_Z^2} \right| \approx \frac{2\mu^2}{\mu^2 - |m_{H_d}^2|}. \tag{3.11}$$

This can be rearranged to give the ratio of m_{H_d} and μ as

$$\frac{\sqrt{|m_{H_d}^2|}}{\mu} = \sqrt{1 - \frac{2}{c_\mu}} \simeq 1 - \frac{1}{c_\mu}, \tag{3.12}$$

assuming $c_\mu > 2$. Thus, if we find the sensitivity criteria to be $c_\mu = 100$, this corresponds to μ and $\sqrt{|m_{H_d}^2|}$ being equal to an accuracy of $\sim 1\%$.

Taking the maximum accepted fine-tuning to be for example $c = 100$, approximate upper bounds on the sparticle masses has been derived. In [31], an MSSM scenario finds that higgsinos should be lighter than ~ 600 GeV, stops and left-handed sbottoms lighter than ~ 1 TeV and gluinos and winos lighter than ~ 1.4 TeV. Other sparticles are less constrained by naturalness arguments, due to their smaller couplings to the Higss sector. Note that these predictions rely on the constraint $c = 100$, and must be taken to be rough estimates only. In fact, Barbieri and Giudice proposed in [30] that the amount of acceptable fine-tuning should be $c = 10$, as this gives cancellations among the parameters in eq. (3.7) of at most one order of magnitude.

Even though the Barbieri–Giudice-measure is well-defined, it is also fully subjective, through the interpretation of the numbers given by eq. (3.9). Another important concern, is the question of what parameters to include in the fine-tuning analysis. For instance, should one also include important Standard Model parameters such as the top Yukawa coupling? And finally, there is the question of what fine-tuning measure to use, as there exist several alternative suggestions in litterature, see e.g. [25].

Chapter 4

Statistics and information criteria

The success of a physical theory relies on its agreement with observed data, and how well it is able to predict the outcomes of future experiments. The answer to these questions are related to *hypothesis testing* and *parameter estimation*.

In hypothesis testing we investigate how our model predictions agree with observed data. In parameter estimation, we try to determine what parameter values of the theory are preferred, based on some data.

Both hypothesis testing and parameter estimation are important concepts of *statistical inference* — the process of drawing conclusions about a model, based on the data at hand. This is in contrast to probability theory, where the goal is to predict the outcome for a random variable given a known model. The close connection of statistical inference with probability theory, has lead to two different statistical approches — Bayesian and frequentist — based on how probability is interpreted. Both interpretations will come into play in the process of Bayesian parameter estimation in this thesis, and we begin this section with a brief discussion of the two.

4.1 Bayesian and frequentist statistics

From a frequentist point of view, probability is only meaningful when assigning it to repeatable random samples. In the limit of infinitely many samples N, the true probability $P(A)$ of event A is

$$P(A) = \lim_{N\to\infty} \frac{n_A}{N}, \tag{4.1}$$

where n_A is the number of occurences of A in N. This means probabilities are fundamentally related to the *frequency* of events.

From a Bayesian perspective, however, probability covers *degrees of certainty* about statements, and is related to our prior knowledge about an event. It is not restricted to cover random processes only, and hence extends the range of

possible problems to treat in a probabalistic manner. Rather than measuring the probability of an event, one measures a degree of belief in it, i.e. how well the event is supported by data at hand. In Bayesian statistics we must therefore define our prior knowledge before an experiment.

Both the Bayesian and frequentist interpretation of probability is based on the sum and product rules of probability theory,

$$P(A) + P(\bar{A}) = 1, \tag{4.2}$$

$$P(A, B) = P(A|B)P(B), \tag{4.3}$$

for $0 \leq P(A) \leq 1$, where $P(A)$ is the probability of event A being true and $P(\bar{A})$ is the probability of A being false. Further, if we know the conditional probability of A given B, $P(A|B)$, and the probability of B, $P(B)$, we also know the probability of both A and B, $P(A, B)$. Among the most useful results derived from these rules is Bayes' theorem.

4.2 Bayes' theorem

The central tool in Bayesian statistics is Bayes' theorem [32],

$$P(A|B) = \frac{P(B|A)P(A)}{P(B)}, \tag{4.4}$$

which expresses the probability of A given B, $P(A|B)$, through the probability of B given A, and the unconditioned probabilities $P(A)$ and $P(B)$. As the theorem is a direct consequence of the sum and product rules of probability theory in eqs. (4.2) and (4.3), it is valid in both a frequentist and Bayesian interpretation. However, replacing the condition A with some hypothesis H, B with some data D, and conditioning all probabilities on some background information I, Bayes' theorem takes the form

$$P(H|D, I) = \frac{P(D|H, I)P(H|I)}{P(D|I)}. \tag{4.5}$$

This formulation is only valid in the Bayesian approach, as we assign a prior belief in the hypothesis H. The left hand side is called the Bayesian *posterior probability* (referred to simply as the posterior), and represents our degree of belief in the hypothesis H in light of some new data D. The factor $P(H|I)$ is called the *prior probability* (or just the prior), and expresses our degree of belief in the hypothesis before analyzing any data, on light of the background information only. As the posterior from one experiment is an update of our prior belief, it may be used as the prior in another experiment.

The factor $P(D|H, I)$ expresses the probability of obtaining the observed data D, assuming the hypothesis H is true. This is the *likelihood*, and introduces the

physical predictions from H into the equation. The likelihood describes how the probability of an observation relates to the corresponding theoretical prediction from our theory, and is central in both frequentist and Bayesian approaches. We return to likelihoods in section 4.4.

The denominator of eq. (4.5) is called the Bayesian *evidence*, and is the nominator *marginalized* over all possible realizations of H. Taking H_i to represent a set of discrete parameters, the marginalization reads

$$P(D|I) = \sum_i P(D|H_i, I)P(H_i|I), \tag{4.6}$$

where the set of possible hypothesis must be exhaustive, i.e. $\sum_i P(H_i|I) = 1$. Now, if the hypothesis H represents a point in a continous parameter space, such as the parameter space of the MSSM, the prior and posterior probabilities in eq. (4.4) become probability density functions (pdfs). The evidence then turns into an integral over the entire parameter space of the model, and is nothing but a normalization constant of the posterior. It can be determined post hoc, and does not affect the shape of the posterior.

However, in the case of Bayesian hypothesis testing, the ratio of the evidence of two models takes central stage, controlling our relative confidence in the two.

From this, we can conclude that the Bayesian posterior is a description of how our state of knowledge is modified by experimental measurements. A corresponding frequentist analysis would be based on the likelihood alone, while a Bayesian analysis considers also the prior, and makes inferences based on the posterior.

4.2.1 Bayesian parameter estimation

As an example of Bayesian parameter estimation, consider a model with a set of free parameters $\boldsymbol{\Theta}$ and data $\mathbf{D}$. The posterior p can then be expressed as

$$p(\boldsymbol{\Theta}|\mathbf{D}) = \frac{\mathcal{L}(\boldsymbol{\Theta})\pi(\boldsymbol{\Theta})}{\mathcal{Z}}, \tag{4.7}$$

where $\mathcal{L}$ is the likelihood and π is the prior.[1] The evidence is given from the marginalization over all possible $\boldsymbol{\Theta}$,

$$\mathcal{Z} = \int \mathcal{L}(\boldsymbol{\Theta})\pi(\boldsymbol{\Theta})\mathrm{d}\boldsymbol{\Theta}. \tag{4.8}$$

In addition to the posterior distributions of the model parameters themselves, we may also be interested in the distribution of a function of them. If the interesting

[1] All quantities are still conditioned on the overall model and background information being true, even if the notation is simplified.

quantity is $f = f(\mathbf{\Theta})$, this means we want to change variables in e.g. the posterior from $\mathbf{\Theta}$ to f. From eq. (4.3), the joint posterior can be expressed as[2]

$$p(f, \mathbf{\Theta}) = p(f|\mathbf{\Theta})p(\mathbf{\Theta}), \tag{4.9}$$

where the value of f is determined by the parameters, and may be equal for different $\mathbf{\Theta}$. As it does not rely on the background data D, a pdf for f conditional $\mathbf{\Theta}$ is a delta function, [33] and the posterior becomes

$$p(f, \mathbf{\Theta}) = \delta(f(\mathbf{\Theta}) - f)p(\mathbf{\Theta}). \tag{4.10}$$

The posterior in f alone is the marginalization over the model parameters,

$$p(f) = \int \delta(f(\mathbf{\Theta}) - f)p(\mathbf{\Theta})\mathrm{d}\mathbf{\Theta}. \tag{4.11}$$

Hence, the posterior is found by weighting all values of f by the posterior in the corresponding value of $\mathbf{\Theta}$. This approach is valid for all pdfs, hence it is also applicable to the prior.

Unfortunately, this analytic approach can not be taken in practice, as we do not have analytic expressions for the pdfs. In this thesis, we will typically draw random samples $\mathbf{\Theta}_i$ in our scan parameters from their prior and posterior distributions, before calculating the interesting quantity $f_i = f(\mathbf{\Theta}_i)$. Then, we histogram the sampled values f_i, giving the distributions in f. The histogramming in terms of f_i without reference to the parameters $\mathbf{\Theta}$, corresponds numerically to the marginalization in eq. (4.11).

4.2.2 Assigning priors

In order to calculate a posterior, we are in need of a prior distribution. It is assigned according to how we believe prior information — or the lack thereof — should be encoded in a pdf, and there are many important principles for how this should be done. We will here explain the two principles behind the priors we use in this thesis.

The first principle is applied to location parameters, such as the mean x of a Gaussian distribution. Having no information about this parameter (other than its rôle in our theory), the principle of *transformation group invariance* is used. This means that our prior knowledge should not be affected if our parameter is transformed in a way considered to be irrelevant for the problem. Said in other words, the prior $\pi(x)$ should be invariant under the coordinate translation $x' = x + a$,

$$\pi(x)\mathrm{d}x = \pi(x + a)\mathrm{d}(x + a), \tag{4.12}$$

[2]In the simplified notation where the data conditioning is omitted.

and since $\mathrm{d}(x+a) = \mathrm{d}x$, the requirement is

$$\pi(x) = \pi(x+a). \tag{4.13}$$

This is referred to as a *flat* or *uniform* prior, and is fulfilled if $\pi(x)$ is constant.

Another important class of parameters are *scale parameters*, e.g. mass parameters such as the common GUT scale scalar and gaugino masses in supersymmetry, m_0 and $m_{1/2}$, respectively. Their dimension introduces a definite scale into the problem. Ignorance as to what scale is correct for a mass m, implies that the prior should be invariant under the transformation $m' = cm$, where c is a constant scaling. This means we require

$$\pi(m)\mathrm{d}m = \pi(cm)\mathrm{d}(cm) = c\pi(cm)\mathrm{d}m, \tag{4.14}$$

which is satisfied by the prior $\pi(m) \propto 1/m$. By a change of variables, we see that this means $\pi(\log(m))$ is uniform, and hence we call this a *log* prior.

Both priors discussed above are *improper* pdfs, as they do not integrate to unity. Nevertheless, they may be used in Bayesian analysis as long as the resulting posterior is normalizable. Improper pdfs can also be used when we have good arguments for restricting the parameter range. If so, one simply construct the priors in some given parameter range $[\theta_{\min}, \theta_{\max}]$, and define them to be zero everywhere else. This is typically what we do in this thesis, as we have restricted our scans to finite intervals in the scan parameters. The motivation behind this, is that we simulate scenarios that can be searched for at the LHC and a possible future International Linear Collider (ILC). This implies mass scales in the GeV–TeV range, putting upper limits on the scan intervals. Lower limits arise naturally by results from LEP.

4.2.3 Prior dependence

To what extent the posterior is affected by the choice of prior, depends upon the strength of the data available, i.e. how narrow our likelihood is. Large variations in posteriors based on different priors (but equal likelihoods), means the data are not strong enough to dominate the prior information. Conclusions based on weak data should therefore be interpreted with care, as they may be strongly affected by the assumption of prior information.

To see the effect on the posterior from a weak study, see figures 4.1(a) and 4.1(b). The likelihood is based on some data having a large uncertainty, which is not strong enough to dominate both priors — hence the posteriors differ in shape depending on the choice of prior. The opposite effect can be illustrated with a particle physics experiment and determination of a particle mass. Say the prior range of the mass is 100–1000 GeV, and the likelihood from the experiment is a peak with a width of a few GeV. This would dominate all (reasonable) priors, and the posterior would look much the same regardless of what prior was assigned.

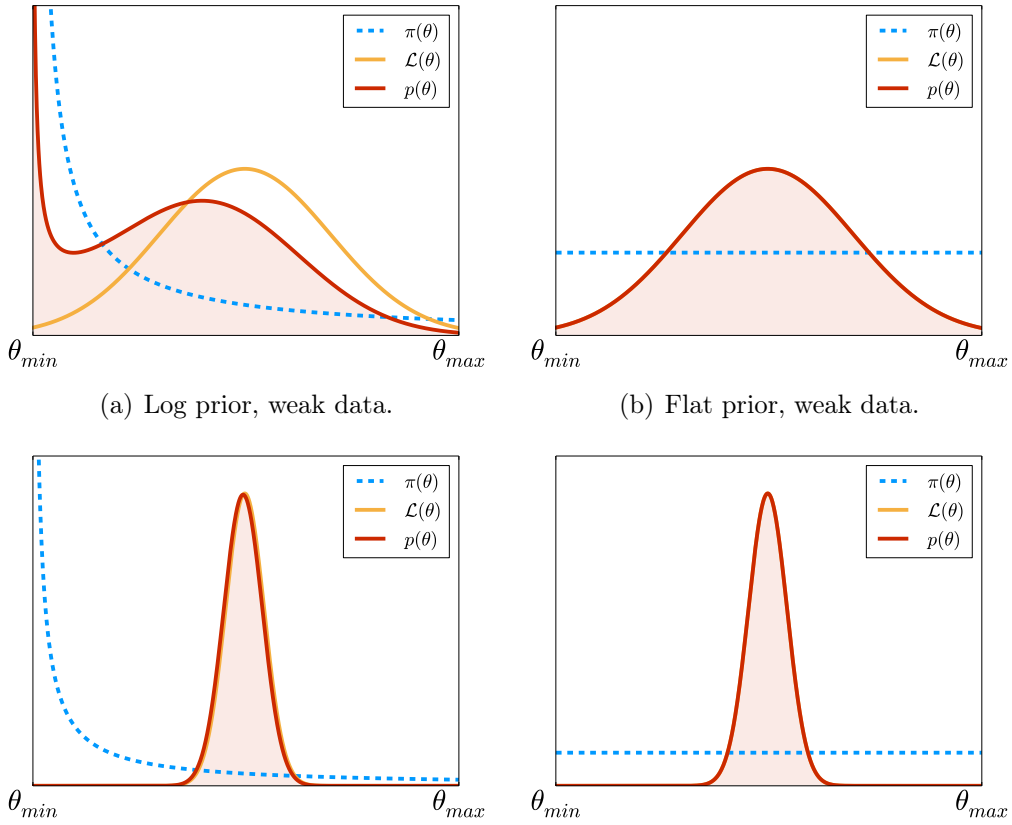

(a) Log prior, weak data.

(b) Flat prior, weak data.

(c) Log prior, strong data.

(d) Flat prior, strong data.

Figure 4.1: Illustration of the sensitivity of the posterior distribution to the choice of prior.

This is illustrated in figures 4.1(c) and 4.1(d). In the limit of very strong data, the Bayesian interpretation would give the same result as a frequentist interpretation, meaning the result would not depend upon what is the underlying statistical philosophy.

4.3 The Kullback–Leibler divergence

We have earlier seen how experiments can be used to construct likelihoods, updating our prior beliefs of e.g. model parameters. As a formal measure of the information gain in updating our prior knowledge,[3] we are using the *Kullback–Leibler (KL) divergence* [34] from information theory. It appears from literature that this has never previously been used in the context of particle physics. The

[3]Or, the information lost when using the prior to approximate the posterior.

Kullback–Leibler divergence is defined as

$$D_{KL} = \int p(\mathbf{\Theta}|\mathbf{D}) \ln \frac{p(\mathbf{\Theta}|\mathbf{D})}{\pi(\mathbf{\Theta})} \mathrm{d}\mathbf{\Theta}, \tag{4.15}$$

where $\pi(\mathbf{\Theta})$ is the prior probability of the model parameters $\mathbf{\Theta}$, and $p(\mathbf{\Theta}|\mathbf{D})$ is the posterior from eq. (4.7). This measures the amount of information provided by $\mathbf{D}$ on the parameters $\mathbf{\Theta}$,[4] and has the property $D_{KL} \geq 0$, with equality only if the two distributions are equal almost everywhere. Hence, if our knowledge about the parameters a priori equals the knowledge a posteriori, no information is gained from the experiment.

To illustrate the concept of the KL-measure, we look at a toy model of one parameter as an example.

4.3.1 Example

Consider a theory with the parameter θ, in which we investigate how a uniform, log and normal distributed prior affect the KL-measure. The priors we define as

$$\pi_1(\theta) = C_1/\theta, \tag{4.16}$$

$$\pi_2(\theta) = C_2, \tag{4.17}$$

$$\pi_3(\theta) = N(\theta|\alpha, \sigma), \tag{4.18}$$

where $N(\theta|\alpha, \sigma)$ denotes a normal distribution of mean $\alpha = 0.9$ and standard deviation $\sigma = 0.2$, and C_1 and C_2 are normalization constants. As the priors are pdfs, they must integrate to unity over all possible θ. Obviously, we need to restrict the parameter interval, as neither π_1 nor π_2 are normalizable for $\theta \in [-\infty, \infty]$. Therefore, we specify the range of the parameters such that $\theta \in [\theta_{\min}, \theta_{\max}] = [0.05, 1.5]$.

Now assume the model predicts the value of an observable $x(\theta)$, whose measured value is α_0. We assume the likelihood to be a normal distribution, $\mathcal{L} = N(\theta|\alpha_0, \sigma_0)$, of mean $\alpha_0 = 1$ and standard deviation $\sigma_0 = 0.09$. The posterior distribution $p_i(\theta)$ for prior i is then

$$p_i(\theta) = \frac{\mathcal{L}(\theta)\pi_i(\theta)}{\mathcal{Z}_i}, \tag{4.19}$$

and we can calculate the corresponding KL-measure D^i_{KL} from eq. (4.15).

The resulting KL-measures are $D^1_{KL} = 2.2$, $D^2_{KL} = 1.36$, and $D^3_{KL} = 0.56$, and can be seen in figure 4.2. The largest information gain is achived for π_1, reflected in the fact that $D^3_{KL} < D^2_{KL} < D^1_{KL}$. This prior distribution in θ had the largest discrepancy compared to the posterior obtained in taking experiment into consideration. The smallest information gain was for π_3, which had the greatest relative coincidence with the posterior.

[4] It can also be regarded as the distance between the two distributions, even if the measure is not a metric, as it is not symmetric in p and π.

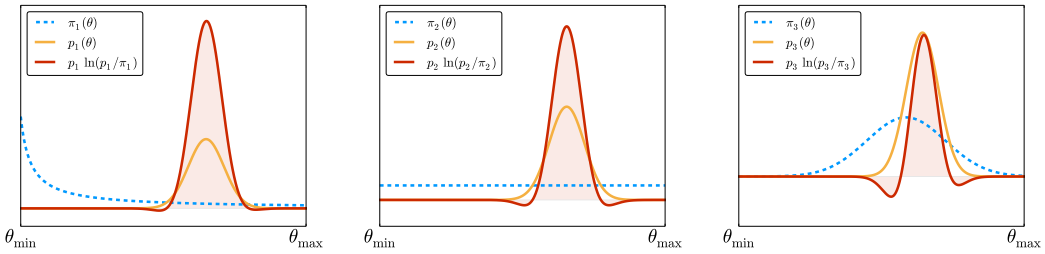

(a) Log prior. (b) Flat prior. (c) Normal distributed prior.

Figure 4.2: Illustration of how prior knowledge affects the KL-measure.

4.4 Likelihoods

4.4.1 Signal events

In this thesis, we generate particle collisions using Monte Carlo event generators. The ultimate goal of a Monte Carlo event generation is to determine the *detection efficiency*, or simply efficiency, of a given parameter point. The efficiency is defined as

$$\mathcal{E} = N_{\text{acc}}^{MC}/N_{\text{tot}}^{MC}, \tag{4.20}$$

where N_{acc}^{MC} is the number of *accepted events*, and N_{tot}^{MC} is the total number of generated events. The accepted events are those events passing a set of requirements, called *selection cuts*, needed to be fulfilled. The selection cuts are imposed to isolate a supersymmetric process from a Standard Model *background event*. A supersymmetric decay chain may just as well end in the same final-state as from a Standard Model process, thus resulting in the same signature. Luckily we are able to distinguish between a supersymmetric event and a background event by evalutaing e.g. the kinematic configuration of the two. Consequently we can filter out the supersymmetry processes by imposing cuts on for example the amount of total missing energy or individual energies of the final-state particles of the event. The efficiency constitutes the fundament in further calculations, as it ables us to determine the physical number of expected *signal events*.

We can find the number of expected signal events of a parameter point by assuming that the (constant) ratio in nature between the physical number of signal events, $s = N_{\text{acc}}$, and the total number of all events N_{tot}, equals the same ratio as from an MC generation — if that particular parameter point is realized in nature. In other words, we assume that

$$\frac{N_{\text{acc}}^{MC}}{N_{\text{tot}}^{MC}} = \frac{N_{\text{acc}}}{N_{\text{tot}}}. \tag{4.21}$$

The number of accepted events from the MC generation is easy to keep under control, as well as the total number of generated events. This ables us to find the

physical number of signal events as

$$s = N_{\text{acc}} = \mathcal{E} N_{\text{tot}}, \tag{4.22}$$

where the total number of events can be found from

$$N_{\text{tot}} = \sigma_{\text{tot}} \int L \, \mathrm{d}t = \sigma \mathcal{L}. \tag{4.23}$$

Here, $\mathcal{L}$ is the integrated luminosity, characterizing the performance of the particle accelerator, and σ_{tot} is the total cross section for the process. Hence, the number of signal events for a given process, at a given parameter point, is given by

$$s = \mathcal{E} \sigma_{\text{tot}} \mathcal{L}. \tag{4.24}$$

The efficiency is a result from a counting experiment, as we either keep an event as an accepted supersymmetry event, or we do not. The number of generated collisions for each parameter point is large ($N_{\text{tot}}^{\text{MC}} \to \infty$), the probability of keeping an event is low ($p \to 0$), and the expected number of events is constant ($N_{\text{tot}}^{\text{MC}} p \to \nu$). Therefore, the actual number of kept events follows a Poisson distibution, given by

$$P(n; \nu) = \frac{\nu^n e^{-\nu}}{n!}. \tag{4.25}$$

Here, $P(n; \nu)$ gives the probability of getting n events when we expect to have ν. In our case, we expect to have b background events from the Standard Model, in addition to s supersymmetry signal events predicted from our model, hence $\nu = (b + s)$. Thus, we can write eq. (4.25) as

$$P(n; s + b) = \frac{(s + b)^n e^{-(s+b)}}{n!}. \tag{4.26}$$

The number of accepted events $N_{\text{acc}}^{\text{MC}}$ follows a Poisson distribution, and consequently the error on the efficiency is given by $\delta\mathcal{E} = \sqrt{N_{\text{acc}}^{\text{MC}}}/N_{\text{tot}}^{\text{MC}}$.

4.4.2 Likelihoods from collider experiments

We interpret as likelihoods two different distributions in the presention of our results in this thesis. The first distribution is a Gaussian distribution, where the experimentally measured Higgs mass m_h^{exp} plays the rôle of the observation. Given model parameters $\boldsymbol{\Theta}$, the model predicts a Higgs mass $m_h^0(\boldsymbol{\Theta})$, and we interpret the likelihood as

$$\mathcal{L}(m_h | m_h^{\text{exp}}) = \frac{1}{\sqrt{2\sigma^2\pi}} \exp\left[-\frac{(m_h(\boldsymbol{\Theta}) - m_h^{\text{exp}})^2}{2\sigma^2} \right], \tag{4.27}$$

where σ is the uncertainty in the *theoretical* prediction of the Higgs mass m_h, taken to be 2 GeV.[5] In this way, the model parameters are introduced into the calculations through m_h, and the likelihood quantifies the level of agreement between model and experiment across the parameter space. If a predicted m_h is close to m_h^{exp}, the likelihood in that particular parameter point is large, reflecting that model and experiment agree. If our prior belief in that point was low, the posterior belief is increased in comparison, as a consequence of the large likelihood.

As our second likelihood we use the so-called *p-value*. It is defined from the cummulative Poisson distribution,

$$P(n \leq b; (s+b)) = \sum_{n=0}^{b} \frac{(s+b)^n e^{-(s+b)}}{n!}, \tag{4.28}$$

which quantifies the significance through the probability of observing b events *or less*, when the expected number is $(s+b)$.

We set *exclusion limits* to define what areas of parameter space are disfavored by experiment, i.e. what parameters are likely to be realized in nature and not. By convention, we exclude points with $p < 0.05$, referred to as exclusion at *95% confidence level* (CL). We will always use the strongest signal by minimizing the p-value over all *signal regions* in each parameter point.[6]

An exclusion limit should not be confused with a *discovery limit*, where the latter is much more stringent. For an observation to be classified as a discovery, one needs a discovery at so-called 5σ, corresponding to a p-value of $3 \cdot 10^{-7}$.

[5] The experimental uncertainty, however, is much smaller.

[6] A parameter point may have different set of selection cuts, defining different signal regions.

Chapter 5

Future collider searches for supersymmetry

To investigate the potential of planned searches for electroweak and strong supersymmetry production at a high-luminosity Large Hadron Collider (HL-LHC) [35], we perform two-dimensional grid scans in the parameter spaces of two supersymmetric models. By calculating the p-value of each parameter point we set exclusion limits, defining what parameter values and sparticle masses are disfavored by experiment. We also explore the naturalness reach of the HL-LHC, by evaluating likelihoods using the measured Higgs mass in addition to the potential likelihoods from future searches. From the prior and posterior distributions of naturalness, we determine the KL-measure from eq. (4.15), describing the information gain in the update of our prior beliefs. We include also results for the possible future ILC [1, 36], to explore how the two colliders can complement each other.

In this chapter, we discuss the practical software set-up of these scans, and give the selection cuts from the original analyses in [35] and [36]. We also give results from benchmark testing, validating our implementations. Results from the analysis validation will be referred to as T (test), and the original results as O. A short discussion of uncertainties will be given in section 5.5.

5.1 Model scenarios

The grid scans are performed in the parameter space of mSUGRA and NUHM2, described in section 2.7. We study two parameter choices for mSUGRA and one for NUHM2, in the following referred to as mSUGRA10, mSUGRA30 and NUHM2, respectively. Their parametrizations are given in table 5.1. As we fix some of the free parameter values, the effective model dependence upon these are removed, and we only maximize over the specific MSSM scan parameters in the evaluation of naturalness.

The scan ranges are chosen to enable comparison with the results in [2]

Table 5.1: The three scenarios and their parameter ranges. In the scan we sample $\mathcal{O}(100)$ points in each direction.

Scenario	Parameter	Prior range [GeV]	Fixed parameters
mSUGRA10	m_0	$[50, 5000]$	$\tan\beta = 10,\ A_0 = 0,$
	$m_{1/2}$	$[72, 1854]$	$\mathrm{sgn}(\mu) = +.$
mSUGRA30	m_0	$[50, 5000]$	$\tan\beta = 30,\ A_0 = -2m_0,$
	$m_{1/2}$	$[36, 1818]$	$\mathrm{sgn}(\mu) = +.$
NUHM2	$m_{1/2}$	$[30, 2010]$	$\tan\beta = 15,\ A_0 = -1.6m_0,$
	μ	$[42, 636]$	$m_0 = 4$ TeV.

and [25].[1] We do not scan over areas where the mass of the lighter chargino is $m_{\tilde{\chi}_1^\pm} \lesssim 45$ GeV, as these areas are already excluded by LEP [13], and should be reflected in our prior. This sets natural lower bounds on $m_{1/2}$ and μ.

5.2 Scan set-up

To calculate the supersymmetric mass spectrum from the GUT scale parameters in table 5.1, the corresponding naturalness from eq. (3.9), and to ensure consistent EWSB for a given parameter point, we use RGE codes of `SOFTSUSY` [37], generating a *SUSY Les Houches Accord* (SLHA) file [38], describing the model point. This is used as input to `SUSY-HIT` [39], calculating, and adding to the file, the sparticle decays. The SLHA file is further passed to `FeynHiggs` [40–45], improving the calculations of masses and couplings for the MSSM Higgs bosons. We further use two versions of the Monte Carlo event generator `PYTHIA` [46, 47] to generate the signal samples. To make file operations on the SLHA files, we use the `Python` interface `PySLHA` [48]. All program versions and their non-standard settings can be found in appendix A, table A.1.

For the electroweak processes in both e^+e^-- and pp-collisions, we use the leading order (LO) plus leading log (LL) cross sections calculated by `PYTHIA`, except where noted otherwise. We use `NLL-fast` [49–52] for the calculation of decoupled next-to-leading order (NLO) plus next-to-leading log (NLL) production cross sections for strong processes at the LHC. These corrections are of importance in strong processes, as $\alpha_s \gg \alpha_{\mathrm{em}}$. Beyond the extra NLL corrections, we use `NLL-fast` is as it is many orders of magnitude faster than the alternative, `Prospino` [53], even though the latter is more flexible in terms of processes. As the 14 TeV version of

[1] In the case of NUHM2, we reduced the value of m_0 by 1 TeV compared to [25] in order to bring the Higgs mass into closer agreement with the measured value. The difference in Higgs mass is due to the use of different RGE codes and the use of the more precise calculation in `FeynHiggs` in this thesis.

Table 5.2: Cross sections σ used in the benchmark testing.

Benchmark point [GeV]	Process	σ [fb]	Origin
$m(\tilde{g}, \tilde{\chi}_1^0) = (1425, 1400)$	$\tilde{g}\tilde{g}$	32.4	`NLL-fast`
$m(\tilde{g}, \tilde{\chi}_1^0) = (1950, 1)$	$\tilde{g}\tilde{g}$	2.14	`NLL-fast`
$m(\tilde{q}, \tilde{\chi}_1^0) = (1050, 900)$	$\tilde{q}\tilde{q} + \tilde{q}\tilde{q}^*$	85.4	`Prospino`
$m(\tilde{q}, \tilde{\chi}_1^0) = (2250, 1)$	$\tilde{q}\tilde{q} + \tilde{q}\tilde{q}^*$	0.245	`Prospino`
$m(\tilde{\chi}_2^0, \tilde{\chi}_1^0) = (400, 1)$	$\tilde{\chi}_1^\pm \tilde{\chi}_2^0$	130.4	`Prospino`
$m(\tilde{\chi}_2^0, \tilde{\chi}_1^0) = (600, 1)$	$\tilde{\chi}_1^\pm \tilde{\chi}_2^0$	23.09	`Prospino`
$m(\tilde{\chi}_2^0, \tilde{\chi}_1^0) = (800, 1)$	$\tilde{\chi}_1^\pm \tilde{\chi}_2^0$	5.53	`Prospino`
$m(\tilde{\chi}_2^0, \tilde{\chi}_1^0) = (1000, 1)$	$\tilde{\chi}_1^\pm \tilde{\chi}_2^0$	1.646	`Prospino`
Benchmark point in eq. (5.11)	$\tilde{\chi}_1^\pm \tilde{\chi}_1^\mp$	187.27	`PYTHIA 6.428`

`NLL-fast` has no option for squark–squark ($\tilde{q}\tilde{q}$) production, this process is omitted in the scan, and we only look at gluino–gluino ($\tilde{g}\tilde{g}$) and squark–anti-squark ($\tilde{q}\tilde{q}^*$) processes in the respective limits where squark and gluino masses are decoupled.

This means we will underestimate the cross section in areas where the squark and gluino masses are not decoupled, as we leave open fewer possible channels for production than what is reality. The consequence is that we will set *conservative* limits, as we underestimate the number of signal events, and we do not run the risk of excluding more than we should. For the benchmark testing, however, production cross sections are generated by both `NLL-fast`, `PYTHIA` and `Prospino`, as listed in table 5.2.

The resources needed to perform a parameter scan is highly model dependent. In mSUGRA10 and NUHM2 we generate in `PYTHIA 8` a total of 1 200 000 events for each point for electroweak production and 800 000 events for strong production. In mSUGRA30 the statistics are halved. In `PYTHIA 6`, used for the ILC analysis, we generate 100 000 events for each parameter point in all scenarios. In mSUGRA10, this costs $\sim$ 30 000 CPU hours (CPUh), while for mSUGRA30 the cost is 25 000 CPUh. The most expensive scenario is NUHM2, in which we utilise $\sim$ 39 000 CPUh. Since the parameter scanning is a complex process involving parallell processing and many scripts, we give a flowchart in figure 5.1, describing the routine for one worker process.

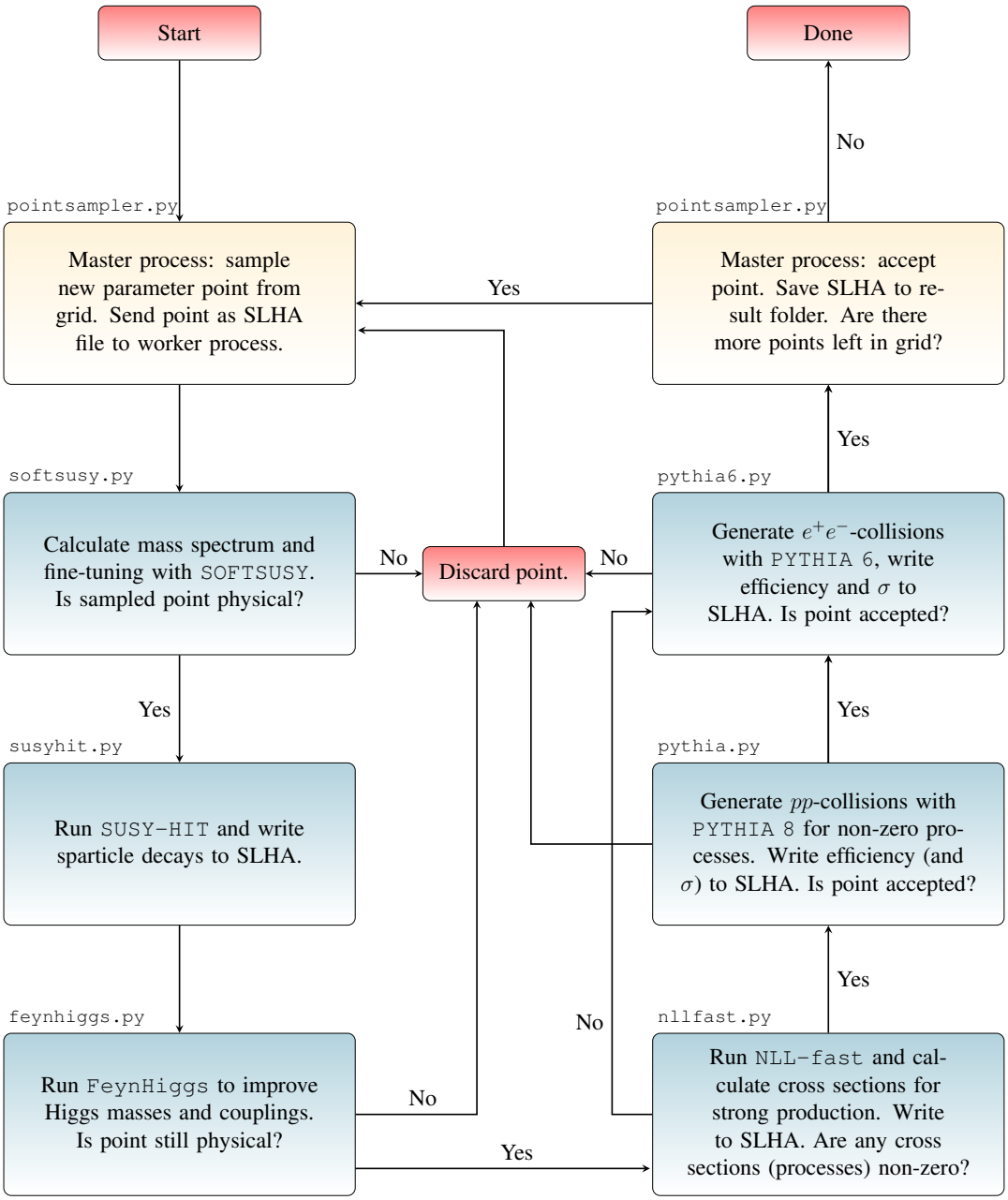

Figure 5.1: Flowchart describing the program flow of the grid scanning process. One process handles one parameter point at the time. Points are unphysical if the EWSB eqs. (2.52) and (2.52) are not fulfilled, tachyons appear in the particle spectrum or the LSP is not the lightest neutralino. Points are accepted by PYTHIA if event generation finishes during a given time limit.

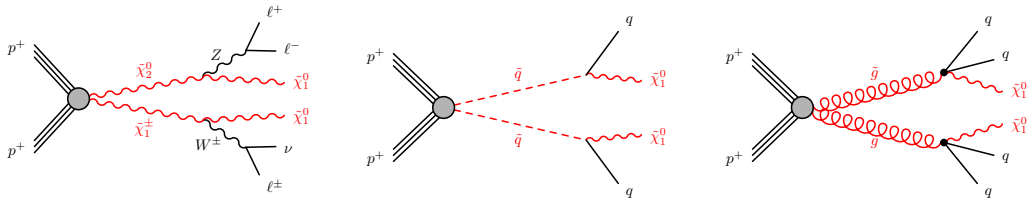

(a) Chargino and neutralino. (b) Squark. (c) Gluino.

Figure 5.2: Decay cascades for the simplified models for supersymmetry production at the LHC used in [35].

5.3 Supersymmetry production at the high-luminosity LHC

The Large Hadron Collider is expected to deliver 300 fb^{-1} of collected data by 2022, before the accelerator has a foreseen upgrade. After the high-luminosity upgrade, it is expected to reach 3000 fb^{-1} within 2032, and can hence access processes with small cross sections or poor detection efficiencies.

We implement searches for electroweak direct production of charginos and neutralinos and direct production of gluino and squark–anti-squark pairs. All collisions are at the ultimate centre-of-mass energy $\sqrt{s} = 14$ TeV, and results are presented for luminosities $\mathcal{L} = 300$ fb^{-1} and $\mathcal{L} = 3000$ fb^{-1}.

The following supersymmetric searches are motivated by the simplified models defined by ATLAS in [35], giving the signatures in figure 5.2. The simplified models are described in more detail in section 5.3.3. However, in this thesis we apply the searches to more general models, and to a wider range of parameter points.

5.3.1 Search for chargino and neutralino production

If squarks and gluinos are out of kinematic reach, electroweak production of supersymmetry can dominate at the LHC. Smoking gun signals for processes beyond the Standard Model are large amounts of missing energy E_T^{miss} due to LSPs escaping detection,[2] in addition to isolated leptons [54].[3] Therefore, a possible signature from production of charginos and neutralinos are three isolated leptons and missing energy, as illustrated in figure 5.2(a). In this section, we describe our implementation of the planned search for this particular signature given in [35].

Jets are identified and reconstructed by `FastJet` with the anti-k_T-algorithm [55], with a size parameter of $\Delta R = 0.4$. Pile-up effects are not concidered in this thesis, but to simulate some detector imperfections, we smear all jet four-momenta

[2]For clarity, by missing energy we mean missing transverse momentum.

[3]But there are of course Standard Model background processes to these signals as well.

by 3%. Candidate jets are then selected from clusters with transverse momenta $p_T > 20$ GeV, and pseudo-rapidity $|\eta| < 2.5$,[4] whereas candidate leptons, electrons and muons only, are selected with $p_T > 10$ GeV and $|\eta| < 2.4$.

For all tracks[5] i of the event with $p_T^i > 1$ GeV and within a cone of $\Delta R = \sqrt{\Delta\eta^2 + \Delta\phi^2} = 0.3$ around the lepton candidate j we define

$$S_{p_T} = \sum_{i \neq j} p_T^i. \tag{5.2}$$

All candidate leptons are required to be isolated by imposing $S_{p_T} < 0.15 p_T^j$, with p_T^j being the transverse momentum of the lepton candidate itself. Further, all lepton candidates must be isolated also from each other, through the distance requirement between lepton ℓ and ℓ', $\Delta R(\ell, \ell') > 0.1$.

The analysis is optimized for heavy sparticle masses, as events are selected with exactly three surviving high-p_T (candidate) leptons, all with $p_T^i > 50$ GeV.[6] We also require one same-flavour opposite-sign (SFOS) pair, choosing the one with invariant mass m_{SFOS} closest to the Z-boson mass. This is further restricted to $|m_{\text{SFOS}} - m_Z| < 10$ GeV for the event to include a Z-boson candidate. The lepton *not* forming the SFOS pair is used to construct m_T, the invariant mass of the lepton with the missing energy,

$$m_T^2 = (E_T^{\text{miss}} + E_\ell)^2 - (p_x^{\text{miss}} + p_x^\ell)^2 - (p_{\text{miss}}^y + p_y^\ell)^2, \tag{5.3}$$

The transverse mass is required to be $m_T > m_W$ to eliminate the dominating Standard Model background from WZ production.

To suppress the less dominant background from $t\bar{t}$ and $t\bar{t} + V$ processes,[7] we veto events with b-tagged jets. Jets are labelled as b-jets if the distance between the b-quark and a candidate jet is $\Delta R(j, b) < 0.4$. We further implement a b-tagging efficiency of 70%, with a jet misidentification probabilty of 1%.

The E_T^{miss} and m_T requirements are used to define three (four) signal regions (SR), A, B, and C (D) for $\mathcal{L} = 300$ (3000) fb^{-1}. The first is designed for maximal discovery reach, while SRB and SRC are designed for maximal exclusion reach. The fourth signal region is defined to improve the sensitivity to high mass scenarios. As we set exclusion limits, SRA is not used in our scan results.

These selection cuts are summarized in table 5.3.

[4]Where η is defined as

$$\eta = \text{atanh}\left(\frac{p_L}{|\mathbf{p}|}\right), \tag{5.1}$$

with p_L being the longitudinal momentum component, i.e. momentum along the beam axis.

[5]That is, final state, charged particles.

[6]Where p_T^i defines the i-th hardest (highest p_T) lepton of the event.

[7]For $V = W, Z$.

Table 5.3: Selection cuts for the search for direct production of $\tilde{\chi}_1^{\pm}$ and $\tilde{\chi}_2^0$ at the LHC.

	Electroweak selection cuts. **Signal: $3\ell + \boldsymbol{E_T^{\text{miss}}}$.**	SRA	SRB	SRC	SRD
1)	Candidate lepton p_T [GeV] $>$		10		
2)	Candidate lepton $\lvert\eta\rvert <$		2.4		
3)	Candidate lepton track isolation S_{p_T} [GeV] $<$		$0.15p_T^j$		
4)	Candidate lepton isolation $\Delta R(\ell, \ell') >$		0.1		
5)	Candidate jet p_T [GeV] $>$		20		
6)	Candidate jet $\lvert\eta\rvert <$		2.5		
7)	$\lvert m_{\text{SFOS}} - m_Z\rvert$ [GeV] $<$		10		
8)	Number of b-tagged jets		0		
9)	Lepton $p_T^{1,2,3}$ [GeV] $>$		50		
10)	E_T^{miss} [GeV] $>$	250	300	400	500
11)	m_T [GeV] $>$	150	200	200	200

5.3.2 Search for squark and gluino pair production

Strongly produced supersymmetry, i.e. squarks and gluinos, is expected to have the highest cross section of all supersymmetry processes at the LHC, provided the sparticles are within kinematic reach. Signals from such production are characterized by many high-p_T jets, large E_T^{miss} and no leptons. The hard jets are expected as they originate from massive gluinos and squarks, while the LSP carries away large amounts of E_T^{miss}. In this section we describe the planned search for gluino and squark pair production.

As in section 5.3.1, candidate leptons, i.e. electrons and muons, are selected with $p_T > 10$ GeV and $|\eta| < 2.4$. Jets are selected with transverse momentum $p_T > 20$ GeV and $|\eta| < 4.5$, and are reconstructed and smeared as described in section 5.3.1. The number of required jets come from the typical signatures illustrated in figure 5.2, with an additional possibility for initial and final state gluon radiation, and radiation from beam remnants. The ten signal regions in the search are labelled by the number of high-p_T jets they contain, with corresponding loose (l), medium (m) and tight (t) cuts on the effective mass m_{eff}. This is defined from the missing energy and transverse momentum of jets,

$$m_{\text{eff}} = E_T^{\text{miss}} + \sum_i^{n_{\text{jets}}} |p_T^i|, \tag{5.4}$$

and is applied to reduce the dominant Standard Model background from V + jets, $t\bar{t}$ and diboson production. A total missing energy of $E_T^{\text{miss}} > 160$ GeV and

$p_T > 60$ GeV for the jets are required in all signal regions, to characterize final states originating from cascade decays of supersymmetric particles. We also require the hardest jet to have $p_T(j_1) > 160$ GeV. This will limit us in the case of mass degeneration of the squark and LSP. If these masses have a 10% fine-tuning, i.e. if $m_{\tilde{q}}/m_{\tilde{\chi}_1^0} = 1.1$, this corresponds to ~ 180 GeV of available kinetic energy to the jet from the squark decay. Increasing the fine-tuning of the sparticle masses to e.g. 8% decreases the available energy for the jet to ~ 150 GeV, hence scenarios of fine-tuning much more than 10% in the squark and LSP masses will be hard to detect with this analyis.

To reject QCD multijet events with large E_T^{miss} from bad jet reconstruction, cuts on the azimuth angle $\Delta\phi$ between the missing energy vector $\mathbf{E}_T^{\text{miss}}$ and two different configurations of jets are imposed. One is defined from the three strongest jets of the event, and is required to be $\Delta\phi(j_1, j_2, j_3) > 0.4$. The second is formed from all jets with $p_T > 40$ GeV, and we impose $\Delta\phi(p_T > 40 \text{ GeV}) > 0.2$. We also impose cuts on $E_T^{\text{miss}}/m_{\text{eff}}$ and the so-called E_T^{miss} *significance*, $E_T^{\text{miss}}/\sqrt{H_T}$. Here, H_T is defined to be the scalar sum of the jet p_Ts,

$$H_T = \sum_i^{n_{\text{jets}}} p_T^i. \tag{5.5}$$

The cut selection is summarized in table 5.4.

5.3.3 LHC analysis validation

To validate our implementation of the analyses of the two previous sections, we do benchmark testing of the points given in [35]. They are defined in terms of parameters, decays, and gauge particle content of the mass eigenstates.

We use `Prospino` for cross section calculations for the electroweak processes in order to compare to [35]. The benchmark point is defined with wino-like $\tilde{\chi}_1^\pm$ and $\tilde{\chi}_2^0$, bino-like $\tilde{\chi}_1^0$, and a mass relation between the lighter chargino and next-to-lightest neutralino $m_{\tilde{\chi}_1^\pm} = m_{\tilde{\chi}_2^0}$.[8] Gluinos, squarks, sleptons and sneutrinos are decoupled, and the produced charginos and neutralinos decay according to figure 5.3(b). We generate all four electroweak benchmark points with 200 000 events.

The results are presented in table 5.5. We see that our validation is in good overall agreement with the original ATLAS results, with a few exceptions at the lowest mass. The reason could e.g. be the lack of electromagnetic smearing. We emphasize that ratios $s_T/s_O < 1$ are conservative as our analyses give fewer signal events.

For the strong processes, we use the NLL+NLO cross sections from `NLL-fast` for gluino pair production, and NLO cross sections from `Prospino` for squark–squark

[8] For the original ATLAS results, the neutralino mass is $m_{\tilde{\chi}_1^0} = 0$, but as this gives no open decay channel for the lightest chargino in `PYTHIA`, it is here set to 1 GeV.

Table 5.4: Selection cuts for the ten signal regions in the search for jets and missing energy [35]. Signal regions $2j, 3j$ and $4jl$ target squark production, and have two cuts on m_{eff}. The first is designed for scenarios where the gluino is completely decoupled, the other for the case in which $m_{\tilde{g}} = 4.5$ TeV. In the scan we make use of the latter.

	Strong selection cuts. **Signal: jets + $\boldsymbol{E_T^{\text{miss}}}$.**	Signal region									
		2jl	2jm	3j	4jl	4jm	4jt	5j	6jl	6jm	6jt
1)	Number of leptons	0	0	0	0	0	0	0	0	0	0
1)	$p_T(j_1)$ [GeV] $>$	160	160	160	160	160	160	160	160	160	160
2)	$N_{\text{jets}}(p_T > 60 \text{ GeV}) \geq$	2	2	3	4	4	4	5	6	6	6
3)	E_T^{miss} [GeV] $>$	160	160	160	160	160	160	160	160	160	160
4)	$\Delta\phi(j, \mathbf{E}_T^{\text{miss}})_{\text{min}} >$	$0.4(j_1, j_2, j_3)$ and 0.2(all jets with $p_T > 40$ GeV)									
		$\boldsymbol{\mathcal{L} = 300 \text{ fb}^{-1}}$									
5)	$E_T^{\text{miss}}/m_{\text{eff}} >$	-	-	0.3	0.4	0.25	-	0.20	0.3	0.15	0.2
6)	$E_T^{\text{miss}}/\sqrt{H_T}$ [GeV$^{1/2}$] $>$	8	15	-	-	-	10	-	-	-	-
7)	m_{eff} [GeV] $>$	3600	(3100, 4300)	(3600, 3000)	(3000, 2200)	3200	3400	3000	2800	3400	3400
		$\boldsymbol{\mathcal{L} = 3000 \text{ fb}^{-1}}$									
8)	$E_T^{\text{miss}}/m_{\text{eff}} >$	-	-	0.3	0.35	0.25	-	0.25	0.25	0.35	0.15
9)	$E_T^{\text{miss}}/\sqrt{H_T}$ [GeV$^{1/2}$] $>$	8	15	-	-	-	10	-	-	-	-
10)	m_{eff} [GeV] $>$	(4500, 4000)	(4500, 4900)	4000	(4000, 3800)	4000	4500	4000	3400	3500	5000

Table 5.5: Benchmark testing of expected number of signal events in direct production of $\tilde{\chi}_1^{\pm}$ and $\tilde{\chi}_2^0$ at the LHC. Errors are statistical only.

	$\mathcal{L} = 300$ fb^{-1}			$\mathcal{L} = 3000$ fb^{-1}				
$m(\tilde{\chi}_2^0, \tilde{\chi}_1^0)$ [GeV]	SRA	SRB	SRC	SRA	SRB	SRC	SRD	
$(400, 1)$	42.4 ± 2.9	27.6 ± 2.3	10.8 ± 1.5	424.5 ± 28.8	275.8 ± 23.2	107.6 ± 14.5	52.8 ± 10.2	s_T
	38.5 ± 0.6	20.1 ± 0.5	5.47 ± 0.23	407 ± 6	224 ± 5	67.9 ± 2.6	19.7 ± 1.4	s_O
	1.1 ± 0.1	1.4 ± 0.1	2.0 ± 0.3	1.0 ± 0.1	1.2 ± 0.1	1.6 ± 0.2	2.7 ± 0.5	s_T/s_O
$(600, 1)$	20.2 ± 0.8	16.1 ± 0.7	8.7 ± 0.5	201.9 ± 8.4	161.4 ± 7.5	86.9 ± 5.5	40.9 ± 3.8	s_T
	19.40 ± 0.20	14.69 ± 0.17	7.76 ± 0.12	194.8 ± 2.0	148.9 ± 1.7	81.6 ± 1.3	33.5 ± 0.8	s_O
	1.04 ± 0.04	1.1 ± 0.1	1.1 ± 0.1	1.04 ± 0.04	1.1 ± 0.1	1.1 ± 0.1	1.2 ± 0.1	s_T/s_O
$(800, 1)$	6.6 ± 0.2	5.7 ± 0.2	4.1 ± 0.2	66.1 ± 2.3	56.7 ± 2.2	41.1 ± 1.8	24.5 ± 1.4	s_T
	6.97 ± 0.06	5.90 ± 0.06	4.21 ± 0.05	69.6 ± 0.6	59.1 ± 0.6	42.4 ± 0.5	25.2 ± 0.4	s_O
	0.94 ± 0.03	0.96 ± 0.04	0.98 ± 0.05	0.95 ± 0.03	0.96 ± 0.04	0.97 ± 0.05	0.97 ± 0.06	s_T/s_O
$(1000, 1)$	2.1 ± 0.1	1.8 ± 0.1	1.4 ± 0.1	20.9 ± 0.7	18.3 ± 0.7	13.6 ± 0.6	9.8 ± 0.5	s_T
	2.31 ± 0.02	2.05 ± 0.02	1.64 ± 0.02	22.94 ± 0.19	20.42 ± 0.18	16.36 ± 0.16	11.55 ± 0.14	s_O
	0.90 ± 0.03	0.89 ± 0.03	0.83 ± 0.04	0.91 ± 0.03	0.90 ± 0.03	0.83 ± 0.04	0.85 ± 0.04	s_T/s_O
SM background	12.4 ± 0.4	5.89 ± 0.28	2.35 ± 0.16	239 ± 6	75.6 ± 3.3	27.7 ± 1.8	10.3 ± 1.1	[35]

and squark–anti-squark production, assuming a gluino mass of 4.5 TeV. The benchmarks defined by ATLAS in [35] have 100% branching fraction of the decaying sparticles according to figure 5.2. We generate one million events in the benchmark points with degenerate masses, and 100 000 otherwise.

The validation for gluino pair production is presented in table 5.6, and for squark–squark + squark–anti-squark production in table 5.7. The mass degenerate squark point at $\mathcal{L} = 300$ fb^{-1} has a relative large disagreement, especially pronounced in the 3j and 4jl signal regions. We did not succeed to uncover the reason for this discrepancy. However, the other benchmark points seem to be in relatively good compliance.

The errors in tables 5.5, 5.6 and 5.7 are statistical only, and calculated under the very reasonable the assumption that the two results (testing and original) are uncorrelated. Hence, the error of the ratio s_T/s_O is calculated as

$$\delta\left(\frac{s_T}{s_O}\right) = \frac{s_T}{s_O}\sqrt{\left(\frac{\delta s_T}{s_T}\right)^2 + \left(\frac{\delta s_O}{s_O}\right)^2}. \tag{5.6}$$

5.4 Supersymmetry production at the ILC

This section is a summary of the search for sleptons and charginos at the ILC, presented in [1]. These searches are motivated by the analyses in [36], searching for the signatures in figure 5.3. Collisions are assumed to be at the centre-of-mass energies $\sqrt{s} = 0.5$ TeV and $\sqrt{s} = 1$ TeV, and results are presented for an integrated luminosity of $\mathcal{L} = 100$ fb^{-1}.

5.4.1 Detector simulation

For the calorimeter simulation, the covered regions are $-4 < \eta < 4$, with cell sizes $\Delta\eta \times \Delta\phi = 0.05 \times 0.05$. Both the electromagnetic E_{em} and hadronic E_h energy is smeared according to the energy resolutions given in [36]

$$\frac{\sigma_{\text{em}}}{E_{\text{em}}} = \frac{0.15}{\sqrt{E_{\text{em}}}} \oplus 0.01, \tag{5.7}$$

and

$$\frac{\sigma_h}{E_h} = \frac{0.5}{\sqrt{E_h}} \oplus 0.02. \tag{5.8}$$

Here, σ is the standard deviation of the energy smearing, and the $\oplus$ denotes addition in quadrature. The smeared energy is then given by $E_{\text{smear}} = E + \sigma \cdot N(0,1)$, where E is the unsmeared energy, and $N(0,1)$ is a normal distribution around zero with standard deviation one.

The term of the resolution proportional to $1/\sqrt{E}$ is the *stochastic term*, and simulates the fluctuations related to the physical development of the electromagnetic and hadronic showers. The constant term simulates energy independent

Table 5.6: Benchmark testing of extepcted number of signal events for $\tilde{g}\tilde{g}$ production with decoupled squarks at the LHC. Errors are statistical only.

(a)

Gluino production	$\mathcal{L} = 300$ fb^{-1}										
$m(\tilde{g}, \tilde{\chi}_1^0)$ [GeV]	2jl	2jm	3j	4jl	4jm	4jt	5j	6jl	6jm	6jt	
	6.5 ± 0.3	1.5 ± 0.1	13.1 ± 0.4	15.9 ± 0.4	4.7 ± 0.2	3.6 ± 0.2	3.0 ± 0.2	1.4 ± 0.1	0.6 ± 0.1	0.6 ± 0.1	s_T
$(1425, 1400)$	12.6 ± 1.2	3.7 ± 0.6	8.5 ± 1.0	7.5 ± 0.9	8.1 ± 0.9	6.2 ± 0.8	4.7 ± 0.7	1.6 ± 0.4	1.05 ± 0.33	1.05 ± 0.33	s_O [35]
	0.5 ± 0.1	0.4 ± 0.1	1.5 ± 0.2	2.1 ± 0.3	0.6 ± 0.1	0.6 ± 0.1	0.6 ± 0.1	0.9 ± 0.2	0.6 ± 0.2	0.6 ± 0.2	s_T/s_O
	85.2 ± 0.7	14.9 ± 0.3	61.4 ± 0.6	17.9 ± 0.3	72.7 ± 0.7	99.8 ± 0.8	90.6 ± 0.8	24.6 ± 0.4	48.3 ± 0.6	37.4 ± 0.5	s_T
$(1950, 1)$	68.8 ± 0.6	12.48 ± 0.27	35.4 ± 0.5	18.41 ± 0.33	70.6 ± 0.7	102.4 ± 0.8	83.4 ± 0.7	25.6 ± 0.4	44.6 ± 0.5	35.4 ± 0.5	s_O [35]
	1.24 ± 0.02	1.20 ± 0.04	1.74 ± 0.03	0.97 ± 0.03	1.03 ± 0.01	0.97 ± 0.01	1.09 ± 0.01	0.96 ± 0.02	1.08 ± 0.02	1.06 ± 0.02	s_T/s_O
SM background	183 ± 5	23.6 ± 1.7	64.9 ± 2.9	72.6 ± 3.1	125 ± 4	300 ± 8	138 ± 5	38.3 ± 2.5	28.1 ± 2.2	18.8 ± 1.7	[35]

(b)

Gluino production	$\mathcal{L} = 3000$ fb^{-1}										
$m(\tilde{g}, \tilde{\chi}_1^0)$ [GeV]	2jl	2jm	3j	4jl	4jm	4jt	5j	6jl	6jm	6jt	
	4.9 ± 0.7	4.1 ± 0.6	21.4 ± 1.4	15.3 ± 1.2	12.2 ± 1.1	4.5 ± 0.7	5.1 ± 0.7	5.8 ± 0.8	4.3 ± 0.6	0.6 ± 0.2	s_T
$(1425, 1400)$	10.5 ± 3.3	15 ± 4	48 ± 7	19 ± 4	23 ± 5	8.4 ± 3.0	14 ± 4	7.4 ± 2.8	5.3 ± 2.4	0.00 ± 0.00	s_O [35]
	0.5 ± 0.2	0.3 ± 0.1	0.4 ± 0.1	0.8 ± 0.2	0.5 ± 0.1	0.5 ± 0.2	0.4 ± 0.1	0.8 ± 0.3	0.8 ± 0.4	–	s_T/s_O
	48.4 ± 1.8	72.3 ± 2.2	126.5 ± 2.9	99.3 ± 2.5	188.7 ± 3.5	130.2 ± 3.0	157.0 ± 3.2	257.1 ± 4.1	66.8 ± 2.1	24.1 ± 1.2	s_T
$(1950, 1)$	55.8 ± 1.8	43.4 ± 1.6	163.9 ± 3.1	75.2 ± 2.1	191.0 ± 3.4	159.1 ± 3.1	152.7 ± 3.0	257 ± 4	73.4 ± 2.1	36.0 ± 1.5	s_O [35]
	0.87 ± 0.04	1.7 ± 0.1	0.77 ± 0.02	1.32 ± 0.05	0.99 ± 0.03	0.82 ± 0.02	1.03 ± 0.03	1.00 ± 0.02	0.91 ± 0.04	0.67 ± 0.04	s_T/s_O
SM background	76 ± 10	72 ± 9	269 ± 18	104 ± 11	176 ± 14	292 ± 23	99 ± 11	141 ± 14	48 ± 8	5.6 ± 2.4	[35]

Table 5.7: Benchmark testing of expected number of signal events for squark–squark and squark–anti-squark production at the LHC, with a gluino mass of $m_{\tilde{g}} = 4.5$ TeV. Errors are statistical only.

(a)

Squark production	$\mathcal{L} = 300$ fb^{-1}										
$m(\tilde{q}, \tilde{\chi}_1^0)$ [GeV]	2jl	2jm	3j	4jl	4jm	4jt	5j	6jl	6jm	6jt	
$(1050, 900)$	8.1 ± 0.4	2.0 ± 0.2	23.9 ± 0.8	37.0 ± 0.9	13.5 ± 0.6	9.4 ± 0.5	13.0 ± 0.6	7.9 ± 0.4	3.0 ± 0.3	3.0 ± 0.3	s_T
	2.5 ± 1.1	1.5 ± 0.9	2.0 ± 1.0	3.5 ± 1.3	6.4 ± 1.8	4.0 ± 1.4	7.4 ± 1.9	3.5 ± 1.3	1.5 ± 0.9	1.5 ± 0.9	s_O [35]
	3.2 ± 1.4	1.4 ± 0.8	11.9 ± 6.0	10.6 ± 3.9	2.1 ± 0.6	2.3 ± 0.8	1.8 ± 0.5	2.3 ± 0.8	2.0 ± 1.2	2.0 ± 1.2	s_T/s_O
$(2250, 1)$	151.3 ± 0.7	65.9 ± 0.5	112.8 ± 0.6	37.0 ± 0.4	51.5 ± 0.4	51.6 ± 0.4	22.2 ± 0.3	5.6 ± 0.1	5.9 ± 0.1	5.6 ± 0.1	s_T
	141.7 ± 0.9	60.1 ± 0.6	82.1 ± 0.7	39.2 ± 0.5	59.3 ± 0.6	58.9 ± 0.6	28.4 ± 0.4	7.84 ± 0.21	8.00 ± 0.21	7.57 ± 0.20	s_O [35]
	1.07 ± 0.01	1.10 ± 0.01	1.37 ± 0.01	0.94 ± 0.01	0.87 ± 0.01	0.88 ± 0.01	0.78 ± 0.01	0.72 ± 0.03	0.73 ± 0.03	0.74 ± 0.03	s_T/s_O
SM background	183 ± 5	23.6 ± 1.7	64.9 ± 2.9	72.6 ± 3.1	125 ± 4	300 ± 8	138 ± 5	38.3 ± 2.5	28.1 ± 2.2	18.8 ± 1.7	[35]

(b)

Squark production	$\mathcal{L} = 3000$ fb^{-1}										
$m(\tilde{q}, \tilde{\chi}_1^0)$ [GeV]	2jl	2jm	3j	4jl	4jm	4jt	5j	6jl	6jm	6jt	
$(1050, 900)$	5.2 ± 1.1	5.4 ± 1.1	31.5 ± 2.8	28.2 ± 2.6	26.5 ± 2.5	8.9 ± 1.5	16.6 ± 2.0	28.0 ± 2.6	12.4 ± 1.7	1.5 ± 0.6	s_T
	5 ± 5	10 ± 7	15 ± 9	10 ± 7	15 ± 9	15 ± 9	10 ± 7	25 ± 11	5 ± 5	5 ± 5	s_O [35]
	1.0 ± 1.1	0.5 ± 0.4	2.1 ± 1.3	2.8 ± 2.0	1.8 ± 1.1	0.6 ± 0.4	1.7 ± 1.2	1.1 ± 0.5	2.5 ± 2.5	0.3 ± 0.3	s_T/s_O
$(2250, 1)$	200.1 ± 2.6	167.3 ± 2.4	540.0 ± 4.3	258.0 ± 2.9	278.0 ± 3.0	162.2 ± 2.3	103.8 ± 1.8	51.5 ± 1.3	33.6 ± 1.0	9.8 ± 0.5	s_T
	186 ± 3	208.2 ± 3.4	558 ± 6	254 ± 4	320 ± 4	182.6 ± 3.2	136.4 ± 2.7	75.2 ± 2.0	50.9 ± 1.7	13.6 ± 0.9	s_O [35]
	1.08 ± 0.02	0.80 ± 0.02	0.97 ± 0.01	1.02 ± 0.02	0.87 ± 0.01	0.89 ± 0.02	0.76 ± 0.02	0.69 ± 0.02	0.66 ± 0.03	0.72 ± 0.06	s_T/s_O
SM background	76 ± 10	72 ± 9	269 ± 18	104 ± 11	176 ± 14	292 ± 23	99 ± 11	141 ± 14	48 ± 8	5.6 ± 2.4	[35]

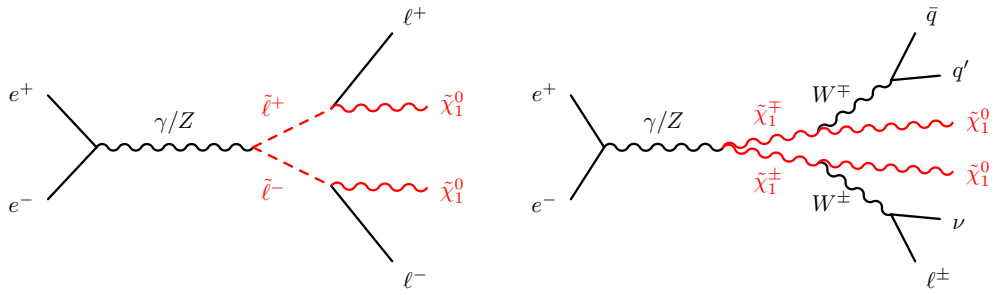

(a) Slepton. (b) Chargino.

Figure 5.3: Example of slepton and chargino production and decay at the ILC.

contributions, e.g. imperfections in the mechanical structure and geometry of the detector. The constant term becomes important at high energies, while the stochastic term dominates at low energies.

The electromagnetic smearing of leptons, that is electrons and muons in the event, happens in the analysis itself, while the hadronic smearing is implemented by changing jet reconstruction subroutine `PYCELL` of `PYTHIA 6`. This has been modified to cluster on energy rather than transverse energy to enable comparison with results in [36]. The modified code is given in appendix C. `PYCELL` is used with a fixed cone size of $\Delta R = 0.6$, and labels jets from clusters with $E > 5$ GeV and $|\eta| < 2.5$.

5.4.2 Search for slepton production

A typical signal of slepton pair production at the ILC can be a pair of opposite sign same flavour leptons and E_T^{miss} as illustrated in figure 5.3(a). In this section, we describe the search for these signatures as investigated in [36]. The reach is evaluated by running with right-polarized electron beams, $P_L(e^-) = -0.9$, to minimize Standard Model W^+W^- background, and maximize pair production of right handed sleptons. To reduce more of the W^+W^- background, a missing energy of $E_T^{\text{miss}} > 25$ GeV is required, and events with jets are vetoed.

Candidate leptons, that is electrons and muons, are selected with $E > 5$ GeV and $|\eta| < 2.5$, and are classified as isolated if the visible activity within a cone of $\Delta R = 0.5$ about the lepton direction is less than $\max(E/10\text{ GeV}, 1\text{ GeV})$.

It has been shown in [56] that a range of backgrounds[9] are efficiently removed by the cuts listed in table 5.8, at least for $\sqrt{s} = 0.5$ TeV. The bulk of these backgrounds is removed also at $\sqrt{s} = 1$ TeV, though not completely eliminated.

[9]Such as $e^+e^- \to \nu\nu Z$, $e^+e^- \to e^+e^- Z$, $e^+e^- \to e^\pm \nu W^\mp$ and $e^+e^- \to e^+e^- W^+W^-$.

Table 5.8: Selection cuts for slepton pair production. The lepton cuts must be fulfilled for both ℓ^+ and ℓ^-.

	Slepton selection cuts. **Signal: $\boldsymbol{\ell^+\ell^- + E_T^{\text{miss}}}$.**	
1)	$E_\ell < 200$ GeV.	Energy E_ℓ of lepton.
2)	20 GeV $< E_{\text{vis}} < \sqrt{s} - 100$ GeV.	All visible energy E_{vis} in event.
3)	$\lvert m_{\ell\ell} - m_Z \rvert > 10$ GeV.	Invariant mass $m_{\ell\ell}$ of lepton pair.
4)	$\lvert \cos\theta_\ell \rvert < 0.9$.	Polar angle θ with beam axis for lepton.
5)	$-Q_\ell \cos\theta_\ell < 0.75$.	Charge Q and polar angle θ of lepton.
6)	$\theta_{\text{acop}} > \pi/6$.	Acoplanar angle of leptons.
7)	$E_T^{\text{miss}} > 25$ GeV.	Missing energy of event.
8)	No jets.	Discard all events with jet activity.

The visible energy of the event is required in the range 20 GeV $< E_{\text{vis}} < \sqrt{s} - 100$ GeV, and both lepton energies must have $E_\ell < 200$ GeV to suppress backgrounds from W^+W^- production with leptonic decays.

To avoid signals from background with Z-production, $|m_{\ell\ell} - m_Z| > 10$ GeV is required, where $m_{\ell\ell}$ is the invariant mass of the lepton pair. Further, the polar angle θ with the beam axis must fulfill $|\cos\theta_\ell| < 0.9$ for both leptons. This prevents mismeasurements of the missing energy due to leptons going down the beam pipe, and therefore suppresses possible fake signals. A more stringent cut, $-Q_\ell \cos\theta_\ell < 0.75$, eliminates events where we suspect the final state leptons to come from the beam itself. To reduce the dominant portion of the $e^+e^-W^+W^-$ background from $\gamma\gamma$-collisions, a cut on the acoplanar angle between the two leptons is introduced, $\theta_{\text{acop}} > \pi/6$, with the acoplanar angle defined as

$$\theta_{\text{acop}} \equiv \pi - \arccos(\hat{p}_x^1 \hat{p}_x^2 + \hat{p}_y^1 \hat{p}_y^2), \quad \hat{p}_x = \frac{p_x}{|\mathbf{p}|}, \tag{5.9}$$

where $\hat{p}_x^i$ referes to lepton i for $i = 1, 2$.

5.4.3 Search for chargino production

The chargino search targets chargino pair production with one hadronic and one leptonic W-boson decay, as illustrated in figure 5.3(b). The signal one may search for is then one isolated lepton, two jets and missing energy. The complete list of selection cuts is given in table 5.9. The signal samples are generated without beam polarization as in [36].

As for the typical slepton signal, an important Standard Model background to the chargino signal is W^+W^- production, and it is desirable to suppress as

Table 5.9: Selection cuts for chargino production. The jet cuts must be fulfilled for both jets.

	Chargino selection cuts. **Signal: $1\ell + 2j + E_T^{\text{miss}}$.**	
1)	$20\text{ GeV} < E_{\text{vis}} < \sqrt{s} - 100\text{ GeV}$.	All visible energy E_{vis} in event.
2)	If $E_{jj} > 200$ GeV, then $m_{jj} < 68$ GeV.	Total energy E_{jj} and invariant mass m_{jj} of jets.
3)	$E_T^{\text{miss}} > 25$ GeV.	Missing energy of event.
4)	$\lvert m_{\ell\nu} - m_W \rvert > 10$ GeV.	Invariant mass $m_{\ell\nu}$ of lepton and neutrino.
5)	$\lvert \cos\theta_j \rvert < 0.9$.	Polar angle θ_j with beam axis for jet.
6)	$\lvert \cos\theta_\ell \rvert < 0.9$.	Polar angle θ_ℓ with beam axis for lepton.
7)	$-Q_\ell \cos\theta_\ell < 0.75$.	Charge Q_ℓ of lepton.
8)	$Q_\ell \cos\theta_{jj} < 0.75$.	Polar angle θ_{jj} of jet momentum vector sum.
9)	$\theta_{\text{acop}}^{WW} > \pi/6$.	Acoplanar angle of WW-pair.

much of this as possible. Therefore, it is required that $|m_{\ell\nu} - m_W| > 10$ GeV, where $m_{\ell\nu}$ is the invariant mass of the lepton with the neutrino, where the latter is represented by the missing energy of the event. Further, if the total jet energy $E_{jj} > 200$ GeV, it is required that the invariant mass of the jets, $m_{jj} < 68$ GeV. It is also required that the acoplanar angle of the reconstructed W-pair is $\theta_{\text{acop}}^{WW} > \pi/6$. As in the search for sleptons, the visible energy of the event is required to be $20\text{ GeV} < E_{\text{vis}} < \sqrt{s} - 100\text{ GeV}$ and the total missing energy $E_T^{\text{miss}} > 25$ GeV. The cut on the polar angle of both the jet θ_j and the isolated lepton θ_ℓ yields $|\cos\theta_j|, |\cos\theta_\ell| < 0.9$. Again, we impose $-Q_\ell \cos\theta_\ell, Q_\ell \cos\theta_{jj} < 0.75$, where the polar angle θ_{jj} is the angle between the beam axis and the momentum vector sum of two jets. This supresses events where we are in risk of loosing particles down the beam pipe.

5.4.4 Extended search for chargino production

To extend the reach of the ILC for chargino production in areas where the chargino and neutralino are almost degenerate in mass, a new set of selection cuts are introduced in [36], given here in table 5.10.

The low energy release of the chargino decays expected in this scenario is reflected in the stringent cut on the visible energy, $20\text{ GeV} < E_{\text{vis}} < 100\text{ GeV}$. This also removes the bulk of Standard Model background such as W^+W^-, ZZ and $t\bar{t}$ production. The upper bound is chosen to lie well over the endpoint of the signal distribution for the cut to be valid also in areas where the mass gap of the charginos and neutralinos are larger. To reduce possible backgrounds from

Table 5.10: Selection cuts for extended chargino production. The lepton isolation cuts are those defined in the beginning of section 5.4.1.

	Chargino extended selection cuts. **Signal: $1\ell + 2j + \boldsymbol{E}_{\boldsymbol{T}}^{\mathbf{miss}}$.**	
1)	$\lvert\eta\rvert, E, \Delta R$.	Lepton (isolation) cuts.
2)	20 GeV $< E_{\text{vis}} <$ 100 GeV.	All visible energy E_{vis} in event.
3)	$\cos\phi_{jj} > -0.6$.	Transverse dijet opening angle ϕ_{jj}.
4)	$m_{\ell j} > 5$ GeV.	Invariant mass $m_{\ell j}$ of lepton with jet.

$\gamma\gamma \to c\bar{c}, b\bar{b}$,[10] a cut on the transverse dijet opening angle,

$$\cos\phi_{jj} = \frac{\mathbf{p_1} \cdot \mathbf{p_2}}{|\mathbf{p_1}||\mathbf{p_2}|}, \tag{5.10}$$

where $\mathbf{p} = (p_x, p_y)$, is required to be $\cos\phi_{jj} > -0.6$. The SM b-quarks will typically emerge back-to-back in the transverse plane, and the distribution in $\cos\phi_{jj}$ for this process peaks at $\cos\theta_{jj} \sim -1$ [36]. If the two jets come from a supersymmetry decay cascade such as in figure 5.3(b), $\cos\phi_{jj}$ will peak at $\cos\theta_{jj} \sim 1$ as the jets are the decay products of a W-boson. Some additional background removal at low cost to signal is gained by requiring $m_{\ell j} > 5$ GeV, where $m_{\ell j}$ is the invariant mass of the isolated lepton with the closest jet in space angle. This also targets Standard Model events with leptonic b-decays because of the b-quark mass $m_b \simeq 5$ GeV.

5.4.5 ILC analysis validation

The only benchmark point shown for supersymmetry production at the ILC in [36] is for the chargino extended analysis, an mSUGRA point

$$(m_0, m_{1/2}, A_0, \tan\beta, \text{sgn}(\mu)) = (4625 \text{ GeV}, 885 \text{ GeV}, 0, 30, +). \tag{5.11}$$

For this benchmark point we have available the cut-flow of the analysis in terms of the effective cross section $\sigma\mathcal{E}$. The validation of this analysis is given in table 5.11 for 100 000 generated events, and is in quite good agreement with [36], although an overestimation of the signal events is the tendency for this benchmark point.

5.5 Discussion of uncertainties

The errors given in the benchmark point tests are statistical only, and originate from the detection efficiency $\mathcal{E}$ due to the Monte Carlo sampling of events. In

[10] Where the incoming particles escape detection due to scattering at small angles with the beam direction.

Table 5.11: Effective cross section $\sigma_{\text{eff}} = \mathcal{E}\sigma$ for the chargino extended benchmark point from [36] at $\sqrt{s} = 0.5$ TeV. Errors are statistical and from the testing, as they are not specified in [36].

Cut		σ^T_{eff} [fb] [1]	σ^O_{eff} [fb]	$\sigma^T_{\text{eff}}/\sigma^O_{\text{eff}}$
1)	$\lvert\eta\rvert, E, \Delta R$	15.81 ± 0.29	16.2	0.98 ± 0.02
2)	E_{vis}	15.52 ± 0.29	14.4	1.08 ± 0.02
3)	$\cos\phi_{jj}$	14.10 ± 0.27	13.5	1.04 ± 0.02
4)	$m_{\ell j}$	13.96 ± 0.27	12.0	1.16 ± 0.02

reality, however, the error in the number of signal events s comes not only from our estimate of the efficiency, but also the luminosity and cross section. For simplicity, we will ignore the uncertainty in the luminosity since it is typically small, and we can express the total error on s as

$$\delta s = s\sqrt{\left(\frac{\delta\sigma}{\sigma}\right)^2 + \left(\frac{\delta\mathcal{E}}{\mathcal{E}}\right)^2}. \tag{5.12}$$

The estimate of error in cross section from (the absence of) higher order corrections is often referred to as the *renormalization* or *factorization error*, and with both NLO and NLL corrections included, it has shown to be as low as 10% of the total cross section for strong production [51]. However, we need also to include the PDF and α_s uncertainties, which give rise to the dominant cross section errors in the case of strong processes. These increase with increasing sparticle mass, since the PDFs are most poorly constrained at high scales and high parton x.

As an example with gluino pair production at 14 TeV with a gluino mass of $m_{\tilde{g}} = 3$ TeV, `NLL-fast` gives errors of $(+48.0\%, -28.4\%)$ and $(+10.2\%, -6.6\%)$ from the PDFs and α_s, respectively. The same analysis for squark pair production with $m_{\tilde{q}} = 3$ TeV gives the errors $(+61.9\%, -36.5\%)$ and $(+13.9\%, -9.1\%)$. This means the total error budget from PDFs and α_s — in a worst case scenario with heavy squarks and gluinos — will not drop much below 50% and 64% for gluinos and squarks, respectively. Reducing the gluino and squark masses to 1 TeV, the total error is reduced to $\sim 16\%$ in both cross sections.

In the case of electroweak processes, the cross section error is much smaller due to the dependence on α rather than α_s. This means δs at the ILC will be dominated by the statistical error on the efficiency in the scan, while at the LHC, $\delta\sigma$ can be a dominating effect in regions with large squark and gluino masses.

However, there are regions of the parameter space where the uncertainty in efficiency will dominate also for the LHC results. These are the areas where the efficiency is very low, giving a large relative error $\delta\mathcal{E}/\mathcal{E} \simeq 1/\sqrt{N_{\text{acc}}}$. The last square of eq. (5.12) would be close to unity, and one single accepted event would

for instance give $\delta s \simeq s$, but with potentially large s due to large cross section (and luminosity). Exclusion limits in these areas will fluctuate due to the poor efficiencies, giving undesired effects caused by the statistical limitations.

While the errors discussed here can be sizeable, they are difficult to reduce significantly. The error on the efficiency would require an infeasible amount of statistics to eliminate, while the cross section errors can only be reduced by future improved knowledge of PDFs from LHC measurements. Although the above errors are known to a certain degree, it is hard to predict how they will impact our calculation of the likelihood. Due to the time constraints inherant to a thesis, we have been unable to include these errors properly in the statistical discussion of parameter estimation and limit setting. We leave this for future work.

Chapter 6

Results and discussion

We will now present and discuss our results from the simulation of future searches for supersymmetry at the high-luminosity Large Hadron Collider. In each of the three scenarios studied,[1] we discuss our results for the exclusion limits at the 95% CL, and what parameter values, masses and naturalness scores they disfavour. Apart from giving the naturalness reach in terms of the minimum non-excluded score, we also give a more sophisticated evaluation of the reach by interpreting naturalness posterior distributions, and their corresponding KL-measures.

As the focus of this thesis is on the HL-LHC, we refer the reader to [1] for a more thorough discussion of the ILC results for the same scenarios.

6.1 mSUGRA10

Within the chosen prior ranges for this scenario, the calculated Higgs mass is too small to reach the measured Higgs mass, but we include this scenario to enable comparison with the results by Allanach et al. from [2], given here in figure 6.1 for ease of reference.

6.1.1 Exclusion limits

In figure 6.2 we give the 95% CL exclusion limits in the mSUGRA10 scenario. The red lines represent the search for the production of gluinos and squarks ($\tilde{g}\tilde{g}/\tilde{q}\tilde{q}^*$) and charginos and neutralinos ($\tilde{\chi}_1^\pm\tilde{\chi}_2^0$) for the two integrated luminosities $\mathcal{L} = 300$ fb^{-1} and $\mathcal{L} = 3000$ fb^{-1}. The light green and light blue lines represent the slepton ($\tilde{\ell}\tilde{\ell}^*$), chargino ($\tilde{\chi}^+\tilde{\chi}^-$) and extended chargino searches ($\tilde{\chi}^+\tilde{\chi}^-$E) at the ILC at 0.5 TeV and 1 TeV, respectively. We have also included some mass contours of interest, seen in black for the Higgs, yellow for the LSP, turquoise for

[1] Defined in section 5.1, table 5.1.

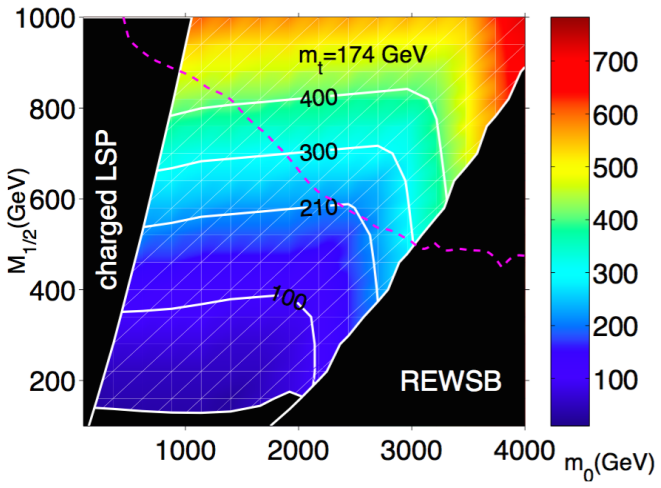

Figure 6.1: Naturalness values in the mSUGRA10 mass plane with predicted discovery reach for the $\sqrt{s} = 14$ TeV LHC with 10 fb^{-1} (dashed line). Taken from [2].

the lighter chargino, dark blue for the slepton[2], dark green for the squark[3] and purple for the gluino.

We observe that the planned search for strongly produced supersymmery at the HL-LHC successfully excludes large squark and gluino masses, where the highest reach is obtained with $\mathcal{L} = 3000$ fb^{-1}, represented by the dashed red line. It excludes all values of $m_{1/2} \lesssim 800$ GeV, corresponding to all gluino masses below ~ 1.9 TeV and all squark masses below ~ 2.1 TeV, which is close to the kinematic reach at $\sqrt{s} = 14$ TeV. It is evident that this exclude higher masses than in [2], as in figure 6.1 we see that their bound excludes only $m_{1/2} \lesssim 460$ GeV. Our bound is similar to that of Allanach et al. in that both decrease with increasing m_0, but the shapes are otherwise rather dissimilar. Allanach et al. use an integrated luminosity of $\mathcal{L} = 10$ fb^{-1} and have set a discovery limit, in contrast to our exclusion limit with an integrated luminosity of $\mathcal{L} = 3000$ fb^{-1}. These are good reasons for our increased reach and the different m_0 dependence in the two results. Another important difference between the two results is the shift in the no REWSB-area, due to the improvements of RGE codes since the year 2000, and possibly the different RGE codes used, `SOFTSUSY` versus `ISAJET`.

As the squark masses are driven by the m_0 parameter, they will only be kinematically accessible at sufficiently low m_0. The increasing squark production with decreasing m_0 is evident in the small bumps in the strong exclusion bounds to the left in figure 6.2. Thus, the bound at $m_0 \gtrsim 1.1$ TeV mainly represents

[2]The slepton mass is minimized over the left- and right-handed selectron.

[3]The squark mass is the average of the two first generations, as this is where we expect to have the best reach. Stop and sbottom production often leads to leptons in the final state, thus the event is rejected by the jets and missing energy search described in section 5.3.2.

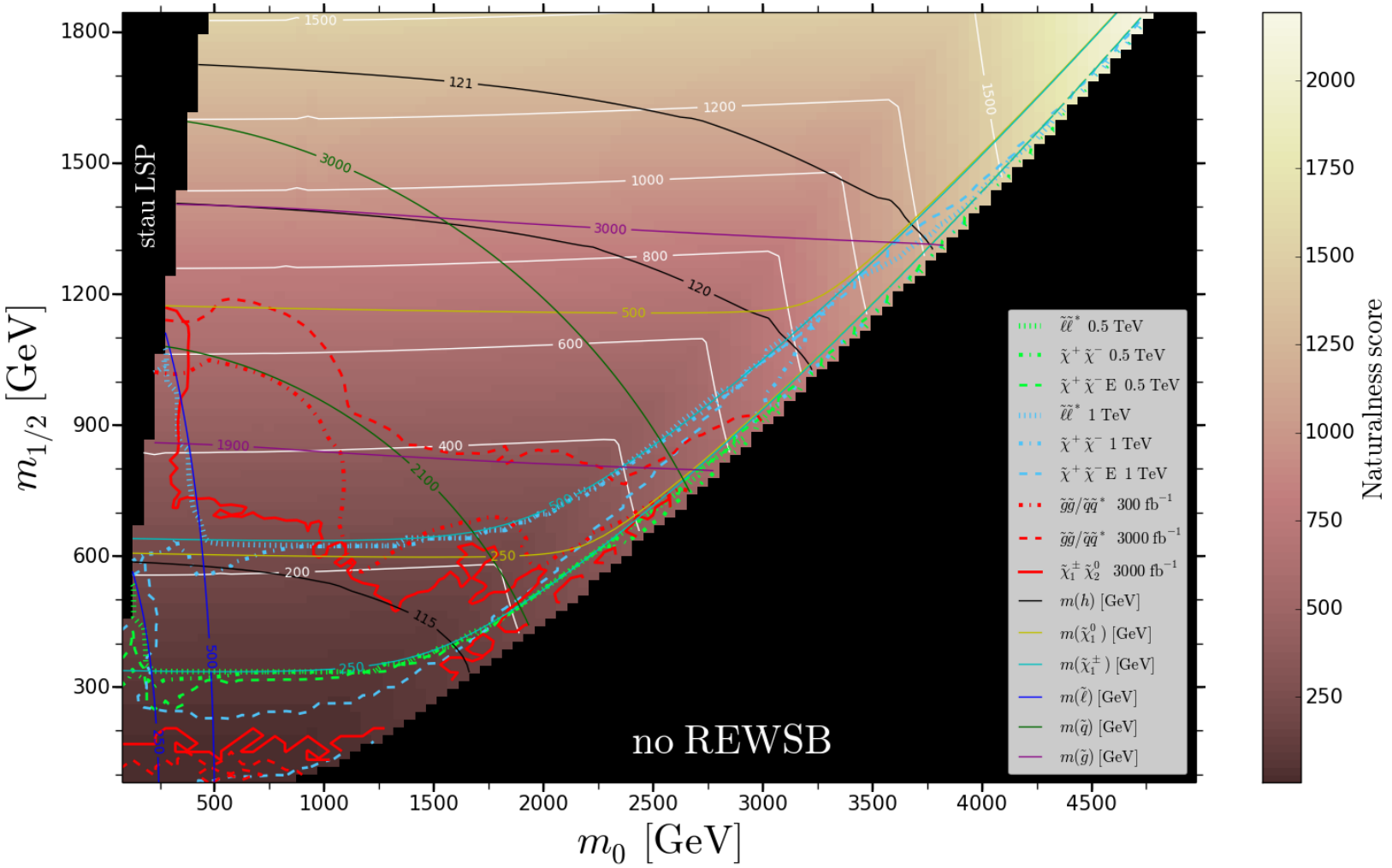

Figure 6.2: The mSUGRA10 scenario with $A_0 = 0$, $\tan\beta = 10$, $\mathrm{sgn}(\mu) = +$. The white lines are contours for the naturalness score.

gluino production. The limits roughly follow the isocurves of the gluino mass when $m_{\tilde{g}} < m_{\tilde{q}}$, and the isocurves of the squark mass when $m_{\tilde{q}} < m_{\tilde{g}}$. We observe that the gluino mass is driven slightly down as m_0 increases, due to loop effects from squarks in the RGE running of the gluino mass parameter M_3. The strong search with $\mathcal{L} = 300$ fb^{-1}, given as the red dashed-dot line, follows the same pattern as with $\mathcal{L} = 3000$ fb^{-1}, as expected.

The search for charginos and neutralinos with $\mathcal{L} = 3000$ fb^{-1}, represented by the red solid line, extends the strong reach slightly at $m_0 \lesssim 250$ GeV. In this area, production of squarks happens at high rate. A "fake" signal resembling direct production of charginos and neutralinos can occur if the squark–anti-squark pair decays to $\tilde{q} \to q\tilde{\chi}_2^0$ and $\tilde{q}^* \to q'\tilde{\chi}_1^\pm$. The resulting jets are not vetoed by the analysis, and the event is accepted as a signal in the electroweak search. Other than the small area mentioned above, the electroweak limit is consistently weaker than the limit from the search for squarks and gluinos. This is as expected in this plane, as electroweak production cross sections are much smaller than the strong. The corresponding bound using $\mathcal{L} = 300$ fb^{-1} reaches up to maximally $m_{1/2} \sim 900$ GeV, and is consequently weaker than all the other bounds. To ease the readability of the plot, it is therefore omitted.

We observe that the search for electroweak production with $\mathcal{L} = 3000$ fb^{-1} suffers from statistical fluctuations, as the bounds have rather large fluctuations. It also fails to exclude areas at very low $m_{1/2}$, due to the small energy release in the sparticle decays. Thus, leptons in this area of parameter space are too soft to pass the selection cuts given in section 5.3.1, and the detection efficiency drops. Since the analysis targets scenarios where the supersymmetric particles are assumed to be heavy, the analysis is well suited in such areas of parameter space, while it suffers under the same assumptions elsewhere. The same pecularity is also seen in the search for squarks and gluinos with $\mathcal{L} = 3000$ fb^{-1}, at very low $m_{1/2}$. However, these areas are already covered by previous searches at 7 and 8 TeV, and by LEP [13].

The HL-LHC dominates the ILC in the entire parameter space, apart from a small strip following the edge of the no REWSB-area at high m_0. Here, squarks and gluinos are out of kinematic reach, and the lighter charginos $\tilde{\chi}_1^\pm$ and neutralinos $\tilde{\chi}_1^0$ have a substantial higgsino component, with masses $\sim \mu$.[4] As expected, the extended search for charginos at 1 TeV remains efficient the furthest into the high m_0-region and gives the best reach here, as it is optimized for such mass degenerate scenarios. This degenerate scenario will not give sufficient E_T^{miss} in the electroweak search at the HL-LHC, and therefore lies beyond its reach. We observe that the ILC bounds in general follow the kinematic limit at 0.5 TeV (1 TeV), as the exclusion limits from the different searches follow the mass contours of 250 GeV (500 GeV) of the sparticles they are optimized to look for.

[4]Note that the mass contours for the lighter chargino (turquoise) and neutralino (yellow) give unfortunate color mixing as they meet along the no REWSB-area.

6.1.2 Naturalness reach

Taking the same approach as Allanach et al. in [2], we look for the minimum non-excluded naturalness. In figure 6.2 we see that the HL-LHC excludes all naturalness below ~ 400, in contrast to ~ 210 in figure 6.1. The maximal reach from the ILC is obtained from the slepton search at 1 TeV, excluding all naturalness below ~ 250. The contours of naturalness agree, and the increased reach of the HL-LHC compared to the reach found in [2] is probably due to the difference in luminosity and type of limits,[5] and that the analysis from [2] is based on 16 year old estimates from ATLAS. Therefore we expect the recent analyses in the ATLAS note [35] to give more realistic predictions. The electroweak search with $\mathcal{L} = 3000$ fb^{-1} however, has a reach similar to that of [2], as it excludes all naturalness below ~ 200.

The somewhat naive definition of the naturalness reach in Allanach et al. does not reflect the fact that for example the HL-LHC can exclude naturalness as high as ~ 700. To overcome this, we have used Bayesian parameter estimation to explore how the two prior distributions of naturalness in figure 6.3 will be affected by the future searches for supersymmetry and by measurements of the Higgs mass, using as likelihoods the p-value and a Gaussian function, respectively, as described in section 4.4.2. This better measures the reach, as it gives the distribution of all naturalness scores, reflecting the likelihood of the various values. For readability, we include in figure 6.3 only the posteriors from the likelihoods with greatest impact. The LHC300 (LHC3000) posterior is based on the product of likelihoods from both the strong and electroweak searches with $\mathcal{L} = 300$ fb^{-1} ($\mathcal{L} = 3000$ fb^{-1}),[6] while the ILC05 (ILC1) is based on the product of the slepton and two chargino likelihoods at 0.5 TeV (1 TeV). The total likelihood is the product of the likelihoods of LHC300, LHC3000, ILC05, ILC1 and the Higgs.

In figure 6.3(a) we see the prior and posterior distributions of naturalness with flat priors in $m_0, m_{1/2}$, obtained as described in section 4.2.1. Within the prior range in this scenario, the LHC3000 likelihood impacts the total distribution of naturalness more than ILC1 (blue), but less than Higgs (green). The Higgs likelihood is clearly dominant, as the total posterior adopts its shape. As the measured Higgs mass lies outside the chosen prior range, at higher values of m_0 and naturalness, this likelihood prefers the maximum possible fine-tuning in the scan region. Taking all experiments into consideration, the most probable naturalness score in this scenario is $c \sim 1500$.

The small peak for low naturalness in the LHC3000 posterior in figure 6.3(a) is an effect from the non-excluded area in the lower left corner of figure 6.2, for the electroweak and strong searches with $\mathcal{L} = 3000$ fb^{-1}. This effect may be alleviated with more statistics, but as the area is already excluded by other experiments, it

[5] We have also used a top mass slightly different from Allanach et al., but we assume this effect to be negligible.

[6] Although we only show three of the total four analyses in figure 6.2.

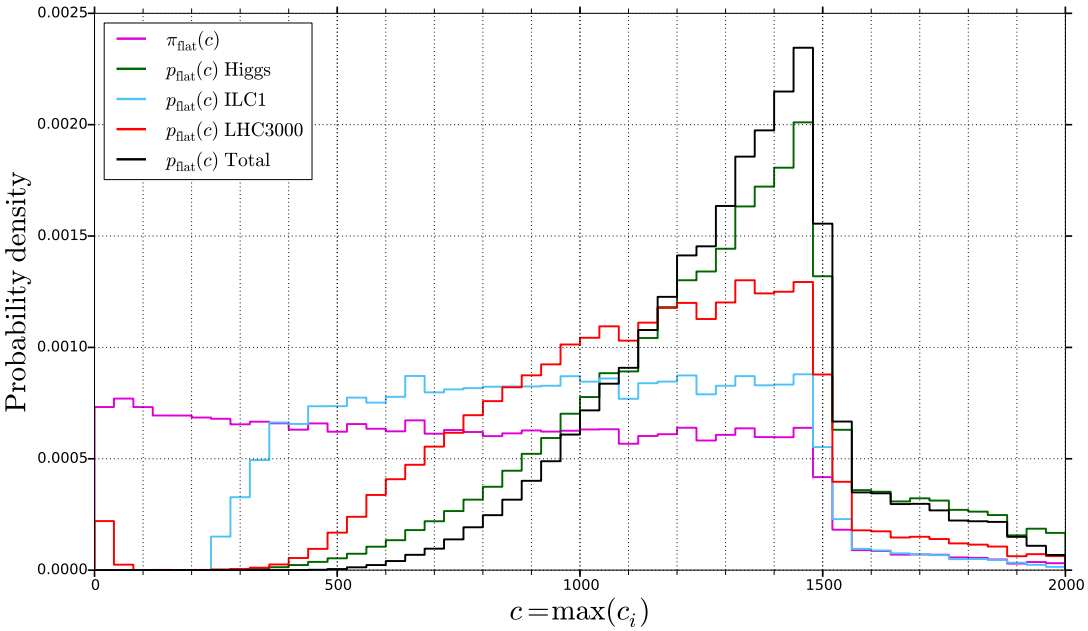

(a) Flat prior in $m_0, m_{1/2}$.

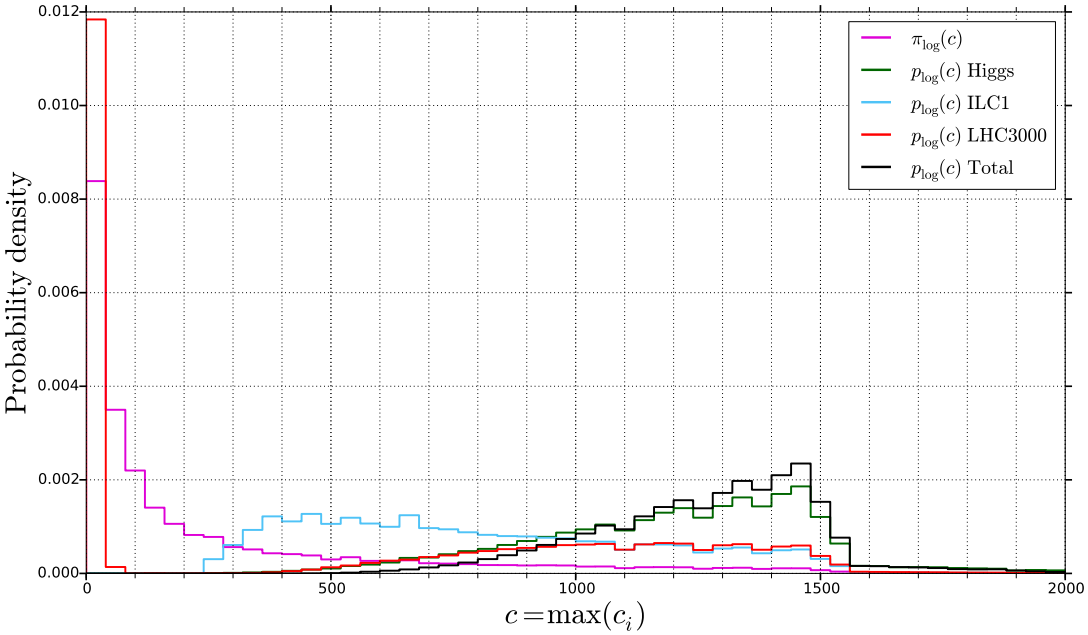

(b) Log prior in $m_0, m_{1/2}$.

Figure 6.3: Prior and posterior distributions of naturalness in the mSUGRA10 scenario.

can be ignored.

The ILC1 results has the least impact on the total posterior in this scenario, and it remains almost unchanged in shape compared to the prior. The exception is a small region of naturalness values below ~ 250, in agreement with what we found previously. Consequently, the posterior is raised above the prior in the rest of the range due to conservation of probability.

The characteristic shape of the prior and posterior distributions, with a sharp cut-off at $c \sim 1500$, is caused by how the naturalness is distributed across parameter space, and our choice of prior ranges. In figure 6.2 we see that we virtually scan over the whole area with $c = 1500$, but very little of the area with higher values. This causes the dramatic fall in naturalness there.

In figure 6.3(b) we give the same results with log priors in $m_0, m_{1/2}$. We see that the total posterior is similar in both shape and maximum, which reflects the strong data from the Higgs likelihood. Due to the large prior at low parameter (and naturalness) values, the weakness of the HL-LHC analyses is more pronounced here. Since these searches fail to exclude low naturalness in this plane on their own, they do not reject our prior belief in low fine-tuning.

This explains why the KL-measure with a log prior for the LHC3000 searches in table 6.1 is smaller than the KL-measure for ILC1. As our prior assumptions are not rejected by LHC3000, the information gain is small. However, the ILC1 mainly excludes in areas with low fine-tuning, which is in contrast to our prior belief, and therefore we learn more.

The KL-measures for various posteriors in table 6.1 reflect our discussion above, as the Higgs posterior gives the largest information gain, followed by the LHC3000 and ILC1 posteriors. We notice that all KL-measures with a log prior are larger than the corresponding measures with a flat prior, as the experiments in general exclude — at least some of — the lowest naturalness. The prior belief in this area is thus rejected, and information gained. Although it is tempting to believe that the KL-measure for the total posterior should be the sum of the KL-measures from which it is composed, the KL-measure for the total posterior is not linear in the individual parts it is constructed from.

Table 6.1: KL-measures for naturalness in mSUGRA10. The priors refer to the priors in m_0 and $m_{1/2}$. The content of the posteriors is defined in the text.

Posterior	Flat prior	Log prior
LHC3000	0.431	0.775
ILC1	0.221	1.313
Higgs	0.708	2.136
Total	0.845	2.434

6.2 mSUGRA30

A plausible realization of supersymmetry is not really present in the parameter space of the previous scenario, as the predicted Higgs mass is too low compared to the experimental measured mass. The parameters of msUGRA30 are therefore chosen to bring the calculated Higgs mass into closer agreement with the measured. The prize to pay is an overall increase in naturalness compared to mSUGRA10.[7]

As the Higgs likelihood no longer gives a — rather artificial — dominating effect, this scenario allows us to inverstigate a more realistic reach and impact on our knowledge of naturalness from the HL-LHC and ILC.

6.2.1 Exclusion limits

In figure 6.4 we give the 95% CL exclusion limits and mass contours for the mSUGRA30 scenario. We find many of the same features as in the previous section, and we will here mainly focus on the differences. We see that the search for strongly produced supersymmetry with $\mathcal{L} = 3000$ fb^{-1} excludes all values of $m_{1/2} \lesssim 900$ GeV, corresponding to squark and gluino masses below ~ 2.25 GeV. Notice that in contrast to the mSUGRA10 scenario, the detection efficiency is maintained at low m_0 to the very left in figure 6.4. In the same figure we also see that the strong searches at both luminosities suffer from poor statistics at very low $m_{1/2}$, indicated by the fluctuations in the lower red lines. We did not have the computational resources to improve this effect.[8]

The searches for electroweak production at the HL-LHC reach up to maximally $m_{1/2} \sim 700$, but are not included in figure 6.4 as they suffer from even larger statistical fluctuations and consistently give the weakest bounds. We have also removed the extended search for charginos at the ILC at 1 TeV, as this bound ran along $m_{1/2} \sim 200$ GeV and did not contribute much to the plot.

We notice that the no REWSB-area is no longer present, but a small region with *tachyons* has appeared. If the soft masses of squarks and sfermions run sufficiently low, they can take on negative values at the electroweak scale. This increases the risk of also having negative physical squared masses — called tachyons. RGE running effects at high $m_{1/2}$ can prevent these negative values, so tachyons appear at low $m_0, m_{1/2}$. The effect is more pronounced at high $\tan\beta$, because this will increase the splitting of the stop (and sbottom) masses, making it easier for the lighter one to become negative.

The bounds from the ILC have the same pattern as in mSUGRA10, following the kinematic limits.

[7] Though not dramatic.

[8] This scenario has the smallest amount of statistics, with only 400 000 generated events for each point for the strong processes.

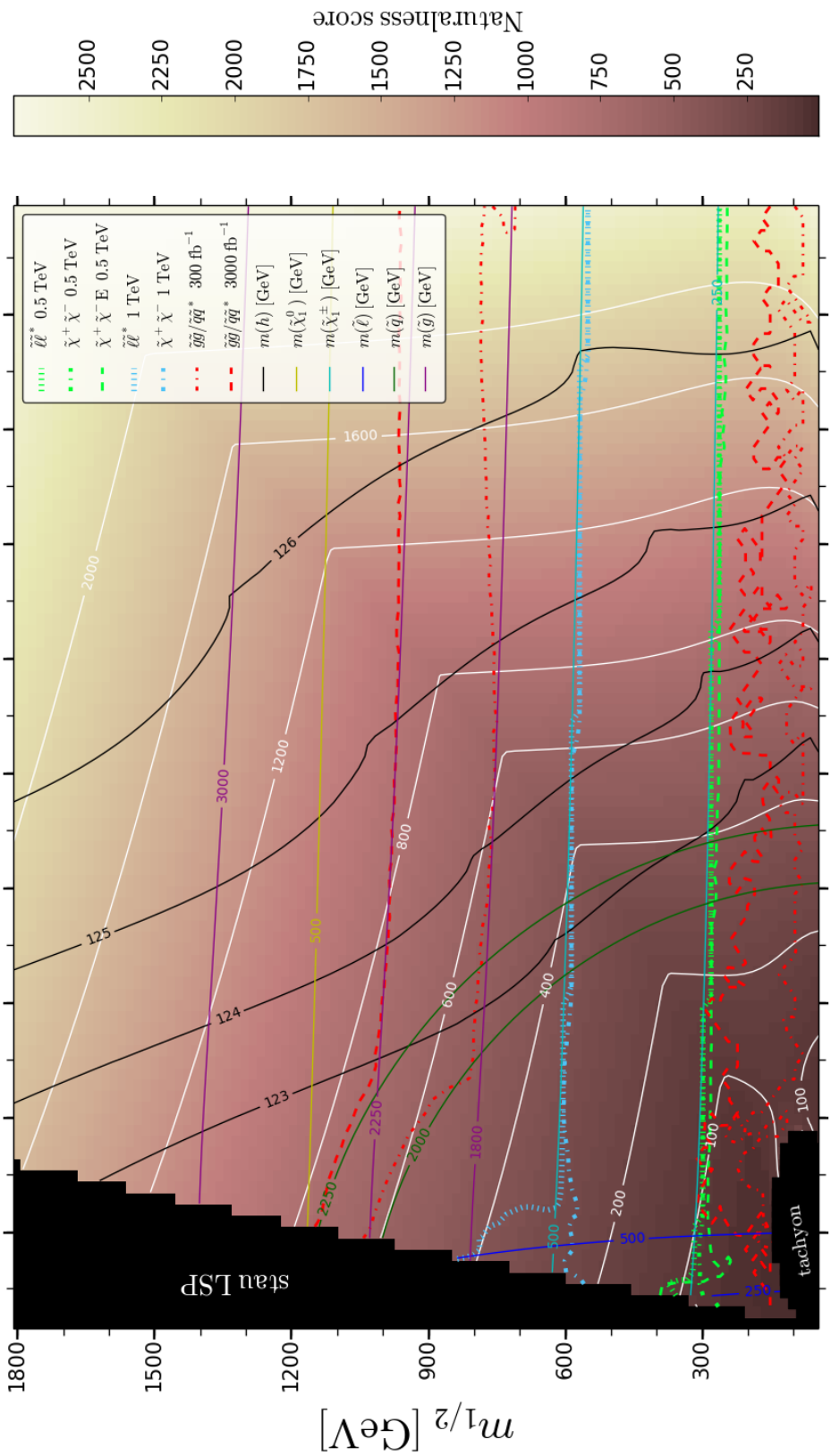

Figure 6.4: The mSUGRA30 scenario with $A_0 = -2m_0$, $\tan\beta = 30$, $\mathrm{sgn}(\mu) = +$. The white lines are contours for the naturalness score.

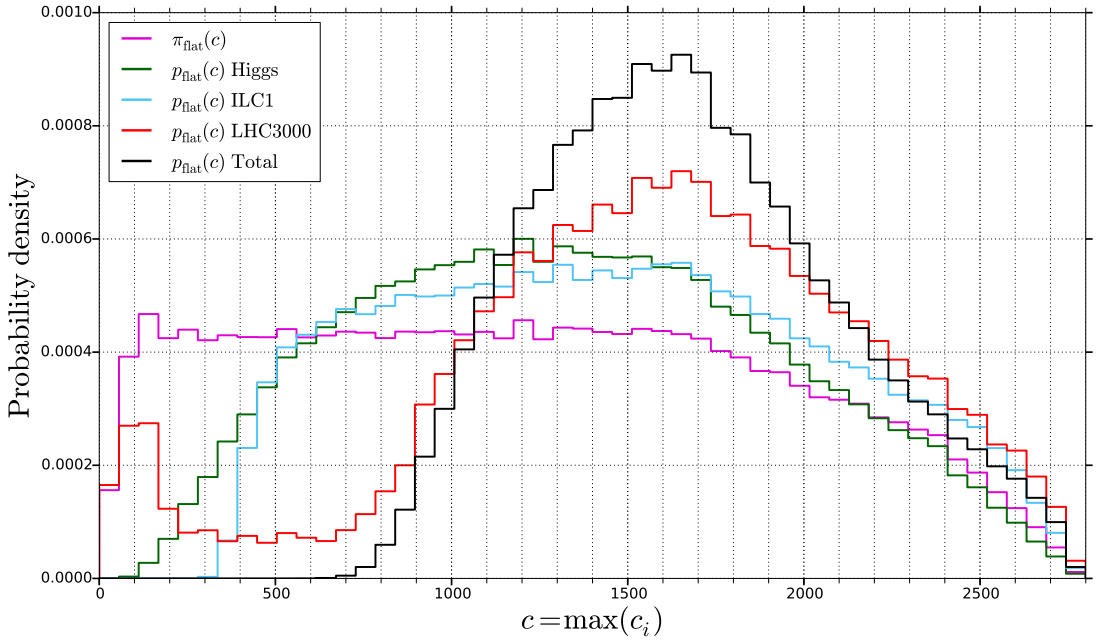

(a) Flat prior in $m_0, m_{1/2}$.

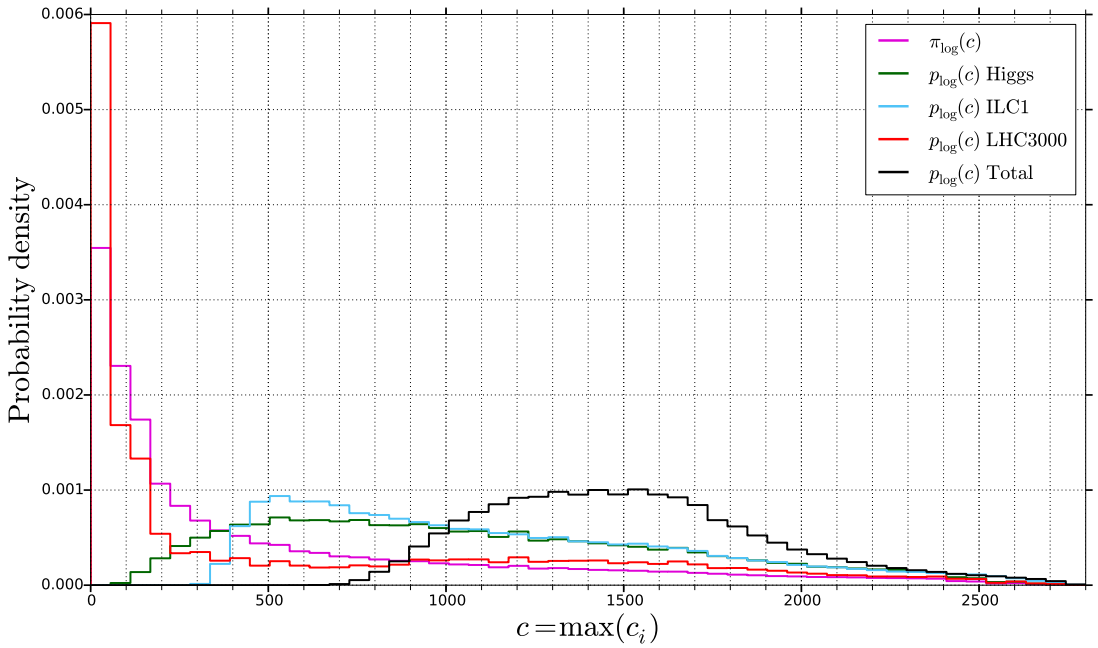

(b) Log prior in $m_0, m_{1/2}$.

Figure 6.5: Prior and posterior distributions of naturalness in the mSUGRA30 scenario.

6.2.2 Naturalness reach

In figure 6.5(a) we see the prior and posterior distributions of naturalness with flat priors in the scan parameters. The LHC3000 and total posteriors no longer contain the likelihood from the much weaker electroweak searches for supersymmetry, but otherwise they are as defined in section 6.1.

Within the prior ranges in this scenario, we see in figure 6.4 that the search for squarks and gluinos at $\mathcal{L} = 3000$ fb^{-1} excludes most of the naturalness below ~ 700 — but not completely, as the search is weak in the region of parameter space where $m_{1/2} \lesssim 200$ GeV. The LHC3000 posterior in figure 6.5(a) has a small plateu at values between approximately $200 - 700$, reflecting this weakness. Even though the ILC slepton search at 1 TeV successfully excludes all naturalness values below ~ 300, and hence complements the problematic areas of the HL-LHC searches, these values are already excluded by previous runs at the LHC at 7 and 8 TeV, and by LEP. As we can see in figure 6.4, the HL-LHC searches exclude little of the very lowest naturalness values, explaining the little peak at $c \sim 100$.

We notice that the Higgs likelihood no longer dominates in the total posterior. This is as expected, since the measured Higgs mass is present in the current scenario. In fact, within the theoretical uncertainty of 2 GeV for the Higgs mass calculation in `FeynHiggs` compared to the measured value, we can have an acceptable Higgs mass in almost the whole prior range scanned. Therefore, the Higgs likelihood allows almost all of the naturalness range in the scan, and is far less dominant than in mSUGRA10. In this plane, the LHC3000 posterior has the greatest impact on the total posterior, while the effect from the ILC1 likelihood is roughly the same as from the Higgs. The most probable naturalness is now $c \sim 1600$, slightly raised compared to the mSUGRA10 scenario.

The total posterior maintains roughly the same shape and maximum in the case of a log prior, shown in figure 6.5(b). However, we find some differences in the individual posteriors. The weak limits at low naturalness are once again pronounced in the LHC3000 posterior, and we notice small shifts towards smaller naturalness also in the ILC1 and Higgs posteriors. The LHC3000 posterior is now the least informative, as can be seen from the KL-measures in table 6.2. From these measures it is also clear that the largest information gain is achieved from ILC1, as this likelihood — similar to the Higgs — mainly excludes low naturalness. The KL-measure for the Higgs posterior with flat priors confirm the very modest information gain from this measurement.

Even though comparison of KL-measures in different scenarios is difficult, we allow for an important observation concerning the information gain in mSUGRA10 versus mSUGRA30. In terms of the definition of naturalness reach by Allanach et al., we have the best reach in the current scenario, as we now exclude all naturalness below ~ 700, versus ~ 400 in mSUGRA10. However, the KL-measure for the total posterior with flat priors in mSUGRA10, given in table 6.1, gives us almost twice as much information as the same measure in mSUGRA30, given

Table 6.2: KL-measures for naturalness in mSUGRA30. The priors refer to the priors in m_0 and $m_{1/2}$. The content of the posteriors is defined in the text.

Posterior	Flat prior	Log prior
LHC3000	0.211	0.115
ILC1	0.164	0.905
Higgs	0.099	0.673
Total	0.469	1.519

in table 6.2. This means that despite the higher allowed minimal naturalness value in mSUGRA30, we actually learn less about naturalness in this scenario compared to mSUGRA10. This illustrates that the approach of Allanach et al. is somewhat naive compared to the one followed here.

6.3 NUHM2

Both models studied up to now have been mSUGRA models, motivated by the wish for GUT unification of scalar masses in m_0. We will now study the NUHM2 model described in section 2.7.2, motivated by both the possibility of low fine-tuning, and the prediction of a Higgs mass in agreement with observation. Large squark masses increase the mass of the Higgs, since the loop corrections to the Higgs mass depend upon the masses of the particles running in them. This in turn typically shifts naturalness in the same direction. Hence, such areas do not exist in mSUGRA models, as the prize to pay there is an increase in the overall naturalness score, and vice versa.

The NUHM2 model in [25], given the name Radiatively-driven Natural supersymmetry (RNS), maintainins the features of gauge coupling unification and radiative electroweak symmetry breaking, as well as keeping the fine-tuning low and predicting a correct Higgs mass. This can be seen from eq. (3.8), as

$$c_{m_{H_u}} = \left| \frac{4}{\tan^2 \beta} \frac{m_{H_u}^2}{m_Z^2} \right| \tag{6.1}$$

is low if $|m_{H_u}| \sim m_Z$ and $\tan^2 \beta \gg 1$. This happens naturally in RNS with running from the GUT scale.

We now compare our results with those from [25], given here in figure 6.7 for ease of reference.

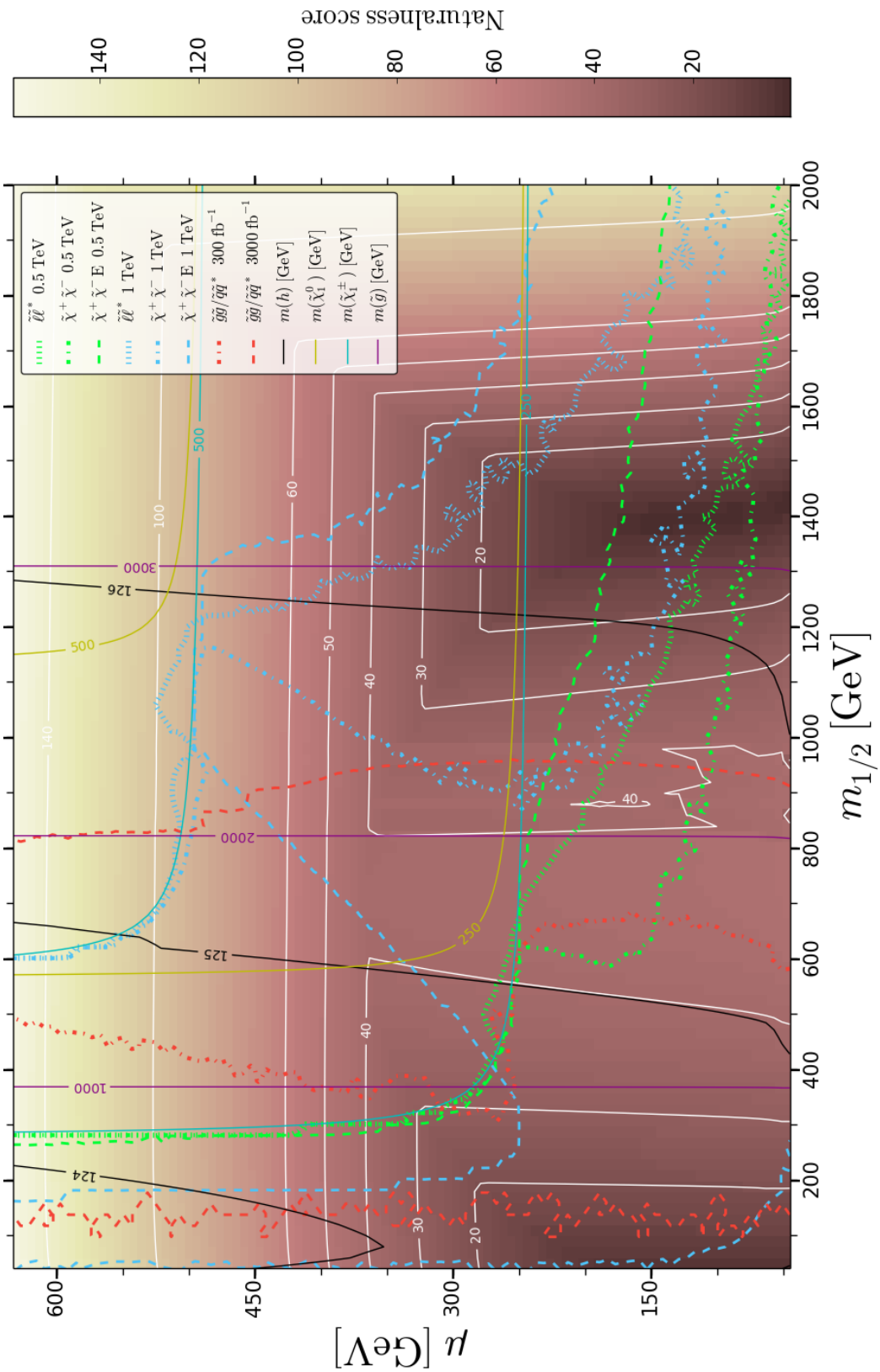

Figure 6.6: The NUHM2 scenario with $m_0 = 4$ TeV, $\tan\beta = 15$, $A_0 = -1.6m_0$, $m_A = 1$ TeV. The white lines are contours for the naturalness score.

6.3.1 Exclusion limits

As $m_0 = 4$ TeV in the NUHM2 mass plane, squarks are out of kinematic reach, and we produce and set limits on the gluino mass. The high value of m_0 also removes the possibility of tachyons, and there are no unphysical areas within the chosen prior ranges.

In figure 6.6 we give the 95% CL exclusion limits for the NUHM2 scenario. We see that the strong production search at the HL-LHC with $\mathcal{L} = 3000$ fb^{-1} will explore all values of $m_{1/2} \lesssim 800$ GeV, corresponding to all gluino masses below ~ 2 TeV. As expected, this reach is similar to those obtained for mSUGRA10 and mSUGRA30, as the kinematics are the same, and 2 TeV gluinos are close to the kinematic reach at $\sqrt{s} = 14$ TeV. This is in contrast to the ILC reach, which in fact is able to exclude models with gluino masses well above this. The electroweak searches for supersymmetry at the HL-LHC once again suffer from large statistical fluctuations,[9] and explore values of at most $m_{1/2} \sim 600$ GeV. Being consistently weaker than the limit from strong production at $\mathcal{L} = 3000$ fb^{-1}, we have left them out of figure 6.6 for readability.

Our reach is increased compared to the results in [25], due to the ten times higher luminosity. The dashed blue line in figure 6.7, representing the search for gluino pair production at $\mathcal{L} = 300$ fb^{-1}, excludes $m_{1/2} \lesssim 700$ GeV, corresponding to gluino masses of $m_{\tilde{g}} \lesssim 1.7$ TeV. The shape of the collider bounds in figures 6.6 and 6.7 are similar, both for the HL-LHC and the ILC. However, the ILC bounds shown in figure 6.7 are purely kinematic, hence it lacks the decreasing detection efficiency at high $m_{1/2}$ from the more realistic simulation shown in figure 6.6. In figure 6.7 we can also see the areas already excluded by LEP, clearly showing that the area poorly covered by the HL-LHC along the lowest values of $m_{1/2}$ is already excluded.

6.3.2 Naturalness reach

We cannot directly relate the shape of the naturalness contours in figure 6.6 with the naturalness contours in figure 6.7, as the former is based on the so-called *electroweak fine-tuning*, and not the Barbieri–Giudice measure defined in eq. (3.9).[10] However, both results are characterized by a low overall fine-tuning, even if quantitatively our results are slightly higher.

A Higgs mass of approximately 125 ± 2 GeV is present throughout the prior ranges in this scenario, and the corresponding likelihood therefore provides little information on naturalness, and has no effect on the total posterior. For these reasons it is omitted in figure 6.8. However, all posteriors used in this scenario are the same as those defined in section 6.2.2, meaning the Higgs likelihood is still included in the total posterior.

[9] Despite the generation of 1 200 000 events for each parameter point.

[10] Although the contours from the two different naturalness definitions bear some resemblance.

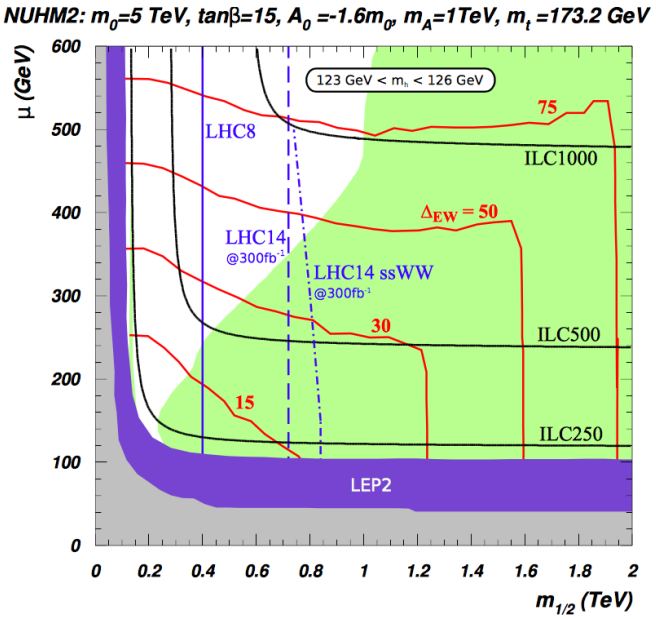

Figure 6.7: Electroweak naturalness scores (red), and predicted LHC (blue) and ILC (black) exclusion bounds for a NUHM2 scenario with $m_0 = 5$ TeV, $\tan\beta = 15$, $A_0 = -1.6m_0$, $m_A = 1$ TeV and $m_t = 173.2$ GeV. Taken from [25].

In figure 6.8(a) we give the prior and posterior distributions of naturalness with flat priors in $m_0, m_{1/2}$. An important discovery in this scenario, is the extremely small information gain — hardly any at all — from the planned searches for strongly produced supersymmetry at the HL-LHC. In terms of the naturalness reach defined by Allanach et al., the HL-LHC has none, since it cannot exclude all naturalness below any value. In contrast to the previous two scenarios, the reason is no longer limitations on detection efficiency, but solely due to the peculiar shape of the naturalness score in the mass plane in combination with the bounds from the HL-LHC experiments at constant $m_{1/2}$. As the LHC3000 posterior in figure 6.8(a) is roughly distributed evenly over all naturalness values, it is effectively just an overall scaling, and the likelihood has no contribution in the total posterior. Our information gain on naturalness from this experiment is very limited, despite the rather large excluded area from the HL-LHC bound at $\mathcal{L} = 3000$ fb^{-1} shown in figure 6.6. However, an interesting effect from this constraint in the mass plane, is its removal of the naturalness plateau for values of $c \sim 40$, for $m_{1/2}$ between $\sim 500 - 1000$ GeV, seen in figure 6.6. We find the plateau in the accumulation of the same values in the prior distribution of figure 6.8(a), and observe that the peak is gone in the LHC3000 posterior. This plateau also explains the rather peculiar behaviour of some of the naturalness isocurves.

The supersymmetry searches at the ILC give the best reach in this scenario,

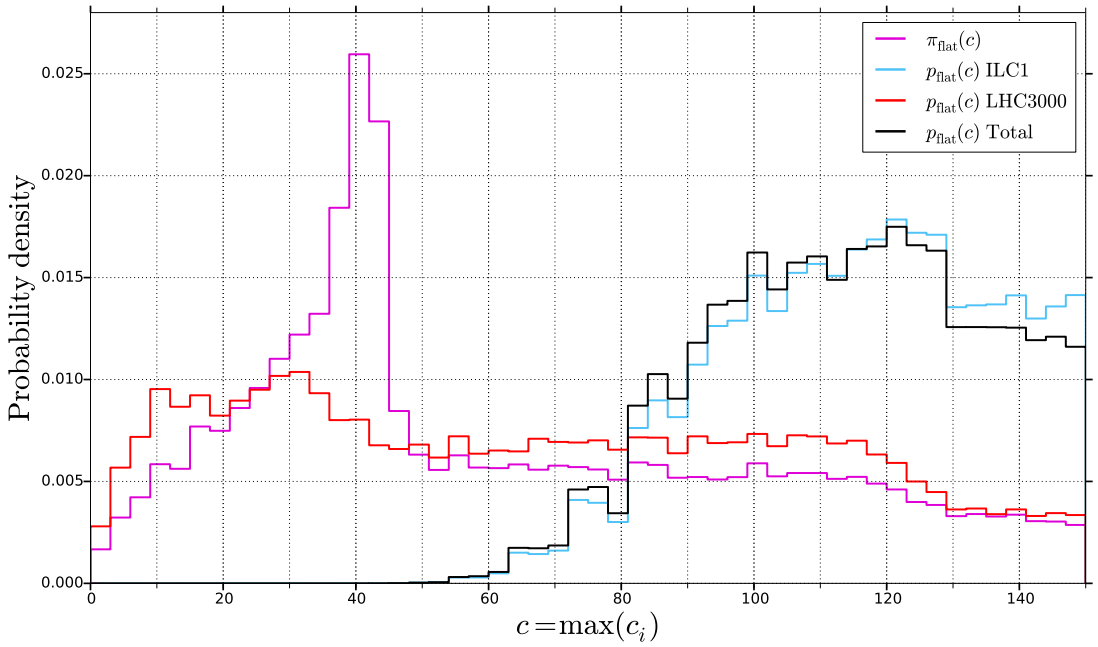

(a) Flat prior in $m_0, m_{1/2}$.

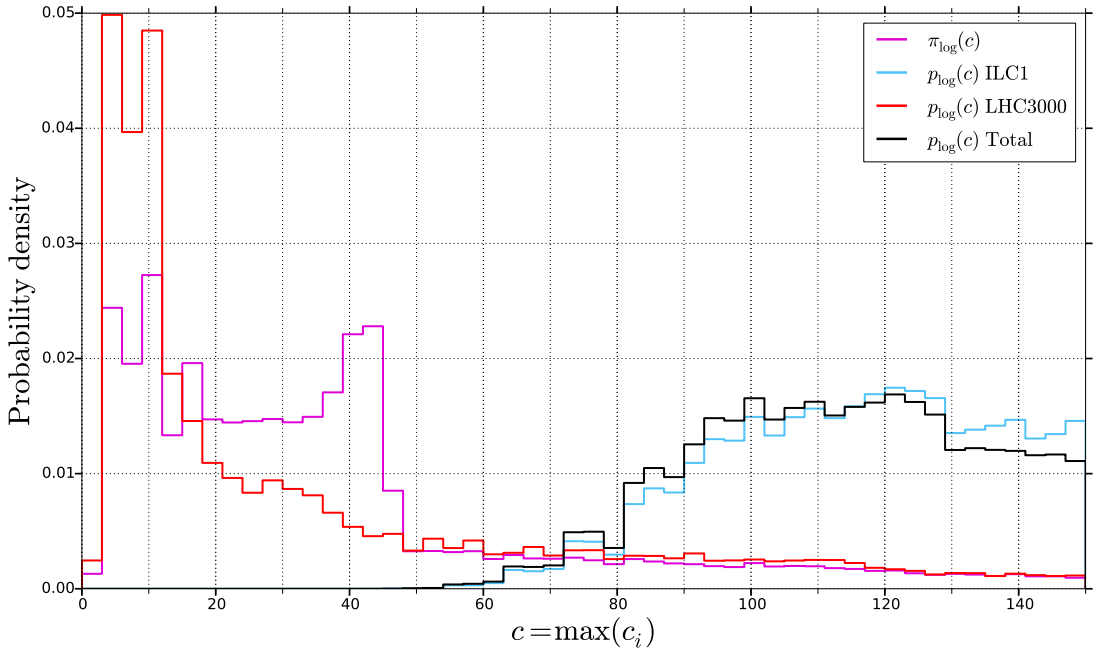

(b) Log prior in $m_0, m_{1/2}$.

Figure 6.8: Prior and posterior distributions of naturalness in the NUHM2 scenario.

and in figure 6.6 we see that the ILC1 posterior excludes all naturalness below ~ 30.

Studying the log priors in figure 6.8(b), we find that the ILC1 and total posteriors are virtually identical in shape and maximum value as with flat priors, indicating the very strong data from the ILC experiments in this scenario. Thus, the other experiments hardly contribute in the total posterior, and the ILC1 posterior predicts a most probable naturalness score of $c \sim 120$. We also observe that the prior peak at $c \sim 40$ is gone.

The KL-measures in table 6.3 reflect the above discussion. The LHC3000 posterior provides close to no information about naturalness, meaning that very natural models may remain even after the HL-LHC searches. If supersymmetry is realized within the parameter space of the scenario studied here, the ILC can provide us with ~ 12 and ~ 16 times the information compared to the HL-LHC assuming flat and log priors in $m_0, m_{1/2}$, respectively. This motivates building such a collider.

Table 6.3: KL-measures for naturalness in NUHM2. The priors refer to the priors in m_0 and $m_{1/2}$. The content of the posteriors is defined in the text.

Posterior	Flat prior	Log prior
LHC3000	0.088	0.183
ILC1	1.063	2.075
Total	1.031	2.016

Conclusions

In this thesis we have scanned the parameter spaces of three supersymmetric scenarios to explore the potential naturalness reach of the HL-LHC at $\sqrt{s} = 14$ TeV in planned searches for supersymmetry. We have set exclusion limits at the 95% confidence level to find the disfavoured naturalness values and sparticle masses. With the likelihoods obtained from these planned experiments, assuming negative results, we have used Bayesian parameter estimation to calculate posterior probability distributions for naturalness. These indicate not only the most probable fine-tuning, but also its spread. We have also used the Kullback–Leibler divergence to quantify the information gain on naturalness from different collider experiments. From the literature it appears that this measure has never been used in the context of particle physics before. This thesis was focused on the planned experiments at the HL-LHC, but we have also compared our results with similar work done for the ILC presented in [1].

In the two mSUGRA scenarios we see that the HL-LHC can exclude all squark and gluino masses below ~ 2 TeV, while virtually all slepton and chargino masses below ~ 0.5 TeV can be excluded by the ILC at 1 TeV. This corresponds to the kinematically accessible sparticles at these energies. In the natural supersymmetric model, the squarks and sleptons were out of kinematic reach, but the reach in the remaining masses was the same as stated above.

The searches for supersymmetry at the HL-LHC were found to have surprisingly weak constraining power in areas of parameter space with low sparticle masses, due to poor detection efficiency and consequently large statistical fluctuations. This is a consequence of the assumptions of high sparticle masses used in the analyses. However, the resultig limitations of the searches are not dramatic, as the problematic areas are already exluded by other searches and experiments. A similar effect is found for the ILC in areas with mass degeneration between charginos and neutralinos. As these areas are not already excluded, an optimized analysis for this mass degenerate case was implemented to extend the reach here.

The favoured fine-tuning in the two mSUGRA scenarios is $c \sim 1500 - 1600$, where the results from the planned searches at the HL-LHC can give substantial contributions to our knowledge about the naturalness of the model. This is in great contrast to the situation in our natural supersymmetry scenario, where the HL-LHC searches cannot provide us with any information about the fine-tuning,

independent on our assumptions of prior beliefs. Thus, natural supersymmetry models may remain viable after the HL-LHC experiments. However, the searches for supersymmetry at the ILC at 1 TeV may push fine-tuning up to $c \sim 120$, and can give over ten times as much information about naturalness as the HL-LHC. This motivates building such a collider.

Appendix A

Formalities

Einsteins summation convention is used throughout this thesis, meaning repeated indices is summed over, i.e.,

$$\alpha_i \theta^i \equiv \sum_i^N \alpha_i \theta^i = \alpha_1 \theta^1 + ... + \alpha_N \theta^N. \tag{A.1}$$

The same convention also applies if both indices are raised or lowered.

We also use natural units $\hbar = c = 1$ and the relativistic four-vector notation, with the contravariant space time vector $x = x^\mu$ defined by

$$x^\mu \equiv (x^0, x^1, x^2, x^3) = (t, \mathbf{x}), \tag{A.2}$$

and the metric tensor in flat space $g_{\mu\nu}$ defined by

$$g_{00} = -g_{11} = -g_{22} = -g_{33} = 1, \tag{A.3}$$

$$g_{\mu\nu} = 0 \quad \text{for} \quad \mu \neq \nu. \tag{A.4}$$

Covariant four vectors are defined using the metric tensor in the following way,

$$x_\mu = g_{\mu\nu} x^\nu = (x^0, -x^1, -x^2, -x^3) = (t, -\mathbf{x}). \tag{A.5}$$

The energy-momentum vector p^μ is defined as

$$p^\mu = (E, p^1, p^2, p^3) = (E, \mathbf{p}). \tag{A.6}$$

The three Pauli matrices σ^i are proportional to the generators of the $SU(2)_L$ gauge group, and are given by

$$\sigma^1 = \begin{pmatrix} 0 & 1 \\ 1 & 0 \end{pmatrix} \quad \sigma^2 = \begin{pmatrix} 0 & -i \\ i & 0 \end{pmatrix} \quad \sigma^3 = \begin{pmatrix} 1 & 0 \\ 0 & -1 \end{pmatrix}, \tag{A.7}$$

with the commutation relations

$$[\sigma^i, \sigma^j] = 2i\epsilon^{ijk}\sigma^k, \tag{A.8}$$

Table A.1: Programs and non-standard settings used.

Generator/program	Application	Tune
`SOFTSUSY 3.7.0` [37]	Mass spectrum and naturalness score.	$\alpha_{\text{em}}^{-1} = 1.279\,44 \cdot 10^2$. $\alpha_s(\text{m}_\text{Z}) = 1.184 \cdot 10^{-1}$. $m_b(m_b) = 4.18$ GeV. $m_t(\text{pole}) = 1.734 \cdot 10^2$ GeV.
`PYTHIA 8.215` [47]	Event generator for pp-collisions.	PDF set CTEQ6.6M NLO. No multiparton interactions. Isotropic tau decays.
`FeynHiggs 2.12.0` [40–45]	Improved Higgs masses and couplings.	Loglevel 2.
`NLL-fast 4.01` [49–52]	Cross section calculations.	PDF set CTEQ6.6M NLO.
`PYTHIA 6.428` [46]	Event generator for e^+e^--collisions.	Modified `PYCELL` subroutine, see appendix C.
`anti-`k_T [55]	Jet reconsruction algorithm used by `FastJet`.	Default.
`FastJet` [57]	Jet reconsruction of `PYTHIA 8.215`.	Default.
`Prospino 2.1` [53]	Cross section calculations.	Default.
`SUSY-HIT 1.5` [39]	Better decays of SUSY particles.	Default.

where ϵ^{ijk} is the Levi–Civita symbol. Further we have that

$$\sigma^\mu = (\mathbf{1}_{2\times 2}, \sigma^i), \tag{A.9}$$

and

$$\sigma^{\mu\nu} = \frac{i}{4}(\sigma^\mu \bar{\sigma}^\nu - \sigma^\nu \bar{\sigma}^\mu), \tag{A.10}$$

where $\bar{\sigma}^\mu = (\mathbf{1}_{2\times 2}, -\sigma^i)$.

The eight Gell-Mann matrices λ^a compose the generators of the $SU(3)_C$ gauge group. They have the commutation relations

$$[\lambda^a, \lambda^b] = 2if^{abc}\lambda^c, \tag{A.11}$$

where the structure constants f^{abc} are antisymmetric in the three indices.

To avoid accumulation of numerical factors, the generators of both $SU(2)_L$ and $SU(3)_C$ are defined as

$$T^i = \frac{1}{2}\sigma^i, \qquad T^a = \frac{1}{2}\lambda^a. \tag{A.12}$$

We also remind the reader of the trace relations for the gamma matrices,

$$\text{Tr}(\gamma^\mu\gamma^\nu) = 4g^{\mu\nu}. \tag{A.13}$$

All program versions and their non-standard settings are found in table A.1.

Appendix B

Loop corrections to the Higgs mass

In this appendix we calculate the fermionic and scalar one-loop corrections to the Higgs mass, using the Feynman rules defined in table B.1.

The tree level mass term of the Higgs boson is present in the Lagrangian as

$$\mathcal{L}_{m_h} = \mu^2 h^\dagger h, \tag{B.1}$$

and is represented by the Feynman diagram in figure B.1. From quantum field theory, we know that a scalar field $h^\dagger$ contains a destruction operator, while h has a creation operator. Figure B.1 therefore describes the destruction and creation of a quanta of the Higgs field. Diagrams such as those in figure B.2 are corrections to the tree level mass, since the initial and final states are exactly the same. It is clear that the tree level mass term in the Lagrangian depends upon the parameter μ. It is important to stress that this is not the same as the *physical* mass of the Higgs boson, m_h. The physical (squared) mass m_h^2, is the sum of the parameter μ^2 and all possible corrections,

$$m_h^2 = \mu^2 + \Delta m_h^2. \tag{B.2}$$

The parameter μ has no predicted value from the Standard Model, and must be determined from experiment.

Table B.1: Feynman rules for calculating fermion and scalar corrections to the Higgs mass.

Diagram element	Expression	Comment
Vertex $h\bar{f}f$	$-i\lambda_f/\sqrt{2}$	λ_f: fermion coupling to the Higgs field
Vertex $(h^\dagger h)(S^* S)$	$-i\lambda_S$	λ_S: scalar coupling to the Higgs field
Fermion propagator	$\frac{(i\not{q}+m_f)}{q^2-m_f^2}$	four-momentum q and mass m_f of fermion
Scalar propagator	$\frac{i}{q^2-m_S^2}$	four-momentum q and mass m_S of scalar
External scalar	1	

Figure B.1: Tree level mass term og the Higgs particle.

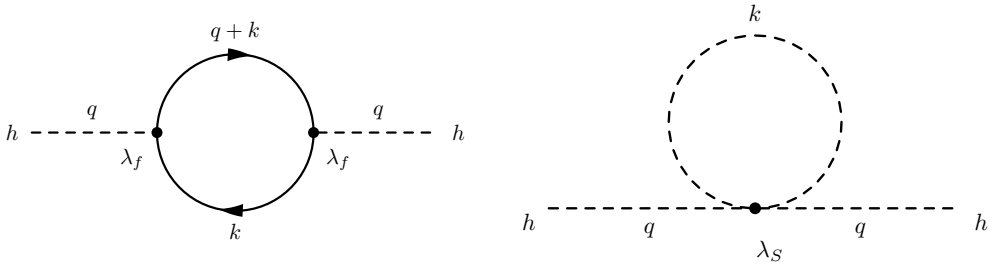

(a) Fermion loop contribution.

(b) Scalar loop contribution.

Figure B.2: First order loop corrections to the Higgs mass.

B.1 Fermionic loop correction

We begin by calculating the correction corresponding to the diagram on the left of figure B.2 which is the contribution from a fermion of mass m_f and coupling λ_f to the Higgs.

Until performing the integral, integration limits will be left for esthetic reasons. The integral is taken over over the unknown loop four-momenta $k_i \in [-\infty, \infty]$. The overall sign of the trace is negative due to the closed fermion loop.

The matrix element to calculate is then

$$i\mathcal{M} = -\frac{|\lambda_f|^2}{2} \operatorname{Tr}\left[\int \frac{\mathrm{d}^4k}{(2\pi)^4} \left(\frac{(\not{q} + \not{k}) + m_f}{(q+k)^2 - m_f^2}\right)\left(\frac{\not{k} + m_f}{k^2 - m_f^2}\right)\right], \tag{B.3}$$

where q is the four-momentum of the Higgs boson.

B.1.1 Feynman parametrization

As a first step to solve the integral, we simplify the denominator by defining

$$A = (q+k)^2 - m_f^2, \tag{B.4}$$

$$B = k^2 - m_f^2. \tag{B.5}$$

Further, we use the Feynman parametrization where we rewrite the expression as an integral:

$$\frac{1}{AB} = \frac{1}{A-B}\left(\frac{1}{B} - \frac{1}{A}\right) = \frac{1}{A-B}\int_B^A \frac{\mathrm{d}z}{z^2}. \tag{B.6}$$

Then we make the substitution

$$x = \frac{z-B}{A-B}, \tag{B.7}$$

where we have

$$z = Ax + (1-x)B. \tag{B.8}$$

Since $z \in [A, B]$, this implies $x \in [0, 1]$ from eq. (B.7). We have also

$$\mathrm{d}x = \frac{\mathrm{d}z}{(A-B)}. \tag{B.9}$$

Substituting back in eq. (B.6), we get

$$\begin{aligned}\frac{1}{AB} &= \frac{1}{A-B}\int_0^1 \frac{(A-B)\mathrm{d}x}{[Ax+(1-x)B]^2} \\ &= \int_0^1 \frac{\mathrm{d}x}{[Ax+(1-x)B]^2}.\end{aligned} \tag{B.10}$$

The (unsquared) denominator in the integral can be expressed in terms of the momenta as

$$\begin{aligned}[Ax+(1-x)B] &= [(q+k)^2 - m_f^2]x + (1-x)[k^2 - m_f^2] \\ &= (k+qx)^2 - \underbrace{(q^2x(x-1) + m_f^2)}_{\equiv\Delta} \\ &= (k+qx)^2 - \Delta(x).\end{aligned} \tag{B.11}$$

We then make the following shift in the unknown four-momentum k to simplify the denominator further,

$$k \to k' = \ell - qx, \qquad \mathrm{d}k' = \mathrm{d}\ell. \tag{B.12}$$

No Jacobi factor is introduced, and the denominator simplifies to

$$[Ax+(1-x)B]^2 = [\ell - \Delta]^2. \tag{B.13}$$

B.1.2 Trace of numerator

Next, we write out the numerator in the same variables. All odd multiples of gamma matrices are left out, as these are traceless and give no contributions. The trace itself is to be integrated over all four-momenta ℓ. Hence all linear terms in ℓ can be neglected as these do not contribute to the integral.

Using these simplifications, the numerator can be written

$$\begin{aligned}\mathrm{Tr}\{[(\not{q}+\not{k}')+m_f][\not{k}'+m_f]\} &= \mathrm{Tr}([(\not{q}+\not{l}-\not{q}x)+m_f][\not{l}-\not{q}x+m_f]) \\ &= 4(q\ell - q^2x + l^2 - 2q\ell x + q^2x^2 + m_f^2) \\ &= 4(\ell^2 + q^2x^2 - q^2x + m_f^2) \\ &= 4(\ell + \Delta(x)). \end{aligned} \tag{B.14}$$

After the Feynman parametrization and trace evaluation, the matrix element is reduced to

$$i\mathcal{M} = -\frac{2|\lambda_f|^2}{(2\pi)^4}\int_0^1 \mathrm{d}x \int \mathrm{d}^4\ell \; \frac{\ell^2 + \Delta(x)}{[\ell^2 - \Delta(x)]^2}. \tag{B.15}$$

B.1.3 Wick rotation

The next step is to perform a Wick-rotation. The Wick-rotation takes us from integration in Minkowski space, to Euclidean space. This is done by introducing the coordinate ℓ_E which is defined with the following properties,

$$\ell^0 \equiv i\ell_E^0, \qquad \boldsymbol{\ell} \equiv \boldsymbol{\ell}_E. \tag{B.16}$$

This leads to the relations

$$\ell^2 = (\ell^0)^2 - \boldsymbol{\ell}^2 = (i\ell_E^0)^2 - (\boldsymbol{\ell}_E)^2 = -(\ell_E^0)^2 - \boldsymbol{\ell}_E^2 = -\ell_E^2, \tag{B.17}$$

$$\mathrm{d}^4\ell = i\mathrm{d}^4\ell_E. \tag{B.18}$$

We now perform the integral over the four-dimensional Euclidean space, using four-dimensional spherical coordinates,

$$\int \mathrm{d}^4\ell_E = \int \mathrm{d}\Omega_4 \int |\ell_E|^3 \mathrm{d}|\ell_E|, \tag{B.19}$$

where the solid angle integral gives

$$\int \mathrm{d}\Omega_4 = 2\pi^2. \tag{B.20}$$

B.1.4 Regularization

We use a cut-off scale Λ for the momentum ℓ_E to regularize the integral. The integral then yields

$$\begin{aligned} i\mathcal{M} &= -\frac{2|\lambda_f|^2}{(2\pi)^4}\int_0^1 \mathrm{d}x \int \mathrm{d}^4\ell \ \frac{\ell^2+\Delta(x)}{[\ell^2-\Delta(x)]^2} \\ &= \frac{2i|\lambda_f|^2}{(2\pi)^4}\int_0^1 \mathrm{d}x \int \mathrm{d}^4\ell_E \ \frac{\ell_E^2-\Delta(x)}{[\ell_E^2+\Delta(x)]^2} \\ &= \frac{2i|\lambda_f|^2}{(2\pi)^4}\int_0^1 \mathrm{d}x \int \mathrm{d}\Omega_4 \int_0^\Lambda \mathrm{d}|\ell_E| \ \frac{|\ell_E|^2-\Delta(x)}{(|\ell_E|^2+\Delta(x))^2}|\ell_E|^3 \\ &= \frac{i|\lambda_f|^2}{4\pi^2}\int_0^1 \mathrm{d}x \int_0^\Lambda \mathrm{d}|\ell_E| \ \left(\frac{|\ell_E|^5}{(|\ell_E|^2-\Delta(x))^2} - \frac{\Delta|\ell_E|^3}{(|\ell_E|^2+\Delta(x))^2}\right) \\ &\approx \frac{i|\lambda_f|^2}{4\pi^2}\frac{\Lambda^2}{2}\int_0^1 \mathrm{d}x, \end{aligned} \tag{B.21}$$

where we have taken the limit $\Lambda \gg \Delta$, and ignored the innermost integral evaluated at zero, as this subtraction is very small compared to the dominating Λ factors from the upper limit.

Hence, the fermionic mass correction is

$$(\Delta\ m_h^2)_f = -\frac{|\lambda_f|^2}{8\pi^2}\Lambda^2. \tag{B.22}$$

B.2 Scalar loop correction

We also have loop diagrams where Higgs can interact with another scalar particle, see figure B.2(b). The only contributing factors is one vertex and one propagator.

The calculation is similar to that of the fermion, but simpler.

$$\begin{aligned} i\mathcal{M} &= -i\lambda_S \int \frac{\mathrm{d}^4k}{(2\pi)^4} \frac{i}{k^2 - m_S^2} \\ &= \lambda_S \int \frac{\mathrm{d}^4k}{(2\pi)^4} \frac{1}{k^2 - m_S^2} \\ &= -i\frac{\lambda_S}{(2\pi)^4} \int \mathrm{d}^4k_E \ \left(\frac{1}{k_E^2 + m_S^2}\right) \\ &= -i\frac{\lambda_S}{(2\pi)^4} \int \mathrm{d}\Omega_4 \int \mathrm{d}|k_E| \ \left(\frac{1}{|k_E|^2 + m_S^2}\right) |k_E|^3 \\ &= -i\frac{\lambda_S}{8\pi^2} \int_0^\Lambda \mathrm{d}|k_E| \ \left(\frac{|k_E|^3}{|k_E|^2 + m_S^2}\right) \\ &= -i\frac{\lambda_S}{16\pi^2} \left(\Lambda^2 - m_S^2 \ln\left(1 + \frac{\Lambda^2}{m_S^2}\right)\right) \\ &\approx -i\frac{\lambda_S}{16\pi^2} \left(\Lambda^2 - m_S^2 \ln\left(\frac{\Lambda^2}{m_S^2}\right)\right), \end{aligned} \tag{B.23}$$

where we have that $\Lambda \gg m_S$.

To leading order in Λ the correction term from the scalar loop is

$$(\Delta m_h^2)_S = \frac{\lambda_S}{16\pi^2}\Lambda^2. \tag{B.24}$$

B.3 Complete correction

The total correction to leading order in Λ from the fermionic and scalar loops is,

$$\begin{aligned} \Delta m_h^2 &= (\Delta m_h^2)_f + (\Delta m_h^2)_S \\ &= -\frac{|\lambda_f|^2}{8\pi^2}\Lambda^2 + \frac{\lambda_S}{16\pi^2}\Lambda^2. \end{aligned} \tag{B.25}$$

Appendix C

Code

The subroutine PYCELL of PYTHIA 6 is modified to cluster on energy rather than transverse energy, for results to be comparable with those in [36]. In addition, two other modifications are done. To avoid double counting of leptons, we allow neither muons nor electrons to be present in jets. This is implemented in line 40. We also redefine the standard deviation in the electromagnetic smearing to include the constant term of eq. (5.7). This is done in line 100. We mark our modifications and additional code with *-*-*-*.

```
1       SUBROUTINE PYCELL(NJET)
2
3 C.....Double precision and integer declarations.
4       IMPLICIT DOUBLE PRECISION(A-H, O-Z)
5       IMPLICIT INTEGER(I-N)
6       INTEGER PYK,PYCHGE,PYCOMP
7       DOUBLE PRECISION P_E(4000)
8
9 C.....Parameter statement to help give large particle
    numbers
10      PARAMETER (KSUSY1=1000000,KSUSY2=2000000,KTECHN=300000
           0,
11     &KEXCIT=4000000,KDIMEN=5000000)
12
13 C.....Commonblocks
14      COMMON/PYJETS/N,NPAD,K(4000,5),P(4000,5),V(4000,5)
15      COMMON/PYDAT1/MSTU(200),PARU(200),MSTJ(200),PARJ(200)
16      COMMON/PYDAT2/KCHG(500,4),PMAS(500,4),PARF(2000),VCKM(
           4,4)
17      SAVE /PYJETS/,/PYDAT1/,/PYDAT2/
18
19 C.....Initialize, put values to zero for correct start point
20 C     *-*-*-*-*-*-*-*-*-*-*-*-*-*-*-*-*-*-*-*-*-*-*-*-*-*
21      DO 42 II = 1,4000
```

```
22          P_E(II)=0D0
23       42 CONTINUE
24    C     *-*-*-*-*-*-*-*-*-*-*-*-*-*-*-*-*-*-*-*-*-*-*-*-*-*
25
26    C.....Loop over all particles
27    C.....Find cell that was hit by given particle
28    C     *-*-*-*-*-*-*-*-*-*-*-*-*-*-*-*-*-*-*-*-*-*-*-*-*-*
29    C.....Do not allow electrons (11) and muons (13) in jets
30    C     *-*-*-*-*-*-*-*-*-*-*-*-*-*-*-*-*-*-*-*-*-*-*-*-*-*
31          PTLRAT=1D0/SINH(PARU(51))**2
32          NP=0           ! Particle number
33          NC=N           ! Number of cells
34          DO 110 I=1,N   ! Run through particles in event
35            IF(K(I,1).LE.0.OR.K(I,1).GT.10) GOTO 110 ! Go to
                 next particle
36            IF(P(I,1)**2+P(I,2)**2.LE.PTLRAT*P(I,3)**2) GOTO 110
37            IF(MSTU(41).GE.2) THEN
38              KC=PYCOMP(K(I,2)) ! Compressed particle code, abs(
                   ID)
39              IF(KC.EQ.0.OR.KC.EQ.12.OR.KC.EQ.14.OR.KC.EQ.16.OR.
40         &      KC.EQ.11.OR.KC.EQ.13.OR.KC.EQ.18.OR.K(I,2).EQ.
41         &      KSUSY1+22.OR.K(I,2).EQ.39.OR.K(I,2).EQ.KSUSY1+39)
42         &      GOTO 110 ! Invisible particles, e and mu not
               wanted. Go to next particle.
43              IF(MSTU(41).GE.3.AND.KCHG(KC,2).EQ.
44         &     0.AND.PYCHGE(K(I,2)).EQ.0)
45         &      GOTO 110
46            ENDIF
47            NP=NP+1 ! We survived, update particle number
48            PT=SQRT(P(I,1)**2+P(I,2)**2)
49            ETA=SIGN(LOG((SQRT(PT**2+P(I,3)**2)+ABS(P(I,3)))/PT)
                 ,P(I,3))
50            IETA=MAX(1,MIN(MSTU(51),1+INT(MSTU(51)*0.5D0*
51         &  (ETA/PARU(51)+1D0))))
52            PHI=PYANGL(P(I,1),P(I,2))
53            IPHI=MAX(1,MIN(MSTU(52),1+INT(MSTU(52)*0.5D0*
54         &  (PHI/PARU(1)+1D0))))
55            IETPH=MSTU(52)*IETA+IPHI
56
57    C     *-*-*-*-*-*-*-*-*-*-*-*-*-*-*-*-*-*-*-*-*-*-*-*-*-*
58            P_XYZ=SQRT(P(I,1)**2+P(I,2)**2+P(I,3)**2)
59    C     *-*-*-*-*-*-*-*-*-*-*-*-*-*-*-*-*-*-*-*-*-*-*-*-*-*
60
61    C...Add to cell already hit, or book new cell.
62    C...Executes zero times the first time (we have no cell to
```

```
   begin with, so we book a new one)
63        DO 100 IC=N+1,NC ! # of iterations:  max(0,int( (
             final val - initial val + step size) / step size)
             )
64          IF(IETPH.EQ.K(IC,3)) THEN
65            K(IC,4)=K(IC,4)+1
66            P(IC,5)=P(IC,5)+PT
67
68 C     *-*-*-*-*-*-*-*-*-*-*-*-*-*-*-*-*-*-*-*-*-*-*-*-*-*-*
69            P_E(IC) = P_E(IC) + P_XYZ
70 C     *-*-*-*-*-*-*-*-*-*-*-*-*-*-*-*-*-*-*-*-*-*-*-*-*-*-*
71            GOTO 110
72          ENDIF
73   100   CONTINUE
74        IF(NC.GE.MSTU(4)-MSTU(32)-5) THEN
75          CALL PYERRM(11,'(PYCELL:) no more memory left in
               PYJETS')
76          NJET=-2
77          RETURN
78        ENDIF
79        NC=NC+1                  ! Update cell number
80        K(NC,3)=IETPH   ! Some flag
81        K(NC,4)=1      ! Another flag
82        K(NC,5)=2      ! Another flag
83        P(NC,1)=(PARU(51)/MSTU(51))*(2*IETA-1-MSTU(51)) !
             WTF
84        P(NC,2)=(PARU(1)/MSTU(52))*(2*IPHI-1-MSTU(52))  !
             WTF
85        P(NC,5)=PT
86 C     *-*-*-*-*-*-*-*-*-*-*-*-*-*-*-*-*-*-*-*-*-*-*-*-*-*-*
87        P_E(NC)=P_XYZ
88 C     *-*-*-*-*-*-*-*-*-*-*-*-*-*-*-*-*-*-*-*-*-*-*-*-*-*-*
89   110 CONTINUE
90
91 C.....Smear true bin content by calorimeter resolution.
92        IF(MSTU(53).GE.1) THEN
93          DO 130 IC=N+1,NC
94            PEI=P(IC,5)
95            IF(MSTU(53).EQ.2) PEI=P(IC,5)*COSH(P(IC,1))
96 C     Redefine the standard deviation of the normal
   distribution
97 C     E = E + sigma*N(0,1), where N(0,1) is a normal
   distribtion
98 C     around zero, with standard deviation 1
99 C     *-*-*-*-*-*-*-*-*-*-*-*-*-*-*-*-*-*-*-*-*-*-*-*-*-*-*
```

```
  120     PEF = PEI + PARU(55)*SQRT(PEI+(0.0004/PARU(55)**2)
     *PEI**2
     &          *(-2D0*LOG(MAX(1D-10,PYR(0))))*COS(PARU(2)*
        PYR(0))
          IF(PEF.LT.0D0.OR.PEF.GT.PARU(56)*PEI) GOTO 120
          P(IC,5)=PEF
          IF(MSTU(53).EQ.2) P(IC,5)=PEF/COSH(P(IC,1))
C     *-*-*-*-*-*-*-*-*-*-*-*-*-*-*-*-*-*-*-*-*-*-*-*
  130   CONTINUE
      ENDIF

C     *-*-*-*-*-*-*-* IGNORED *-*-*-*-*-*-*-*-*-*
C.....Remove cells below threshold.
      IF(PARU(58).GT.0D0) THEN
        NCC=NC
        NC=N
        DO 140 IC=N+1,NCC
          IF(P_E(IC).GT.PARU(58)) THEN
            NC=NC+1
            K(NC,3)=K(IC,3)
            K(NC,4)=K(IC,4)
            K(NC,5)=K(IC,5)
            P(NC,1)=P(IC,1)
            P(NC,2)=P(IC,2)
            P(NC,5)=P(IC,5)
            P_E(NC)=P_E(IC)
          ENDIF
  140   CONTINUE
      ENDIF

C...Find initiator cell: the one with highest p of not yet
    used ones.
      NJ=NC
  150 EMAX=0D0
      DO 160 IC=N+1,NC
        IF(K(IC,5).NE.2) GOTO 160
C     *-*-*-*-*-*-*-*-*-*-*-*-*-*-*-*-*-*-*-*-*-*-*-*
        IF(P_E(IC).LE.EMAX) GOTO 160
C     *-*-*-*-*-*-*-*-*-*-*-*-*-*-*-*-*-*-*-*-*-*-*-*
        ICMAX=IC
        ETA=P(IC,1)
        PHI=P(IC,2)
C     *-*-*-*-*-*-*-*-*-*-*-*-*-*-*-*-*-*-*-*-*-*-*-*
        EMAX=P_E(IC)
C     *-*-*-*-*-*-*-*-*-*-*-*-*-*-*-*-*-*-*-*-*-*-*-*
```

```
142   160 CONTINUE
143       IF(EMAX.LT.PARU(52)) GOTO 220 ! PARU(52) is now =
             minimum E for a cell to be considered as a jet
             initiator. D=1.5 GeV
144       IF(NJ.GE.MSTU(4)-MSTU(32)-5) THEN
145         CALL PYERRM(11,'(PYCELL:) no more memory left in
               PYJETS')
146         NJET=-2
147         RETURN
148       ENDIF
149       K(ICMAX,5)=1
150       NJ=NJ+1
151       K(NJ,4)=0
152       K(NJ,5)=1
153       P(NJ,1)=ETA
154       P(NJ,2)=PHI
155       P(NJ,3)=0D0
156       P(NJ,4)=0D0
157       P(NJ,5)=0D0
158 C     *-*-*-*-*-*-*-*-*-*-*-*-*-*-*-*-*-*-*-*-*-*-*-*-*-*
159       P_E(NJ)=0D0
160 C     *-*-*-*-*-*-*-*-*-*-*-*-*-*-*-*-*-*-*-*-*-*-*-*-*-*
161
162 C...Sum up unused cells within required distance of
       initiator.
163       DO 170 IC=N+1,NC
164         IF(K(IC,5).EQ.0) GOTO 170
165         IF(ABS(P(IC,1)-ETA).GT.PARU(54)) GOTO 170
166         DPHIA=ABS(P(IC,2)-PHI)
167         IF(DPHIA.GT.PARU(54).AND.DPHIA.LT.PARU(2)-PARU(54))
               GOTO 170
168         PHIC=P(IC,2)
169         IF(DPHIA.GT.PARU(1)) PHIC=PHIC+SIGN(PARU(2),PHI)
170         IF((P(IC,1)-ETA)**2+(PHIC-PHI)**2.GT.PARU(54)**2)
               GOTO 170
171         K(IC,5)=-K(IC,5)
                                ! Used cell in jet, 'flip' it to
               illustrate
172         K(NJ,4)=K(NJ,4)+K(IC,4)
173         P(NJ,3)=P(NJ,3)+P(IC,5)*P(IC,1)
174         P(NJ,4)=P(NJ,4)+P(IC,5)*PHIC
175         P(NJ,5)=P(NJ,5)+P(IC,5)
176 C     *-*-*-*-*-*-*-*-*-*-*-*-*-*-*-*-*-*-*-*-*-*-*-*-*-*
177         P_E(NJ)=P_E(NJ)+P_E(IC)
178 C     *-*-*-*-*-*-*-*-*-*-*-*-*-*-*-*-*-*-*-*-*-*-*-*-*-*
```

```
179   170 CONTINUE
180
181 C.....Reject cluster below minimum E, else accept.
182 C     *-*-*-*-*-*-*-*-*-*-*-*-*-*-*-*-*-*-*-*-*-*-*-*-*-*
183       IF(P_E(NJ).LT.PARU(53)) THEN
184 C     *-*-*-*-*-*-*-*-*-*-*-*-*-*-*-*-*-*-*-*-*-*-*-*-*-*
185         NJ=NJ-1 ! Remove one number of jet if it does not
               pass the energy test
186         DO 180 IC=N+1,NC ! Loop over all cells
187           IF(K(IC,5).LT.0) K(IC,5)=-K(IC,5) ! Unuse cell
188   180   CONTINUE
189       ELSEIF(MSTU(54).LE.2) THEN
190         P(NJ,3)=P(NJ,3)/P(NJ,5) ! Scaling?
191         P(NJ,4)=P(NJ,4)/P(NJ,5) ! Scaling?
192         IF(ABS(P(NJ,4)).GT.PARU(1)) P(NJ,4)=P(NJ,4)-SIGN(
               PARU(2),
193      &  P(NJ,4))                                          !
            SIGN(A,B) returns value of A and sign of B
194         DO 190 IC=N+1,NC        ! Loop over all cells
195           IF(K(IC,5).LT.0) K(IC,5)=0    ! Put something to
                zero
196   190   CONTINUE
197       ELSE
198         DO 200 J=1,4
199           P(NJ,J)=0D0 ! Run through four indices for each
                jet; put to zero
200   200   CONTINUE
201         DO 210 IC=N+1,NC ! Loop over cells
202           IF(K(IC,5).GE.0) GOTO 210
203           P(NJ,1)=P(NJ,1)+P(IC,5)*COS(P(IC,2))  ! ..+ ET*cos
                (phi)
204           P(NJ,2)=P(NJ,2)+P(IC,5)*SIN(P(IC,2))  ! ..+ ET*sin
                (phi)
205           P(NJ,3)=P(NJ,3)+P(IC,5)*SINH(P(IC,1)) ! ..+ ET*
                sinh(phi)
206           P(NJ,4)=P(NJ,4)+P(IC,5)*COSH(P(IC,1)) ! ..+ ET*
                cosh(phi)
207           K(IC,5)=0
208   210   CONTINUE
209       ENDIF
210       GOTO 150
211
212 C.....Arrange clusters in falling E sequence.
213   220 DO 250 I=1,NJ-NC
214         EMAX=0D0
```

```
215           DO 230 IJ=NC+1,NJ
216             IF(K(IJ,5).EQ.0) GOTO 230
217             IF(P_E(IJ).LT.EMAX) GOTO 230
218             IJMAX=IJ
219             EMAX=P_E(IJ)
220     230     CONTINUE
221           K(IJMAX,5)=0
222           K(N+I,1)=31
223           K(N+I,2)=98
224           K(N+I,3)=I
225           K(N+I,4)=K(IJMAX,4)
226           K(N+I,5)=0
227   C     *-*-*-*-*-*-*-*-*-*-*-*-*-*-*-*-*-*-*-*-*-*-*-*-*-*
228           P_E(N+I)=P_E(IJMAX)
229   C     *-*-*-*-*-*-*-*-*-*-*-*-*-*-*-*-*-*-*-*-*-*-*-*-*-*
230           DO 240 J=1,5
231             P(N+I,J)=P(IJMAX,J)
232             V(N+I,J)=0D0
233     240     CONTINUE
234     250   CONTINUE
235         NJET=NJ-NC
236
237   C.....Convert to massless or massive four-vectors.
238         IF(MSTU(54).EQ.2) THEN
239           DO 260 I=N+1,N+NJET
240             ETA=P(I,3)
241             P(I,1)=P(I,5)*COS(P(I,4))
242             P(I,2)=P(I,5)*SIN(P(I,4))
243             P(I,3)=P(I,5)*SINH(ETA)
244             P(I,4)=P(I,5)*COSH(ETA)
245             P(I,5)=0D0
246     260     CONTINUE
247         ELSEIF(MSTU(54).GE.3) THEN
248           DO 270 I=N+1,N+NJET
249             P(I,5)=SQRT(MAX(0D0,P(I,4)**2-P(I,1)**2-P(I,2)**2-
                  P(I,3)**2))
250     270     CONTINUE
251         ENDIF
252
253   C.....Information about storage.
254         MSTU(61)=N+1
255         MSTU(62)=NP
256         MSTU(63)=NC-N
257         IF(MSTU(43).LE.1) MSTU(3)=MAX(0,NJET)
258         IF(MSTU(43).GE.2) N=N+MAX(0,NJET)
```

```
259
260         RETURN
261         END
```

Bibliography

[1] E. B. Rye, "Making SUSY Natural Again — Investigating the Naturalness Reach of the International Linear Collider," Master's thesis, The Faculty of Mathematics and Natural Sciences, University of Oslo, 2016.

[2] B. Allanach, J. Hetherington, M. A. Parker, and B. Webber, "Naturalness reach of the large hadron collider in minimal supergravity," *JHEP* **0008** (2000) 017, `arXiv:hep-ph/0005186 [hep-ph]`.

[3] **ATLAS** Collaboration, G. Aad *et al.*, "Observation of a new particle in the search for the Standard Model Higgs boson with the ATLAS detector at the LHC," *Phys. Lett.* **B716** (2012) 1–29, `arXiv:1207.7214 [hep-ex]`.

[4] **CMS** Collaboration, S. Chatrchyan *et al.*, "Observation of a new boson at a mass of 125 GeV with the CMS experiment at the LHC," *Phys. Lett.* **B716** (2012) 30–61, `arXiv:1207.7235 [hep-ex]`.

[5] E. Noether, "Invariante Variationsprobleme," *Nachr. D. König. Gesellsch. D. Wiss. Zu Göttingen* (1918) 235–257.

[6] R. P. Feynman, "Space-Time Approach to Quantum Electrodynamics," *Phys. Rev.* **76** (Sep, 1949) 769–789.

[7] C. S. Wu, E. Ambler, R. W. Hayward, D. D. Hoppes, and R. P. Hudson, "Experimental Test of Parity Conservation in Beta Decay," *Phys. Rev.* **105** (Feb, 1957) 1413–1415.

[8] T. D. Lee and C. N. Yang, "Question of Parity Conservation in Weak Interactions," *Phys. Rev.* **104** (Oct, 1956) 254–258.

[9] G. S. Guralnik, C. R. Hagen, and T. W. B. Kibble, "Global Conservation Laws and Massless Particles," *Phys. Rev. Lett.* **13** (Nov, 1964) 585–587.

[10] P. W. Higgs, "Broken Symmetries and the Masses of Gauge Bosons," *Phys. Rev. Lett.* **13** (Oct, 1964) 508–509.

[11] P. W. Higgs, "Broken Symmetries and the Masses of Gauge Bosons," *Phys. Rev. Lett.* **13** (Oct, 1964) 508–509.

[12] F. Englert and R. Brout, "Broken Symmetry and the Mass of Gauge Vector Mesons," *Phys. Rev. Lett.* **13** (Aug, 1964) 321–323.

[13] **Particle Data Group** Collaboration, K. Olive *et al.*, "Review of Particle Physics," *Chin. Phys.* **C38** (2014) 090001.

[14] V. C. Rubin and W. K. Ford, Jr., "Rotation of the Andromeda Nebula from a Spectroscopic Survey of Emission Regions," *Astrophys. J.* **159** (1970) 379–403.

[15] M. Thomson, *Modern Particle Physics*. Cambridge University Press, 2013.

[16] S. Coleman and J. Mandula, "All Possible Symmetries of the S Matrix," *Phys. Rev.* **159** (Jul, 1967) 1251–1256.

[17] R. Haag, J. T. Łopuszański, and M. Sohnius, "All possible generators of supersymmetries of the S-matrix," *Nucl. Phys.* **B88** no. 2, (1975) 257 – 274.

[18] H. J. Müller-Kirsten and A. Wiedemann, *Introduction to Supersymmetry*. World Scientific, 2010.

[19] J. Bagger and J. Wess, "Partial breaking of extended supersymmetry," *Phys. Lett.* **B138** no. 1, (1984) 105 – 110.

[20] S. Ferrara, L. Girardello, and F. Palumbo, "General mass formula in broken supersymmetry," *Phys. Rev.* **D20** (Jul, 1979) 403–408.

[21] P. Fayet, "Spontaneous Supersymmetry Breaking Without Gauge Invariance," *Phys. Lett.* **B58** (1975) 67.

[22] P. Batzing and A. Raklev, "Supersymmetry Lecture notes for FYS5190/FYS9190." Lecture notes in the FYS5190 Supersymmetry course given at the University of Oslo, autumn 2015.

[23] S. P. Martin, "A Supersymmetry primer," `arXiv:hep-ph/9709356 [hep-ph]`. *Adv. Ser. Direct. High Energy Phys. 18,1(1998)*.

[24] H. Baer, A. Mustafayev, S. Profumo, A. Belyaev, and X. Tata, "Direct, indirect and collider detection of neutralino dark matter in SUSY models with non-universal Higgs masses," *JHEP* **07** (2005) 065, `arXiv:hep-ph/0504001 [hep-ph]`.

[25] H. Baer, W. others, and X. Tata, "Radiatively-driven natural supersymmetry at the LHC," *JHEP* **12** (2013) 013, `arXiv:1310.4858 [hep-ph]`. [Erratum: JHEP06,053(2015)].

[26] C. Brust, A. Katz, S. Lawrence, and R. Sundrum, "SUSY, the Third Generation and the LHC," *JHEP* **03** (2012) 103, arXiv:1110.6670 [hep-ph].

[27] M. Papucci, J. T. Ruderman, and A. Weiler, "Natural SUSY Endures," *JHEP* **09** (2012) 035, arXiv:1110.6926 [hep-ph].

[28] B. de Carlos and J. A. Casas, "One loop analysis of the electroweak breaking in supersymmetric models and the fine tuning problem," *Phys. Lett.* **B309** (1993) 320–328, arXiv:hep-ph/9303291 [hep-ph].

[29] J. S. Kim, K. Rolbiecki, R. Ruiz, J. Tattersall, and T. Weber, "Natural SUSY: Now or Never?," arXiv:1606.06738 [hep-ph].

[30] R. Barbieri and G. F. Giudice, "Upper Bounds on Supersymmetric Particle Masses," *Nucl. Phys.* **B306** (1988) 63–76.

[31] J. L. Feng, "Naturalness and the Status of Supersymmetry," *Ann. Rev. Nucl. Part. Sci.* **63** (2013) 351–382, arXiv:1302.6587 [hep-ph].

[32] T. Bayes, "An essay towards solving a problem in the doctrine of chances," *Phil. Trans. of the Royal Soc. of London* **53** (1763) 370–418.

[33] A. Kvellestad, *Chasing SUSY through parameter space*. PhD thesis, The Faculty of Mathematics and Natural Sciences, University of Oslo, 2015.

[34] S. Kullback and R. A. Leibler, "On Information and Sufficiency," *Ann. Math. Statist.* **22** no. 1, (03, 1951) 79–86.

[35] "Search for Supersymmetry at the high luminosity LHC with the ATLAS experiment," Tech. Rep. ATL-PHYS-PUB-2014-010, CERN, Geneva, Jul, 2014. https://cds.cern.ch/record/1735031.

[36] H. Baer, A. Belyaev, T. Krupovnickas, and X. Tata, "Linear collider capabilities for supersymmetry in dark matter allowed regions of the mSUGRA model," *JHEP* **02** (2004) 007, arXiv:hep-ph/0311351 [hep-ph].

[37] B. C. Allanach, "SOFTSUSY: a program for calculating supersymmetric spectra," *Comput. Phys. Commun.* **143** (2002) 305–331, arXiv:hep-ph/0104145 [hep-ph].

[38] P. Z. Skands *et al.*, "SUSY Les Houches accord: Interfacing SUSY spectrum calculators, decay packages, and event generators," *JHEP* **07** (2004) 036, arXiv:hep-ph/0311123 [hep-ph].

[39] A. Djouadi, M. M. Muhlleitner, and M. Spira, "Decays of supersymmetric particles: The Program SUSY-HIT (SUspect-SdecaY-Hdecay-InTerface)," *Acta Phys. Polon.* **B38** (2007) 635–644, arXiv:hep-ph/0609292 [hep-ph].

[40] S. Heinemeyer, W. Hollik, and G. Weiglein, "FeynHiggs: A Program for the calculation of the masses of the neutral CP even Higgs bosons in the MSSM," *Comput. Phys. Commun.* **124** (2000) 76–89, arXiv:hep-ph/9812320 [hep-ph].

[41] H. Bahl and W. Hollik, "Precise prediction for the light MSSM Higgs boson mass combining effective field theory and fixed-order calculations," *Eur. Phys. J.* **C76** no. 9, (2016) 499, arXiv:1608.01880 [hep-ph].

[42] T. Hahn, S. Heinemeyer, W. Hollik, H. Rzehak, and G. Weiglein, "High-Precision Predictions for the Light CP-Even Higgs Boson Mass of the Minimal Supersymmetric Standard Model," *Phys. Rev. Lett.* **112** no. 14, (2014) 141801, arXiv:1312.4937 [hep-ph].

[43] M. Frank *et al.*, "The Higgs Boson Masses and Mixings of the Complex MSSM in the Feynman-Diagrammatic Approach," *JHEP* **02** (2007) 047, arXiv:hep-ph/0611326 [hep-ph].

[44] G. Degrassi, S. Heinemeyer, W. Hollik, P. Slavich, and G. Weiglein, "Towards high precision predictions for the MSSM Higgs sector," *Eur. Phys. J.* **C28** (2003) 133–143, arXiv:hep-ph/0212020 [hep-ph].

[45] S. Heinemeyer, W. Hollik, and G. Weiglein, "The Masses of the neutral CP - even Higgs bosons in the MSSM: Accurate analysis at the two loop level," *Eur. Phys. J.* **C9** (1999) 343–366, arXiv:hep-ph/9812472 [hep-ph].

[46] T. Sjostrand, S. Mrenna, and P. Z. Skands, "PYTHIA 6.4 Physics and Manual," *JHEP* **05** (2006) 026, arXiv:hep-ph/0603175 [hep-ph].

[47] T. Sjöstrand *et al.*, "An Introduction to PYTHIA 8.2," *Comput. Phys. Commun.* **191** (2015) 159–177, arXiv:1410.3012 [hep-ph].

[48] A. Buckley, "PySLHA: a Pythonic interface to SUSY Les Houches Accord data," *Eur. Phys. J.* **C75** no. 10, (2015) 467, arXiv:1305.4194 [hep-ph].

[49] W. Beenakker *et al.*, "Squark and Gluino Hadroproduction," *Int. J. Mod. Phys.* **A26** (2011) 2637–2664, arXiv:1105.1110 [hep-ph].

[50] W. Beenakker *et al.*, "Soft-gluon resummation for squark and gluino hadroproduction," *JHEP* **12** (2009) 041, arXiv:0909.4418 [hep-ph].

[51] A. Kulesza and L. Motyka, "Soft gluon resummation for the production of gluino-gluino and squark-antisquark pairs at the LHC," *Phys. Rev.* **D80** (2009) 095004, arXiv:0905.4749 [hep-ph].

[52] A. Kulesza and L. Motyka, "Threshold resummation for squark-antisquark and gluino-pair production at the LHC," *Phys. Rev. Lett.* **102** (2009) 111802, arXiv:0807.2405 [hep-ph].

[53] W. Beenakker, R. Hopker, and M. Spira, "PROSPINO: A Program for the production of supersymmetric particles in next-to-leading order QCD," arXiv:hep-ph/9611232 [hep-ph].

[54] Z. Sullivan and E. L. Berger, "Isolated leptons from heavy flavor decays - theory and data," *Phys. Rev.* **D82** (2010) 014001, arXiv:1003.4997 [hep-ph].

[55] M. Cacciari, G. P. Salam, and G. Soyez, "The Anti-k(t) jet clustering algorithm," *JHEP* **04** (2008) 063, arXiv:0802.1189 [hep-ph].

[56] T. Tsukamoto, K. Fujii, H. Murayama, M. Yamaguchi, and Y. Okada, "Precision study of supersymmetry at future linear e^+e^- colliders," *Phys. Rev.* **D51** (Apr, 1995) 3153–3171.

[57] M. Cacciari, G. P. Salam, and G. Soyez, "FastJet User Manual," *Eur. Phys. J.* **C72** (2012) 1896, arXiv:1111.6097 [hep-ph].